Optical emission produced by proton and hydrogen atom impact on nitrogen and hydrogen molecules
by Duane Arlen Dahlberg

A thesis submitted to the Graduate Faculty in partial fulfillment of the requirements for the degree of
DOCTOR OF PHILOSOPHY in Physics
Montana State University

Abstract:
Optical emissions produced in collisions of protons incident on nitrogen and hydrogen molecules and hydrogen atoms incident on the same molecules were studied in the spectral region from 1200 Å to 6000 Å. Relative emission cross sections were measured in the energy range from 10 kev to 130 kev.

The spectra excited by proton impact with nitrogen and hydrogen molecules were scanned with a monochromator and photomultiplier. The prominent features of the nitrogen spectrum below 2000 Å were the Lyman alpha line and some atomic nitrogen lines. The Lyman-Birge-Hopfield system appeared also, but it was weak. At the longer wavelengths the N2^+ First Negative and the N2 Second Positive systems dominated the spectrum. The Balmer beta and an ionic nitrogen line appeared as well. Both Lyman alpha and the Lyman bands were prominent in the hydrogen molecular spectrum. Lyman alpha, however, was the dominant emission. In addition to the Balmer lines, a few lines of the hydrogen molecular spectrum were present in the longer wavelength spectral region.

Relative emission cross sections were measured for the production of a number of the First Negative bands, the (0,0) Second Positive band, an ionic nitrogen line, atomic nitrogen lines, and Lyman alpha in proton and hydrogen atom collisions with nitrogen gas. Cross sections for the production of the First Negative bands in collisions of hydrogen atoms with nitrogen molecules were nearly constant as a function of energy, and at an energy of 40 kev the cross section was one-half as large as the cross section for proton collisions. The cross section for the Second Positive band due to hydrogen atom impact was about 3 x 10^-18 cm^2 at 25 kev whereas for proton impact the cross section was about 2 x 10^-19 cm^2 at its maximum value. The cross sections for the atomic nitrogen lines produced in hydrogen atom impact were approximately 75% of the cross sections for the same lines produced in proton impact. Hydrogen atom collisions had higher cross sections throughout the energy range for the production of Lyman alpha emission.

Relative emission cross sections for the production of the Lyman bands and Lyman alpha by proton and hydrogen atom impact on hydrogen molecules were also measured. Hydrogen atoms proved to be much less effective than protons in exciting the Lyman bands of hydrogen.

Consideration was given to the possible mechanisms responsible for the various emissions and comparisons were made to the energy dependence predicted in the Born approximation theory.

OPTICAL EMISSION PRODUCED BY PROTON AND HYDROGEN ATOM IMPACT ON NITROGEN AND HYDROGEN MOLECULES

by

DUANE ARLEN DAHLBERG

A thesis submitted to the Graduate Faculty in partial fulfillment of the requirements for the degree

of

DOCTOR OF PHILOSOPHY

in

Physics

Approved:

N. L. Moise
Head, Physics Department

Irving E. Dayton
Chairman, Examining Committee

David K. Anderson
Co-Director of Thesis

Louis D. Smith
Graduate Dean

MONTANA STATE UNIVERSITY
Bozeman, Montana

June, 1967

ACKNOWLEDGMENTS

The author wishes to acknowledge the continued financial support of this research project by the National Aeronautics and Space Administration under the Sustaining University Program Grant NsG-430, the financial support of the National Science Foundation under the Science Faculty Fellowship Program, and the financial support and extended leave of absence from Concordia College, Moorhead, Minnesota. The author is also grateful for the direction and assistance of Professor Irving E. Dayton and Professor David K. Anderson, the helpful discussions of Professor Joseph A. Ball and Professor E. Miller Layton, and the assistance of Ann Romer, Edward Teppo and James White in taking data.

LIST OF TABLES

LIST OF FIGURES

ABSTRACT

Optical emissions produced in collisions of protons incident on nitrogen and hydrogen molecules and hydrogen atoms incident on the same molecules were studied in the spectral region from 1200 Å to 6000 Å. Relative emission cross sections were measured in the energy range from 10 kev to 130 kev.

The spectra excited by proton impact with nitrogen and hydrogen molecules were scanned with a monochromator and photomultiplier. The prominent features of the nitrogen spectrum below 2000 Å were the Lyman alpha line and some atomic nitrogen lines. The Lyman-Birge-Hopfield system appeared also, but it was weak. At the longer wavelengths the N_2^+ First Negative and the N_2 Second Positive systems dominated the spectrum. The Balmer beta and an ionic nitrogen line appeared as well. Both Lyman alpha and the Lyman bands were prominent in the hydrogen molecular spectrum. Lyman alpha, however, was the dominant emission. In addition to the Balmer lines, a few lines of the hydrogen molecular spectrum were present in the longer wavelength spectral region.

Relative emission cross sections were measured for the production of a number of the First Negative bands, the (0,0) Second Positive band, an ionic nitrogen line, atomic nitrogen lines, and Lyman alpha in proton and hydrogen atom collisions with nitrogen gas. Cross sections for the production of the First Negative bands in collisions of hydrogen atoms with nitrogen molecules were nearly constant as a function of energy, and at an energy of 40 kev the cross section was one-half as large as the cross section for proton collisions. The cross section for the Second Positive band due to hydrogen atom impact was about 3×10^{-18} cm^2 at 25 kev whereas for proton impact the cross section was about 2×10^{-19} cm^2 at its maximum value. The cross sections for the atomic nitrogen lines produced in hydrogen atom impact were approximately 75% of the cross sections for the same lines produced in proton impact. Hydrogen atom collisions had higher cross sections throughout the energy range for the production of Lyman alpha emission.

Relative emission cross sections for the production of the Lyman bands and Lyman alpha by proton and hydrogen atom impact on hydrogen molecules were also measured. Hydrogen atoms proved to be much less effective than protons in exciting the Lyman bands of hydrogen.

Consideration was given to the possible mechanisms responsible for the various emissions and comparisons were made to the energy dependence predicted in the Born approximation theory.

CHAPTER I. INTRODUCTION

The homonuclear diatomic molecule represents the simplest molecular structure and the proton is the simplest atomic nucleus. Collisions between these systems would be the least difficult of all ion-molecule collisions to analyze, and the experimental data obtained in studying these collisions would be most useful in evaluating approximate theoretical treatments. Since the hydrogen atom is the simplest atomic structure, collisions between the homonuclear diatomic molecule and the hydrogen atom represent the least complex of the atom-molecule interactions. The hydrogen atom differs from the proton only by the bound electron of the hydrogen atom. Experimental data obtained for collisions in which protons are replaced by hydrogen atoms, therefore, are also of theoretical interest. The least complex of the diatomic molecules is the hydrogen molecule, and consequently, collisions involving this molecule are of the greatest theoretical interest.

One method for studying collisions between two systems is to measure the photon energy which is emitted in optical transitions resulting from the collision. For particular cases a measurement of the photon emission provides a direct means of obtaining cross sections for exciting atomic and molecular states. A comparison of these experimentally obtained excitation cross sections with theoretical predictions can assist in understanding collision mechanisms.

Atmospheric research indicates that fast protons are entering the atmosphere and contribute to the production of auroras[1]. Because of the charge exchange process whereby protons pick up electrons from atmospheric gases, there would also be fast hydrogen atoms present.

It is evident from the work of Allison and others[2] that the equilibrium fraction of hydrogen atoms produced in charge exchange is significant for projectile energies of a few kev to 100 kev. It is of interest, therefore, to determine the effectiveness of the hydrogen atoms in exciting the atmospheric gases and also their contribution to the auroras. The knowledge of hydrogen atom excitation cross sections is also important in studying the history of a proton entering the atmosphere.

For these reasons optical emissions produced in collisions of protons and hydrogen atoms with nitrogen and hydrogen molecules have been studied.

The experimental apparatus used to measure the light emitted in both proton and hydrogen atom collisions represents an integral part of this work and will be discussed next. The proton beam from a Cockroft-Walton accelerator equipped with an RF ion source is focused and mass analyzed. The resulting beam passes through a set of collimating apertures in the charge exchange cell, then into a differentially pumped region, and finally into the excitation chamber. Finally the protons are collected in a Faraday cage at the end of the excitation chamber. If a hydrogen atom beam is desired, a molecular gas is admitted to the charge exchange cell. In passing through the charge exchange cell the initial proton beam becomes a mixture of hydrogen atoms and protons. The protons are electrostatically deflected from the beam in the differentially pumped region, leaving only the hydrogen atoms to enter the excitation chamber. The hydrogen atom beam current is measured by secondary emission techniques. The light which is emitted in the collisions between

the incident particle beam and the target gas is chopped mechanically and spectrally analyzed with a monochromator. A photomultiplier and a phase sensitive detection system are used to measure the light intensity.

Spectral scans of the light emitted in the collisions of protons with both nitrogen gas and hydrogen gas in the spectral region from 1200 Å to 6000 Å indicated which transitions of the molecules, of the atoms and ions originating from molecular dissociation, and of the incident particle produced sufficient light intensities for emission cross section measurements. The results of the scans led to relative emission cross section measurements for the production of the N_2^+ First Negative band system ($B\,^2\Sigma_u^+ \text{---} X\,^2\Sigma_g^+$), the N_2 Second Positive band system ($C^3\Pi_u \text{---} B^3\Pi_g$), atomic and ionic nitrogen lines, Lyman bands in hydrogen, and the Lyman alpha line. The emission cross sections for these molecular vibrational bands and atomic lines were measured as a function of projectile energy from 10 kev to 130 kev. Both protons and hydrogen atoms were used as the incident particles.

Optical emissions produced by protons incident on nitrogen have been studied in the visible and near ultra-violet spectral region by a number of researchers [3,4,5,6]. Some emission cross section measurements of Lyman alpha produced in proton collisions with nitrogen and hydrogen molecules have also been reported [7,8]. Since no emission cross sections for hydrogen atoms incident on nitrogen and hydrogen molecules have been measured, a particular emphasis was placed on the emissions due to hydrogen atom impact. In the vacuum ultra-violet spectral region no emission cross sections for proton and hydrogen atom impact had been measured for

these molecules. An effort was made, therefore, to also measure emission cross sections for optical transitions in the spectral region from 1200 Å to 3000 Å.

In those cases where emission cross sections could be directly related to the excitation cross sections, the measured cross sections were qualitatively related to theory.

CHAPTER II. THEORY

The primary purpose of this discussion is to present briefly some of the most pertinent aspects of the theoretical work involving ion-atom and atom-atom collisions. Some of these theoretical results can be helpful in understanding ion-molecule and atom-molecule collisions. The main body of theoretical work has been centered in collisions of electrons or ions incident on atoms. Discussions of collision processes, collision cross section, some basic theoretical treatments, and a few results are included in this chapter.

COLLISION PROCESSES

There are two basically different processes which occur in a collision. One is the elastic collision in which the kinetic energy is conserved. The second is the inelastic collision in which the kinetic energy is not conserved.

Elastic scattering produces no effect other than changes in kinetic energy and momentum of the colliding particles.

For the inelastic collision the situation is very complex. If an electron is the accelerated particle and A is an atom, the following basic reactions are possible:

$$e + A \text{ --- } e + A^{*} \qquad \text{Excitation}$$

$$e + A \text{ --- } e + A^{+} + e \qquad \text{Ionization}$$

$$e + A_2 \text{ --- } e + A + A \qquad \text{Dissociation}$$

If an atomic ion or atom is the accelerated particle, the additional reactions can occur:

$$B^{+} + A \text{ --- } B + A^{+} \qquad \text{Charge Exchange or Electron Capture}$$

$B + A \text{ --- } B^{+} + A + e$ Stripping

$B^{*} + A \text{ --- } B + A^{*}$ Excitation Transfer

In addition many combinations of these basic processes are possible in a collision. Some examples that will be considered in this paper are charge exchange plus excitation, ionization plus excitation, and dissociation plus ionization plus excitation. For a more complete listing and classification of collision processes the reader is referred to Hasted's work [9].

COLLISION CROSS SECTION

Both elastic and inelastic collision probabilities are defined in terms of the cross section. The total collision cross section, Q_t, can be expressed as $\sum_i Q_i$, where Q_i represents the cross section for an individual type of collision process and the sum is over all possible collision processes.

For two hard spheres of radii r and r' the cross section for elastic collision is defined simply as $Q_e = \pi (r + r')^2$. For inelastic collisions involving ions and atoms the expression for cross section is complex due to the large number of individual processes contributing to the cross sections.

Although many processes are indirectly connected to the work discussed in this paper, the process of direct interest is the excitation process. An expression can be obtained which relates the emission measurements to excitation cross sections.

Consider the excitation produced when a beam of particles passes through a chamber containing a target gas. The change in the number of

excited target atoms in state "i" per second over a path length of one cm, as a consequence of collision with beam particles, is expressed as

$$(dn_i/dt) = NIQ_i + \sum_{k>i} A_{ki} n_k - \sum_{j<i} A_{ij} n_i$$

In this equation n_i is the number of atoms excited to state "i" per cm path length; N is the number of target atoms per cm^3; I is the number of particles passing through a unit surface perpendicular to the beam direction; and A_{ij} is the transition probability from state "i" to "j". Q_i is the cross section for excitation of level "i". The first term on the right in this equation represents the direct excitation to state "i"; the second term is the population by cascading from higher levels, and the third term represents the decay of state "i" to all lower levels. At equilibrium $(dn_i/dt) = 0$. If one neglects the cascading term $Q_i = \sum_{j<i} A_{ij} n_i = \sum_{j<i} Q_{ij}$, where Q_{ij} is the effective cross section for emission of the line representing the transition from "i" to "j". If cascading is included, $Q_i = \sum_{j<i} A_{ij} n_i - \sum_{k>i} A_{ki} n_k$.

The cross section for the excitation of the fast particle consists of the same terms as for the target particle, providing that equilibrium has been established between the formation of the excited state and emission. Absolute measurements, however, require a calculation of the effective path length of observation.

Cross sections normally are expressed in terms of cm^2/ target particle.

THEORETICAL TREATMENTS

Classical Method of Gryzinski

Briefly, Gryzinski's approach[10,11,12] to atomic collisions is based upon the assumption that the interaction between a charged projectile and an atom can be described classically by the coulomb interaction between the projectile and the atomic electrons. This is a classical theory, but its results depend upon the binding energy and the momentum distribution of the atomic electrons which are obtained quantum mechanically. The Gryzinski theory has been used for calculating cross sections for some inelastic collisions, but calculations for excitation processes have not been made. The moderate success of the theory for some inelastic collisions[12] should provide the impetus, however, for excitation calculations.

Quantum Mechanical Methods

Since classical methods are generally not able to predict the behavior of inelastic collisions, quantum theories must be used.

There are two different approaches to the theory which have been exploited. These are the impact parameter treatment and the wave treatment[13]. The impact parameter treatment is applied in particular to collisions of heavy particles. The assumptions are made that the nuclei can be regarded as classical particles and that the nuclei follow classical trajectories which approach straight lines as the particle velocity increases. This treatment is semiclassical since quantum mechanics is used for describing the electron motion. The wave treatment assumes that the incoming and outgoing particles can be treated as waves. This treatment

can, therefore, be used as effectively for electrons as for heavy particles. For collisions involving heavy particles, however, these two treatments have been shown to be mathematically equivalent [14].

In quantum mechanics the motion relative to the center of mass of a system of two colliding particles can be described by the following wave equation [15]:

$$\left[(\hbar^2/2M)\,\nabla_r^2 - H_a(\vec{r}_a) - H_b(\vec{r}_b) + \tfrac{1}{2}Mv^2 + E_o - V(\vec{r},\vec{r}_a,\vec{r}_b)\right]\Psi = 0$$

In order to analyze this wave equation, each section will be considered separately.

First of all, the motion of one particle relative to the other can be represented by the equation:

$\left[(\hbar^2/2M)\,\nabla_r^2 + \tfrac{1}{2}Mv^2\right] F(\vec{r}) = 0$, where $\vec{r}$ and v are, respectively, the relative coordinates and velocity of the two particles and M is the reduced mass.

Second, the internal motion of the two particles can be represented by the equation: $\left[H_a(\vec{r}_a) + H_b(\vec{r}_b) - E_a - E_b\right]\Psi = 0$, where $\Psi(\vec{r}_a,\vec{r}_b)$ is some product of $u(\vec{r}_a)$ and $v(\vec{r}_b)$. The equations, $\left[H_a(\vec{r}_a) - E_a\right] u(\vec{r}_a) = 0$ and $\left[H_b(\vec{r}_b) - E_b\right] v(\vec{r}_b) = 0$ describe the internal motion of particle a and particle b, respectively, where H_a and H_b are respectively the Hamiltonians for particles a and b.

Third is the term which prescribes the interaction between the two particles, $V(\vec{r},\vec{r}_a,\vec{r}_b)$.

In principle the wave equation describing a colliding system can be solved and the cross sections for particular scattering events can be obtained. In practice, however, values for cross sections can be calcu-

lated only by approximate means, even for the simplest system.

The two quantum mechanical approximations which have application here are the Born approximation and the distorted wave approximation.

Born Approximation: The wave treatment of the Born approximation is discussed extensively by Mott and Massey [15] and the impact parameter treatment is considered in detail by Bates [13].

Basically the Born approximation assumes that the incident particle is an undistorted plane wave which is unaffected by the interaction with the target. The interaction producing the excitation is assumed to be small so that the effect on the incident wave can be neglected. Any excitation that occurs results from the direct excitation from the initial to the final state. The coupling between intermediate states is, therefore, ignored.

These assumptions imply that the approximation is valid only at high impact velocities. The term "high" must be expressed more definitely. The only means by which this can truly be accomplished is to compare the theoretical results to experiment. In general terms, however, the velocity is considered high if $(e^2/hv) \ll 1$, where v is the velocity of the incident particle, and if $v^2/u^2 \gg 1$, where u is the orbital velocity of the atomic electrons. In terms of momentum the velocity is high if $K_o^2 \gg K^2$, where $K_o^2 = 2m\,|E_o|\,/\hbar^2$, and E_o is the excitation energy of the target particle. K h is the change in momentum of the incident particle. For example, in the ionization of helium by proton impact, the Born approximation is reasonably good above 60 kev [16]. For further discussion of this subject refer to the work of Bates [13].

In the Born approximation equations for cross section have been formulated also in terms of the energy of the incident particle and transition probabilities [15]. This formulation is sometimes referred to the Bethe-Born approximation and is significant because it provides equations relating the energy dependence of the cross sections for ionization, excitation, and charge exchange produced in collisions of fast ions with atomic systems. The cross section for optical excitation of an allowed transition or outer shell ionization of an atom by a fast ion is:

$$Q_{nl,n'l'} \approx (\text{Constant}/mv^2) \left|x_{nl,n'l'}\right|^2 \ln(2mv^2/E_{n'l'}-E_{nl})$$

$\left|x_{nl,n'l'}\right|^2$ is the square of the dipole transition probability. $E_{n'l'}$ and E_{nl} are energies of the n'l' and nl levels, respectively. If excitation is to a forbidden level and the transition is associated with the quadupole moment, the cross section will have the form:

$$Q_{nl,n'l'} \approx (\text{constant}/v^2) \left|(x)^2_{nl,n'l'}\right|^2 E_{nl}$$ [15].

Distorted Wave Approximation: Mott and Massey have also described the distorted wave approximation and its semiclassical counterpart, the distortion approximation [15]. The two different names are connected, respectively, with the wave treatment and the impact parameter treatment of this approximation.

As in the Born approximation one assumes that the coupling between the two states under consideration is weak. Instead of assuming plane incoming and outgoing waves, as is done in the Born approximation, the distorted wave approximation allows for a distortion of the incoming and outgoing waves by the scattering potential field. The transition matrix

elements, therefore, become a function of the interaction potentials. The distorted wave approximation gives a lower value of cross section than the Born approximation at low energies. At high energies the two approximations approach the same values and are mathematically equivalent.

RESULTS OF THE THEORY

In this section the applications of the theory, comparisons of the Born and distortion approximation, and the general dependence on energy will be discussed.

Applications and Comparisons

In 1953 Bates published a discussion and critique of the various approximations used for describing the inelastic collisions between ions and atoms [17]. At that time the Born approximation was applied at the higher energies and at the lower energies the perturbed stationary state approximation was used. In a more recent publication [18] Bates questioned the validity of ignoring the effect of the scattering field on the incoming and outgoing waves. This led to the distortion approximation for calculating inelastic cross sections for ion-atom collisions. Since then a number of researchers have calculated cross sections for the excitation of hydrogen and helium by proton impact. They have used either the Born or Distortion approximations.

Using both the Born and Distortion approximations Bell [18] has calculated the cross sections for the formation of the $3\,^1P$ excited state of neutral helium by proton impact. These calculations have been compared with experimental results by J. Van Eck, et. al. [20] and E. W. Thomas, et. al. [21].

Bates and Crothers [22] have gone a step further. They have considered atom-atom collisions and have taken into account the exchange of electrons between the incident particle and the target atom. This work was then applied specifically to the excitation produced in the collision of hydrogen atoms on helium.

The exchange of electrons is probably the dominant mechanism in the excitation of a triplet state from a singlet ground state. The calculations were, therefore, compared with the cross sections for the excitation of the $3\,^3P$ state of helium measured by J. Van Eck, et. al. [20]. The comparison was quite good for this triplet state but not so good for some of the other triplet states of helium.

General Energy Dependence of Cross Section

At high incident particle energies the cross sections for inelastic collision processes have a dependence on energy described by the Born approximation. For simple excitation and ionization Q is proportional to $(1/E)\ln E$. For electron capture [9] Q is proportional to E^{-6}. At the high incident particle energies the cross section plotted as a function of energy will, therefore, decrease as the energy increases.

For low energies the cross sections for inelastic collisions will decrease with decreasing energy. Consequently a maximum in the cross section must exist at some intermediate energy. The adiabatic criterion proposed by Massey [23] is useful in predicting the energy dependence at low energies and in predicting the maximum in the electron capture process. At low impact energies where the velocity of relative motion is small, the electron is able to adjust to changes in inter-

nuclear distances. The electron, therefore, has a small probability of making a transition and consequently the cross section for the transition is small. As the relative velocity, v, increases the probability for transition of an electron increases and the time of collision, a/v, decreases. The adiabatic parameter, "a", is the distance in which the electron capture process is assumed to be possible. The assumption is made that the cross section for electron capture has a maximum when the time of collision is equal to the time of transition, $\Delta E/h$, where ΔE is the internal energy defect resulting in the electron capture. For the process $A^+ + B \text{ --- } A + B^+$, the energy defect is defined as $E_B - E_A$, where E_B and E_A are, respectively the ionization energies of atom B and atom A.

This entire argument can now be reversed. If the incident particle velocity at the maximum in the electron capture cross section can be experimentally measured, the Massey criterion provides a method for determining the interaction distance, "a". The determination of "a" has been made for many colliding systems. The interesting result is that the value of "a" is approximately equal to 7 $\mathring{A}$ for most electron capture processes without regard for the particular atoms involved [24].

Hasted [9] points out that there is sufficient justification for applying the adiabatic criterion to other processes also. According to Solov'ev [25] the application of the Massey criterion to ionization process gives values of "a" ranging from 4.7 $\mathring{A}$ to 6.6 $\mathring{A}$.

Hasted [9] also cautions one in using this criterion for collision processes between more complex systems. An example of the necessary

caution is presented in the work of J. Van Eck, et. al.[20]. Applying the criterion to atom-atom collisions which result in excitation of the triplet states of helium, the interaction distance is about 3 Å and this small value of "a" is thought to be due to the formation of intermediate molecular states. If intermediate states are formed, ΔE probably changes in the interaction and the adiabatic criterion can no longer be used.

CHAPTER III. EXPERIMENTAL APPARATUS

The various pieces of experimental apparatus used in the measurements of the emission cross sections produced in collision processes will be discussed. Figures 1 and 2 show the sections of the apparatus which are of special interest in these measurements.

ACCELERATOR

A Cockroft-Walton accelerator manufactured by the Texas Nuclear Corporation (Model 9501-1, Ser. No. 42, Neutron Generator) was modified to provide a stable proton beam of energies from 10 kev to 130 kev. The protons were produced in an Oak Ridge type RF ion source[26] theoretically capable of a total beam of 1 ma, 90% of which would be protons.

A standard resistor equal to 1/10[5] of the measured resistance of the accelerator tube resistor chain was inserted at the low potential end of the chain. This chain of 20 10 meg Ω resistors acted as a potential divider for the accelerating region. The potential across the standard resistor was directly related to the potential across the accelerator tube and was used to measure the proton energy. From direct measurements at low potentials and comparisons with the readings of a voltmeter for the high voltage supply, the author concluded that the error in energy measurements was never more than 10%.

In preparing this machine for use the following modifications were made:

1. The diffusion pump electrical power system was redesigned in order to provide safety switches and controllable power to the heater of the diffusion pump. Figure 3 shows the electrical circuit. This circuit was used also for the vacuum system on the differentially pumped

chamber.

2. The vacuum plumbing was changed to permit roughing the system while the diffusion pump was on.

3. The cold cathode type pressure gauge circuit was removed from the accelerator control panel. A VEECO ionization gauge was used to monitor the pressure in the accelerator tube and served also as a high pressure safety control.

4. The solenoid field coil on the ion source was replaced with a new design which had a heat sink. The control for varying the solenoid field was moved from the high potential end to the low potential end of the accelerator. This modification provided a means of adjusting the magnetic field in the ion source while the accelerator was in operation.

5. The resistor chain on the accelerator tube was replaced after finding the existing resistors unreliable. These faulty resistors led to beam instabilities.

6. Due to fluctuations in line voltage a Sola regulating transformer was installed to control the power input to the high voltage power supply. This regulating transformer also stabilized the power to all the circuits in the high voltage section of the accelerator.

ELECTROSTATIC QUADRUPOLE LENS

To supplement the focusing already built into the accelerator an electrostatic quadrupole strong focusing lens (Texas Nuclear, Model 9515) was added between the accelerator and the analyzing magnet. A beam could then be maintained even at low energies. This lens also served to correct any aberrations produced by the analyzing magnet.

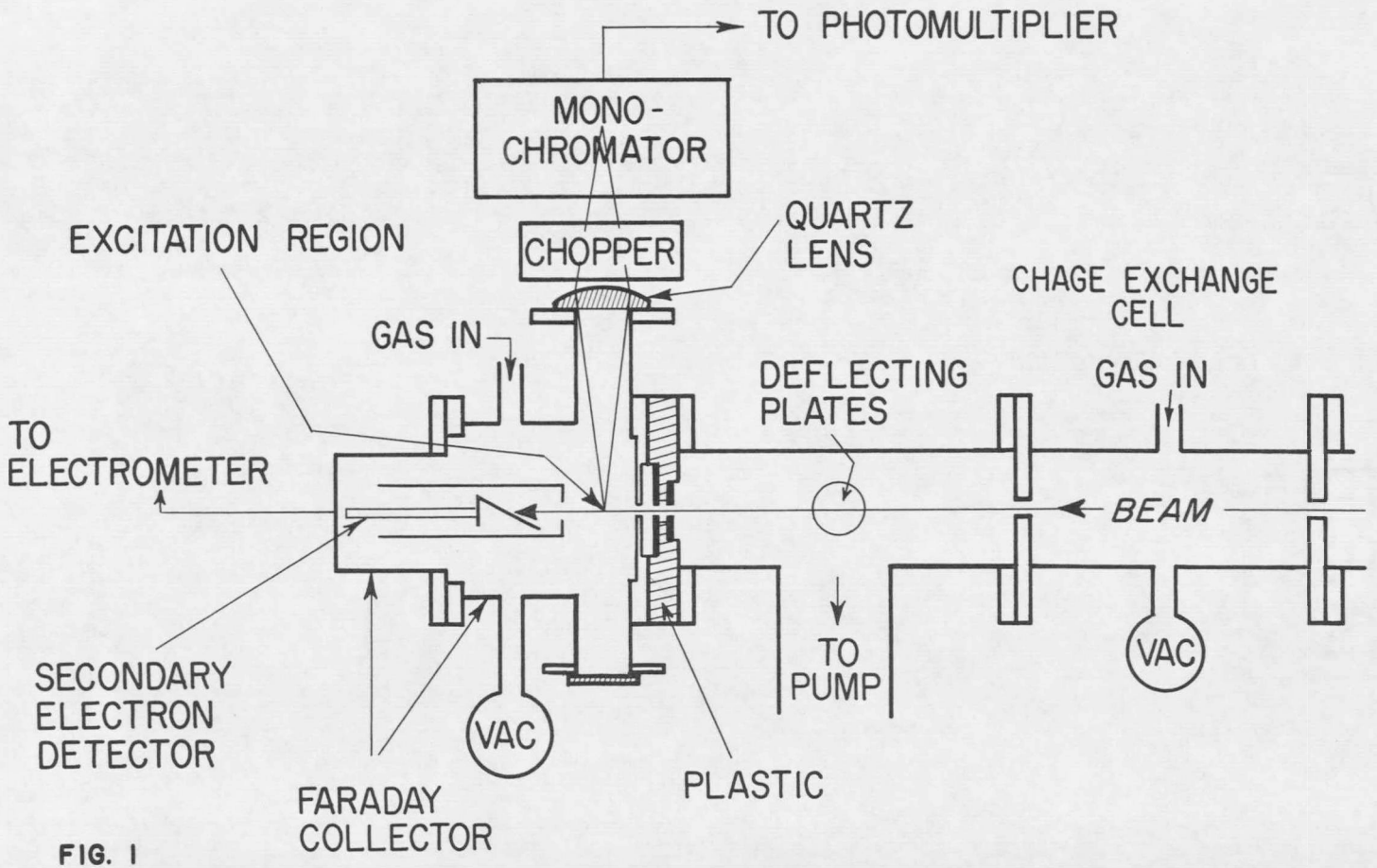
TO PHOTOMULTIPLIER
MONO-
CHROMATOR
EXCITATION REGION
CHOPPER
QUARTZ
LENS
CHAGE EXCHANGE
CELL
GAS IN
DEFLECTING
PLATES
GAS IN
TO
ELECTROMETER
BEAM
SECONDARY
ELECTRON
DETECTOR
VAC
TO
PUMP
VAC
FARADAY
COLLECTOR
PLASTIC

FIG. 1

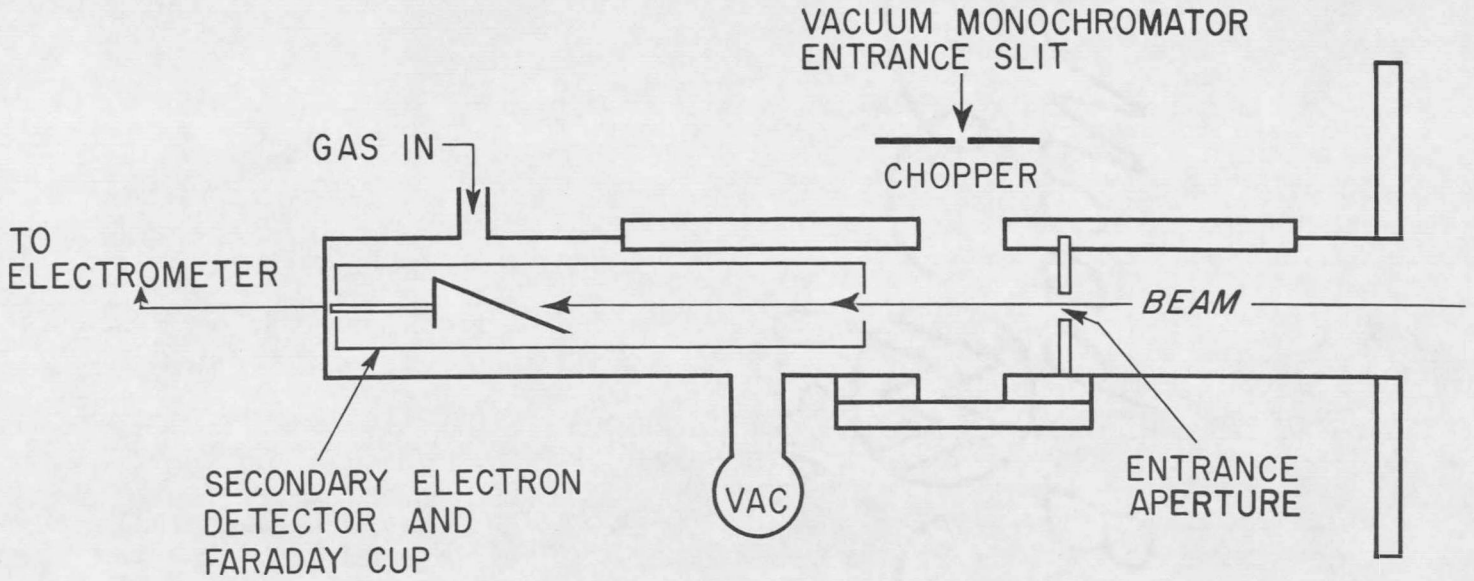

FIG. 2

EXCITATION CHAMBER

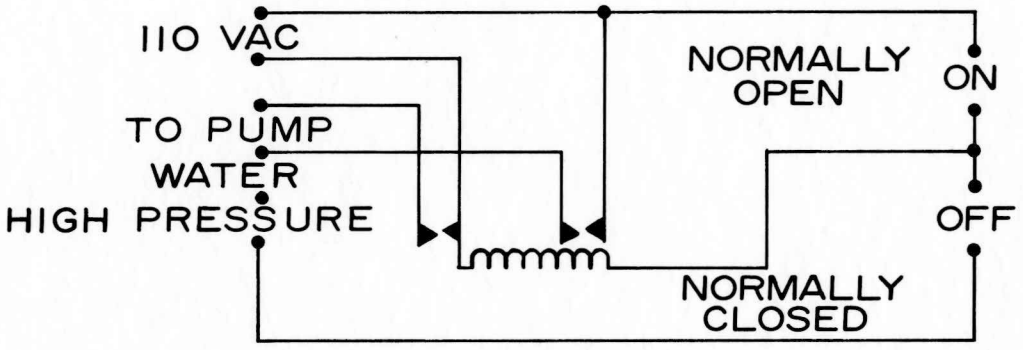
110 VAC
TO PUMP
WATER
HIGH PRESSURE
NORMALLY
OPEN
ON
OFF
NORMALLY
CLOSED

FIG. 3

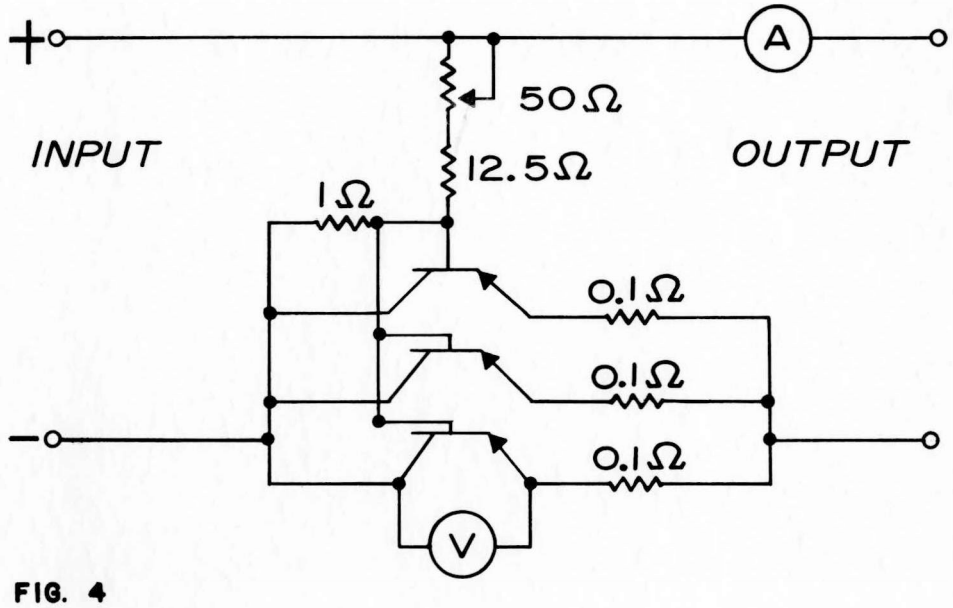
A
50Ω
INPUT
12.5Ω
OUTPUT
1Ω
0.1Ω
0.1Ω
0.1Ω
V

FIG. 4

ANALYZING MAGNET

The protons were separated from the other components inherently present in the beam by the magnetic field of a massive seven inch electro-magnet. A 50 volt and 40 amp partially regulated supply (Kepco, Model PR50-40AM) provided the power for the magnet. The core of the magnet was wound with copper tubing which served both as the electrical conductors as well as the cooling coils. The coils were cast in a rigid polyester resin sold by Fiberlay, Inc. in order to provide physical rigidity and to prevent the shorting of the turns in the coils. Figure 5 shows a graph of the magnetic field as a function of the current in the coils of the magnet.

A fine control which was used in conjunction with the power supply was designed and constructed. The circuit diagram for the fine control is given in figure 4.

CHARGE EXCHANGE CELL AND COLLIMATOR

To produce a beam of hydrogen atoms from a beam of protons a charge exchange cell was designed and constructed. This cell was six inches long and had two adjustable apertures, one at either end of the cell. Except for the two 1/16 inch apertures which served to collimate the beam, the cell was vacuum tight. In order to flow gas into the cell and measure the pressure in the cell, the cell was equipped with two quick connect fittings. With gas flowing into the cell, the proton beam emerged as a mixture of protons and hydrogen atoms. When only a proton beam was desired, the gas inlet valve which permitted gas into the charge cell was closed and the two apertures served simply to collimate the beam.

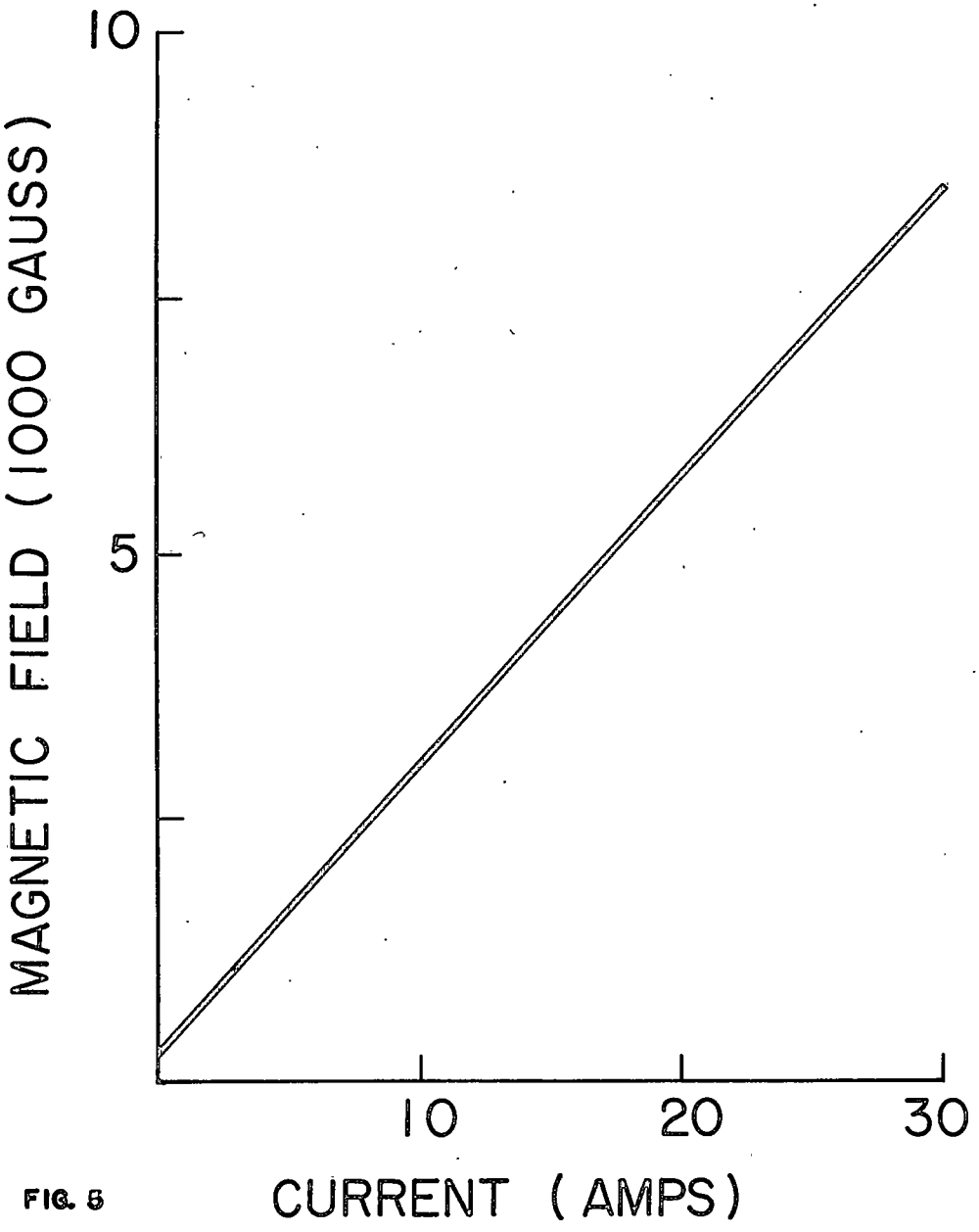

FIG. 5

DIFFERENTIALLY PUMPED CHAMBER

Before the beam reached the entrance to the excitation chamber it passed through a differentially pumped chamber which contained a pair of electrostatic deflecting plates. These plates were used to deflect the protons out of the beam when the atomic hydrogen beam was desired. The chamber was pumped with a four inch liquid air-trapped oil diffusion pump.

EXCITATION CHAMBER FOR THE VISIBLE AND NEAR ULTRAVIOLET WORK

The excitation chamber was a cylinder three inches in diameter and four inches long. There was a series of three apertures at the entrance to the excitation chamber. These apertures can be seen in figure 1. The first aperture through which the beam passed served as the entrance aperture to the excitation region and defined the beam. The diameter of this aperture was 3/32 inches. The second aperture was somewhat larger and served to isolate the entrance aperture from the excitation chamber. The third aperture was in the front face of the excitation chamber and was a little larger than the second aperture. It served to prevent charged ions and secondary electrons produced in the collision of the beam with the gas molecules from leaving the excitation chamber. A plastic disc was used to contain the two metal plates in which the entrance and isolating apertures were drilled and also to electrically isolate them from each other.

Different values of potentials and different polarities were applied to the entrance and isolating apertures in order to determine whether or not electrons were entering the excitation chamber. Electrons produced in the exchange cell or from collisions with surfaces could contrib-

ute to the beam current or the collision processes if they entered the excitation chamber. Investigations led to the conclusion that with the entrance and isolating aperture plates grounded or with a potential on only the entrance aperture plate gave the most consistent results. Applying a potential to the first aperture plate, however, produced no more than a few percent change in the beam current and no measurable change in the optical emission. It was, therefore, concluded that essentially no electrons were entering the excitation chamber through the entrance aperture and contributing to the excitation processes.

The monochromator was orientated so that the entrance slit of the monochromator was perpendicular to the direction of the proton beam. The image of the beam obtained with the quartz lens mounted on the excitation chamber was then focused on the monochromator entrance slit.

The chamber had provisions for gas inlet and for the measurement of the pressure of the gas in the chamber.

EXCITATION CHAMBER FOR THE VACUUM ULTRAVIOLET WORK

The excitation chamber for the vacuum ultraviolet spectral and emission studies had a rectangular cross section with the dimensions one inch by two inches. The important features of this chamber are shown in figure 2.

The vacuum monochromator in this case was attached directly to the chamber so that the slits of the monochromator could be placed as close as possible to the incident particle beam to gain maximum light intensities. The chamber was constructed so that a window could be used to isolate the chamber from the monochromator.

Only one grounded aperture was used at the entrance of this chamber. This chamber also had provisions for gas inlet and for the measurement of the pressure of the gas in the chamber.

BEAM CURRENT MEASUREMENTS

The collection of a fast proton beam could be accomplished quite simply by using a Faraday cage and a secondary electron suppressor screen as long as the pressure in the region of the collector was held below a micron. When the pressure was higher, plasma conditions were such that applying potentials between two points to suppress secondary electrons could set up currents which significantly altered proton beam current measurements. After some study of the problem, the author concluded that a deep, small diameter Faraday cage which essentially trapped the protons and secondary electrons produced in the collision of the protons with the cage was best for measuring the proton beam currents.

Two basic techniques were investigated for measuring the intensity of the hydrogen atom beam. One technique was to measure the power transmitted to a metal target by recording the temperature change with a thermocouple or thermistor. The other technique was to measure the secondary electron current emitted in the collision of the beam with a metal target. The secondary emission method appeared to be the most practical and was selected for measuring the hydrogen atom beam intensity.

In order to be able to measure the proton current and the hydrogen atom current with the same detector, the necessary features of the Faraday cage and the secondary emission techniques were combined into a single

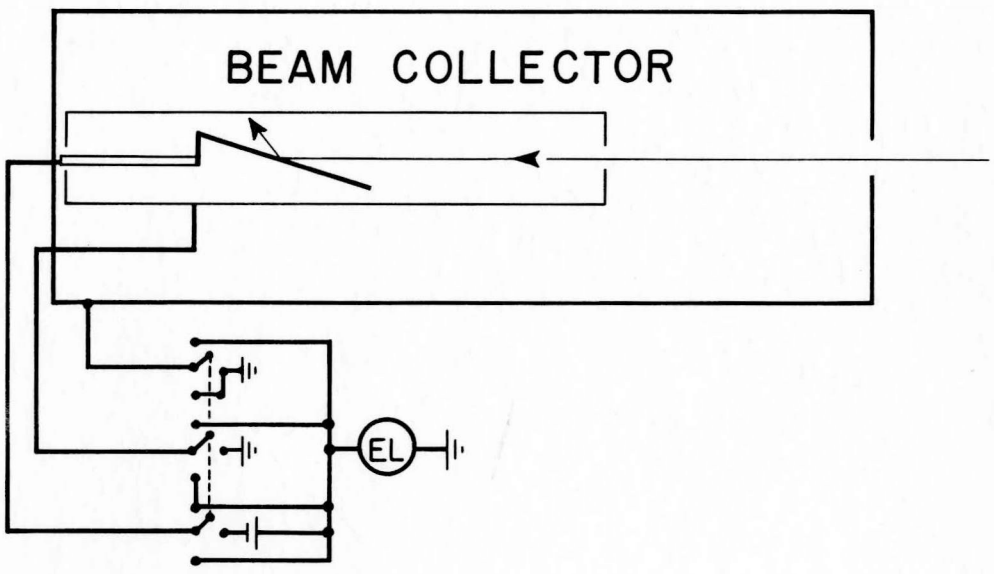

FIG. 6

particle detector. The detector consisted of a molybdenum target called the emitter which is enclosed in a copper tube. This detector is similar to the one designed by Montague[27].

When measuring proton current, the emitter and copper enclosure were electrically connected and the detector was a Faraday cage, figure 6. When a negative potential of from 45-90 volts was applied to the target and the copper tube grounded, the secondary electrons emitted from the target were forced to and collected on the copper tube. Under this operating condition the system was a secondary emission detector. The fact that the molybdenum target made a small angle with the direction of the beam prevented secondary electrons from escaping through the ¼ inch entrance aperture of the detector.

In order to calibrate the detector for measuring the hydrogen atom current, i', the number of electrons emitted per proton colliding with the target, N, was required as a function of proton energy. To obtain N, the detector was first used as a Faraday cage to measure the current, i, due to protons entering the collector. Second, the detector was used to measure the secondary electron current, i_s, emitted from the target under proton bombardment. Finally, N is given by the ratio i_s/i.

Stier, Barnet and Evans[28] have measured the ratio of N'/N as a function of incident particle energy, where N' is the number of electrons emitted per hydrogen atom colliding with the target. From these ratios and measured values of N, N' could, therefore, be calculated as a function of energy. The hydrogen atom current was obtained by measuring i'_s for the hydrogen atom beam and using the calculated values of

N'; $N' = i'_s/i'$.

The excitation chamber used in the visible spectral region was electrically isolated from the other sections of the system. The entire chamber, therefore, served as a Faraday cage and was used to measure the proton current.

The proton currents ranged from 1 microamp at 15 kev to 12 microamps at 100 kev. Beam currents were measured with a General Radio Type 1230 A electrometer.

PRESSURE GAUGES

In the first stages of this experimental work the target gas pressures were measured with either a McLeod gauge or a Westinghouse high pressure ionization gauge calibrated against the McLeod gauge.

Due to the pumping action of a liquid air trapped McLeod gauge [29], a search for a more reliable pressure meter was undertaken. The comparison of pressure gauges conducted by Utterback and Griffith [30] was especially helpful. Their work showed that the capacitance manometer was the most reliable method for measuring pressures in the micron and fraction-of-micron pressure region.

In the later stages of this work, therefore, the MKS Baratron pressure meter (Type 77 with Type 77H-1 head) was obtained and used as the standard pressure measuring device.

LIGHT DETECTION

Two different monochromators and two different photon detectors were used for analyzing and measuring the intensity of the optical emissions.

In the visible and near ultraviolet spectral region a Bausch and Lomb ¼ meter grating monochromator with a dispersion of 33 Å/mm (Cat. Nos. 33-86-40, S/N FD992, f/4.4) was used in conjunction with an EMI 9558 QB photomultiplier. As mentioned previously, the monochromator was orientated in such a manner that the entrance slit was perpendicular to the direction traveled by the proton beam. This alignment was used so that changes in the apparent size of the beam would not cause changes in the amount of light reaching the photomultiplier.

In the vacuum ultraviolet spectral region the McPhearson Model 218, f/5.3, 0.3 meter vacuum monochromator with Czerny-Turner optics was used in conjunction with either a Model 306 Bendix magnetic electron multiplier or an EMI 9558 QB photomultiplier. The grating had a dispersion of 53 Å/m and was ruled at 600 lines /mm. The electron multiplier was useful below 1250 Å where the photon efficiency of the metal cathode was sufficient. Above 1250 Å the photomultiplier with a thin film of sodium salicylate served as the photon detector. The McPhearson monochromator has three reflecting surfaces which are coated with MgF_2. The spectral region below 1150 Å could, therefore, not be studied.

The width of the entrance slit of the monochromator was always adjusted to be the same as the width of the exit slit. The actual slit widths used in the experimental work varied with the monochromator used and the transition that was studied. Except for the case

that will be discussed in the next chapter, the slits were set so that the emissions from transitions near the one being studied were negligible. The relation between the slit widths and the dispersion of the monochromator is discussed in appendix A.

The signal to noise ratio of the photomultiplier output was too small to permit DC measurements of the majority of the transitions. A phase sensitive detection system was, therefore, used for all of the measurements. The optical signal from the excitation chamber was "chopped" before the light entered the monochromator slits. An 100c/sec mechanical "chopper" was used with the Bausch and Lomb monochromator and a 400c/sec American Time Products tuning fork "chopper" was used with the vacuum monochromator. The resulting AC output of the photomultiplier was then fed into a Princeton Applied Research lock-in Amplifier, Model JB-4. Finally the optical signal was recorded with a Honeywell strip chart recorder. In the case of very weak signals a Princeton Applied Research Low-Noise Amplifier, Model CR-4, was inserted between the photomultiplier and the lock-in amplifier.

CHAPTER IV. PROCEDURE

Before considering the results, some elements of the procedure will be presented. In particular there will be a discussion of the observed spectra, the pressure and current linearity measurements, and the methods used in measuring the relative cross section.

SPECTRAL SCANS

Before the cross section measurements were begun the spectrum was scanned to observe which transitions produce sufficient emission to permit a detailed study. The scans also assisted in measuring the approximate ratios of intensities of the transitions. Scans were made of the emission produced from protons incident on nitrogen and hydrogen molecules in the spectral range from 1200 Å to 6000 Å. Since high pressures were required for this work there is some electron and hydrogen atom excitation present. For example, in the spectral scans of the N_2^+ First Negative system and the N_2 Second Positive system, the major contributions to the Second Positive bands were from hydrogen atoms produced by electron capture in the target gas and from secondary electrons produced in the collision of the beam with the target molecules [31].

MOLECULAR SPECTRA

When studying the emission due to atomic transitions, one observes a line spectrum. The spectra from the excitation of simple atoms can be quite easily analyzed and understood.

The spectra of molecules are somewhat more difficult to analyze, however. This is due to the fact that the molecule has, in addition to the quantized electronic states, quantized vibrational and rota-

tional levels. For the diatomic molecule the two nuclei move relative to each other in a vibratory motion producing a definite splitting of the electronic states. The rotational motion of the molecule represents smaller amounts of energy and generally produces a splitting of the vibrational levels. When one observes electronic transitions, therefore, a single electronic transition is made up of numerous lines from the rotational levels of the upper electronic state to the rotational levels of the lower electronic state. These lines usually are grouped into bands each of which represents the transitions from the rotational levels connected with a single vibrational level of the upper state to the rotational levels connected with a single vibrational level of the lower state. The series of bands make up an electronic system. In this work the emission due to vibrational transitions will be measured. The term (v', v'') represents the transitions from the v' vibrational level of the upper state to the v'' level of the lower state.

Figure 7 shows some of the vibrational levels of the electronic states of the nitrogen molecule which are to be considered in this work. Figure 8 presents a few of the potential energy curves of the hydrogen molecule and figure 9 presents some of the vibrational levels of the X, B, and C states.

CURRENT AND PRESSURE DEPENDENCE

In the process of taking data both current and pressure linearity were checked. The linearity of the emitted light intensity per

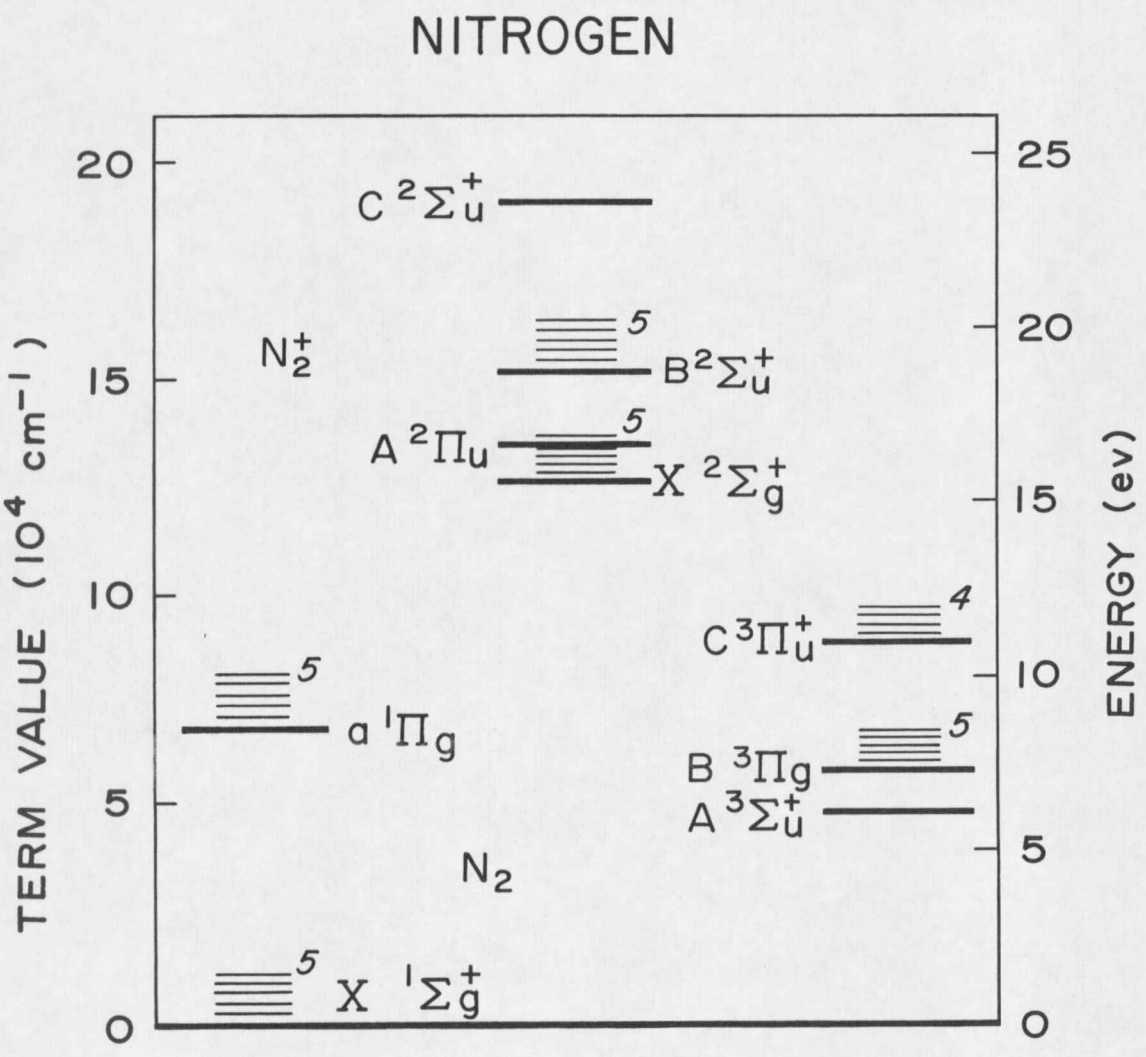
NITROGEN
TERM VALUE (10^4 cm^{-1})
ENERGY (ev)
20
15
10
5
0
25
20
15
10
5
0
$C\,^2\Sigma_u^+$
N_2^+
5
$B\,^2\Sigma_u^+$
$A\,^2\Pi_u$
5
$X\,^2\Sigma_g^+$
$C\,^3\Pi_u^+$
4
5
$a\,^1\Pi_g$
$B\,^3\Pi_g$
5
$A\,^3\Sigma_u^+$
N_2
5
$X\,^1\Sigma_g^+$

FIG. 7

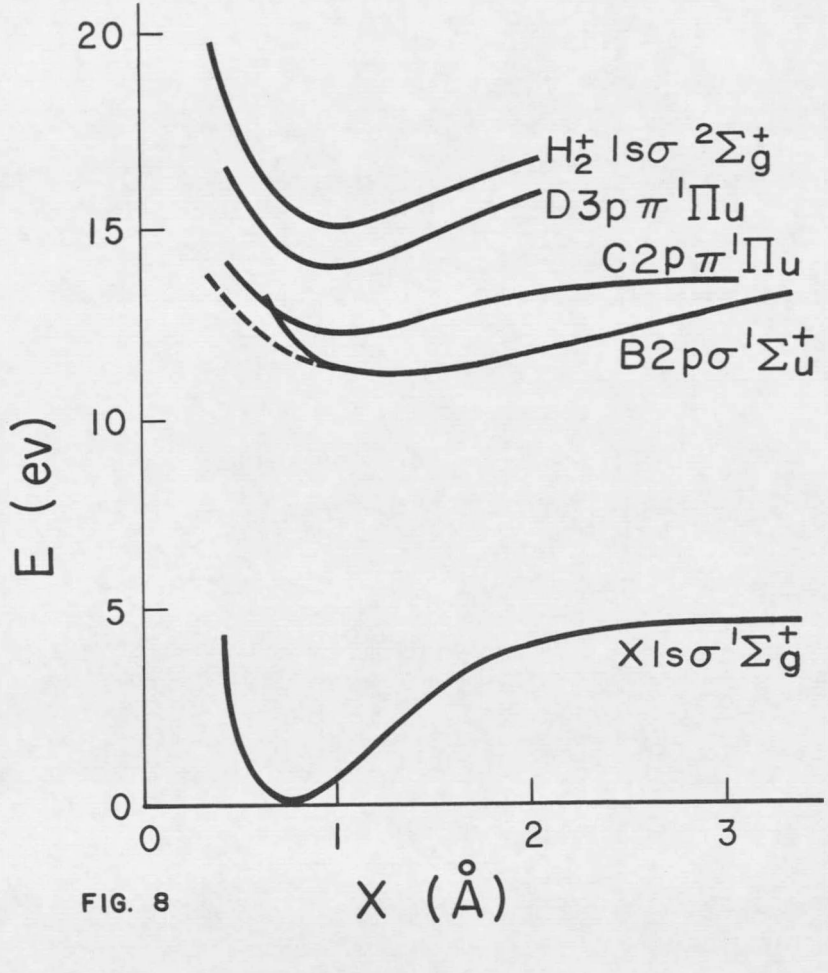
HYDROGEN
20
15
10
5
0
E (ev)
$H_2^+ 1s\sigma\ ^2\Sigma_g^+$
$D3p\pi\ ^1\Pi_u$
$C2p\pi\ ^1\Pi_u$
$B2p\sigma\ ^1\Sigma_u^+$
$X1s\sigma\ ^1\Sigma_g^+$
0
1
2
3
X (Å)

FIG. 8

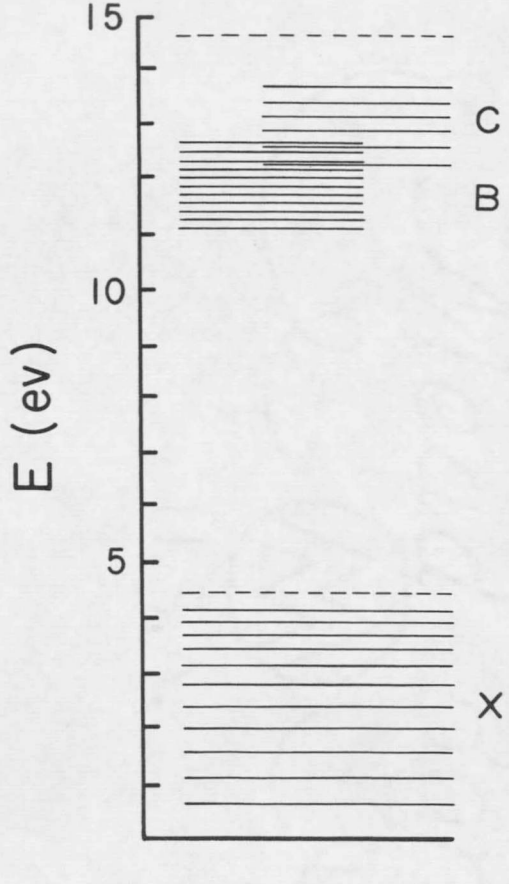
15
10
5
E (ev)
C
B
X

FIG. 9

incident particle, I/i, as a function of the target gas pressure, p, is important since it is used as the criterion for determining the source of optical emissions.

In the following discussion primary particles are those particles which are in the beam before encountering the target gas and secondary particles are those particles which are formed in the collision between the primary particles and the target gas. If the emitted light results from the collisions between the primary incident particles and the target gas, the emission cross section, Q, will be proportional to I/ip. Q is also proportional to I/in, where n is the particle density of the target gas. The secondary particle current, i", is proportional to ni, where i is the primary incident particle current. For the secondary particles, therefore, Q is proportional to I/i"n, where I is, now, the light emitted by the collisions of the secondary particles with the target gas. Substituting for i", Q is proportional to I/in^2. Consequently there is a linear dependence of I/i on pressure for the collisions involving the primary particles and a quadratic dependence of I/i on pressure for collisions involving the secondary particles.

For the emissions from the N_2^+ First Negative vibrational transitions, measurements of I/i as a function p were made at a number of different energies and they all revealed a linear relationship indicating that the emissions were produced by the primary particles. The two sets of data for the (0,0) vibrational transitions taken at 35 kev are shown in figures 10 and 11. In the proton impact work a correction

was required for hydrogen atom production. A correction was also required for the proton production in the hydrogen atom data. These corrections are shown in figures 10 and 11. Appendix B has a discussion of these corrections.

For the $N_2(0,0)$ Second Positive vibrational band, measurements of I/i as a function of pressure were made at a number of different incident particle energies. For hydrogen atom impact a linear relationship of I/i as a function of pressure existed but only for pressure under 5 microns. The author attributed the non linear relationship to the emission caused by secondary electrons produced in the collisions of the incident particles with the target gas. In the case of proton excitation, however, the relationship between I/i and pressure is more complex. Both secondary electrons and also hydrogen atoms in the beam produced by electron capture contribute to the emission. Figure 12 presents a graph of both relative cross section as a function of pressure and I/i as a function of pressure at a proton energy of 43 kev. From these data, the author concluded that the emission due to the primary particles was completely masked by emissions due to secondary particles at pressures above 2 microns. To obtain data for the excitation of the $N_2(0,0)$ band by fast protons, it was, therefore, necessary to work at pressures around one micron.

I/i as a function of the target gas pressure was measured for each of the other transitions studied. Each of these revealed a linear relationahip between I/i and p. The curve in figure 13 shows I/i as a function of pressure for the Lyman bands of hydrogen.

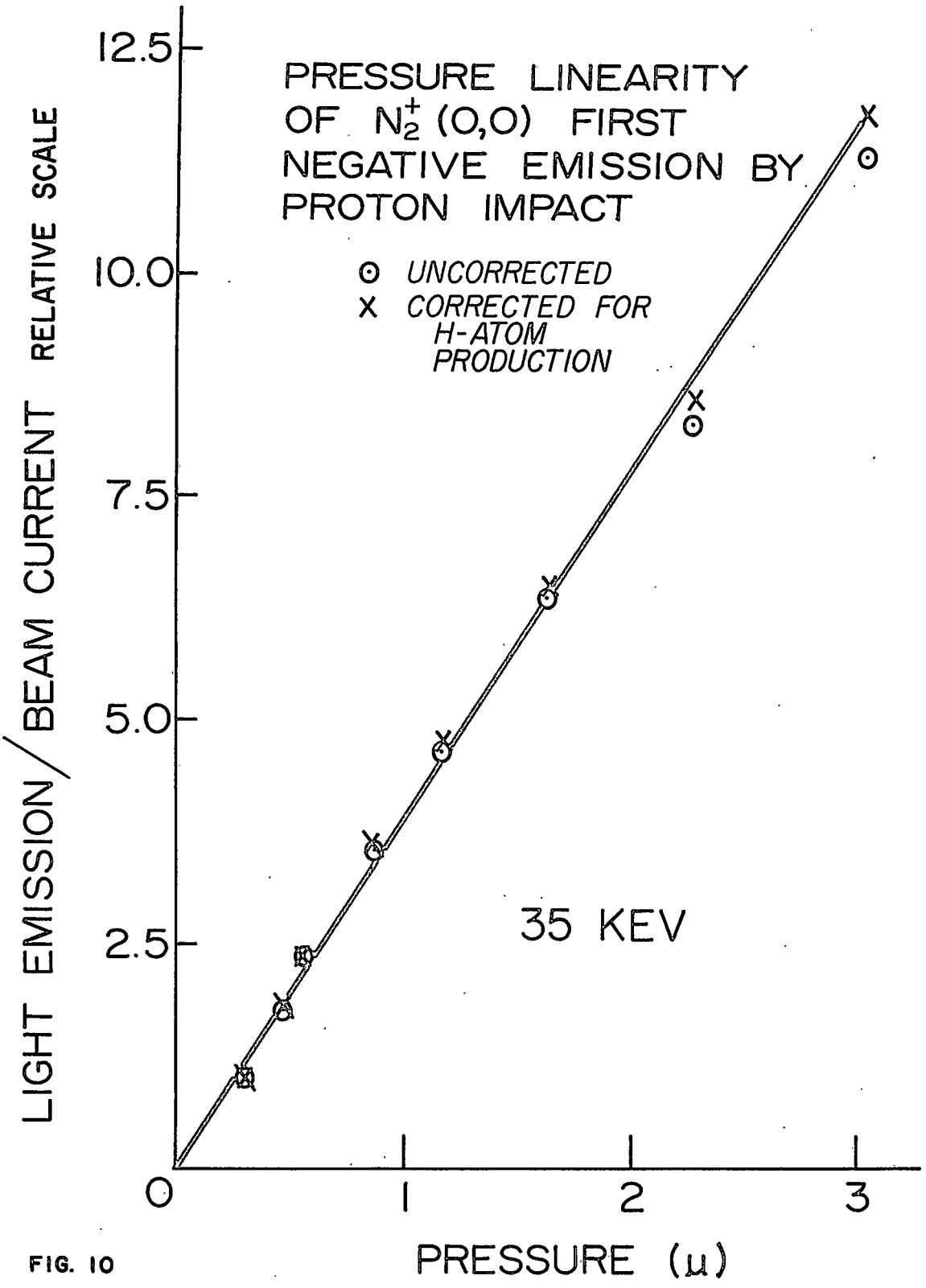
PRESSURE LINEARITY
OF N_2^+ (0,0) FIRST
NEGATIVE EMISSION BY
PROTON IMPACT
⊙ UNCORRECTED
X CORRECTED FOR
H-ATOM
PRODUCTION
35 KEV
LIGHT EMISSION / BEAM CURRENT RELATIVE SCALE
12.5
10.0
7.5
5.0
2.5
0
1
2
3
PRESSURE (μ)

FIG. 10

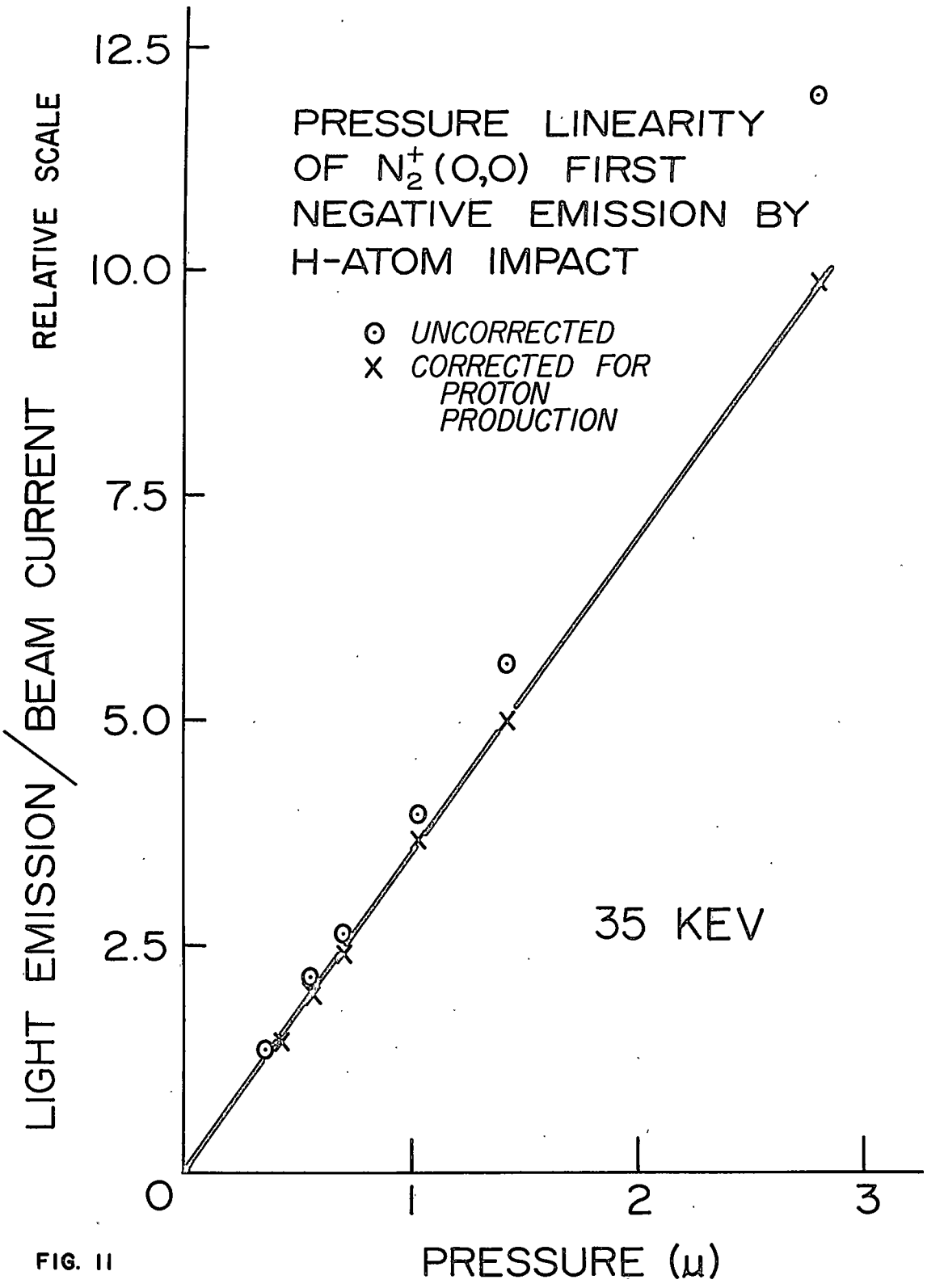
PRESSURE LINEARITY
OF N_2^+(0,0) FIRST
NEGATIVE EMISSION BY
H-ATOM IMPACT
⊙ UNCORRECTED
X CORRECTED FOR
PROTON
PRODUCTION
35 KEV
LIGHT EMISSION / BEAM CURRENT RELATIVE SCALE
12.5
10.0
7.5
5.0
2.5
0
1
2
3
PRESSURE (μ)

FIG. 11

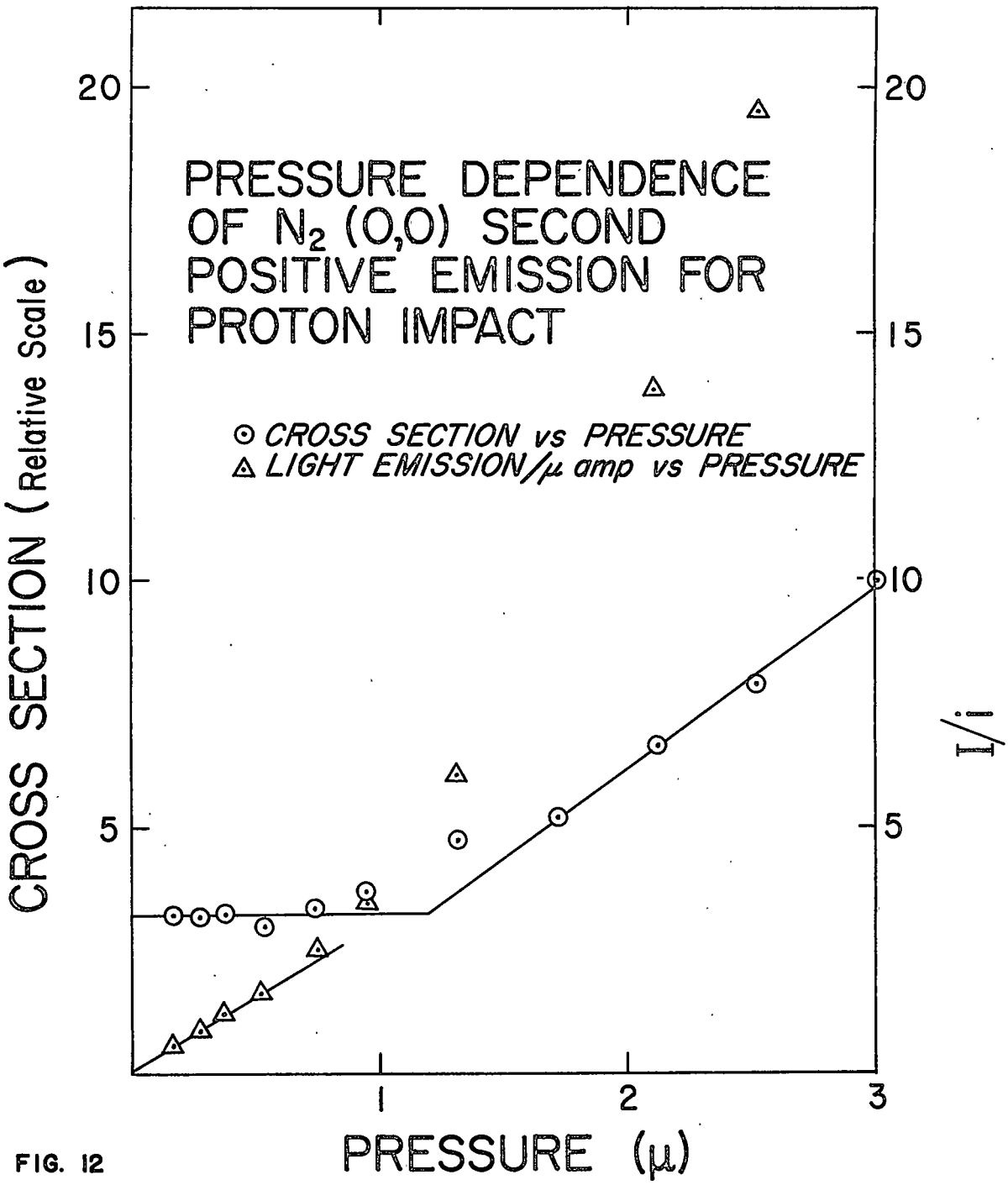
PRESSURE DEPENDENCE OF N_2 (0,0) SECOND POSITIVE EMISSION FOR PROTON IMPACT
⊙ CROSS SECTION vs PRESSURE
△ LIGHT EMISSION/μ amp vs PRESSURE
CROSS SECTION (Relative Scale)
I/i
PRESSURE (μ)
20
15
10
5
1
2
3

FIG. 12

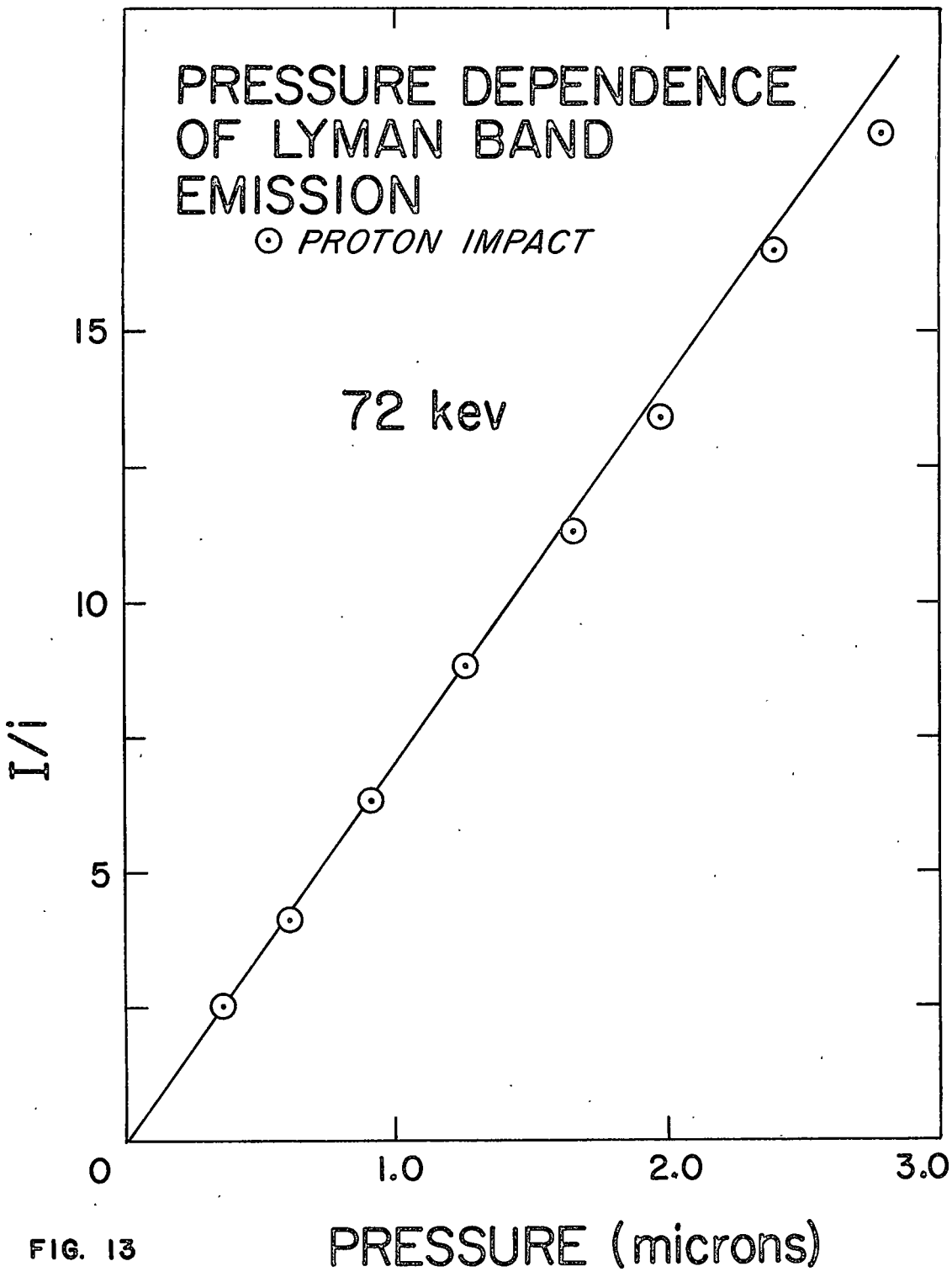
PRESSURE DEPENDENCE
OF LYMAN BAND
EMISSION
⊙ PROTON IMPACT
72 kev
I/i
15
10
5
0
1.0
2.0
3.0
PRESSURE (microns)

FIG. 13

RELATIVE CROSS SECTION MEASUREMENTS

The mass analyzed projectile beam entering the excitation chamber is always a mixture of a hydrogen atom current, i', and a proton current, i. The ratio of i'/i, is a function of both the gas pressure in the exchange cell, p', and the energy E, of the initial proton beam. As p' increases the ratio of i'/i also increases. According to the charge exchange cross sections, as E increases the ratio of i'/i decreases rapidly [2].

The experimental problem is to distinguish the emission produced in the collision of the hydrogen atom with the target gas from the emission produced in the collision of the proton with the target gas. In order to separate these emissions I + I', i + i', and i are measured for p' at background pressure and at a selected value of E, where I and I' are respectively the measured light intensity due to the collision of the protons with the target gas and measured light intensity due to the collision of the hydrogen atoms with the target gas. The protons are then deflected out of the beam leaving only the hydrogen atoms to produce emission. At this point I' and i' are measured. The preceeding procedure is repeated for the same value of E and for one or more values of p'. For each of the measurements the target gas pressure is recorded also. Since I and I' are related to the total emission produced in proton and hydrogen atom collisions, respectively, and p is proportional to the target gas density, the quantity I'/i'p is the relative emission cross section for the hydrogen atom collisions and I/ip is the relative emission cross section for the proton

collisions. Repeating the measurements and calculations for a number of values of E between 10 kev and 130 kev gives relative emission cross sections as a function of energy.

Values of p from 0.5 microns to 3.0 microns were used in these emission cross section measurements. In measuring the relative cross sections for a single line or band, p was held to changes of less than 10% for all values of E.

As previously mentioned, the observation of the light emitted in the collisions of the projectile beam with the target gas is centered at a distance of 3 cm from the entrance aperture. This experimental condition requires some correction for the change in the composition of the beam in traversing the 3 cm in the target gas. This correction is discussed in appendix B.

The emitted light intensity was not absolutely calibrated by the author. Absolute values for the cross sections were obtained by normalizing some of these measured relative cross sections to absolute measurements made by other researchers. These normalization procedures will be discussed with the results.

CHAPTER V. RESULTS AND DISCUSSION

In presenting and discussing the data, the results of the spectral scans and the cross section measurements will be considered.

SPECTRAL SCANS

From the spectral scans for protons incident on nitrogen molecules, figure 14, one observes that above 2000 Å the vibrational bands of the N_2^+ First Negative system ($B\,^2\Sigma_u^+ \text{---} X\,^2\Sigma_g^+$) are dominant. Some of the bands of the N_2 Second Positive system ($C\,^3\Pi_u \text{---} B\,^3\Pi_g$) and two ionic nitrogen lines appeared also. In addition, the Balmer lines of hydrogen produced in the electron capture process were present. In the spectral region below 2000 Å, figure 15, atomic nitrogen lines and Lyman alpha were the most prominent emissions of the spectrum. The forbidden bands of the Lyman-Birge-Hopfield system ($a\,^1\Pi_g \text{---} X\,^1\Pi_g^+$) appeared, but their intensity was significantly weaker than the intensity of the atomic lines. Of interest, also, was the appearance of the unidentified band at 1589 Å reported by Carroll [35].

For hydrogen as the target gas the spectrum was also divided into two sections. The spectral scan of hydrogen above 1800 Å is not shown. With the exception of the Balmer lines the emissions which appeared were quite weak. Below 1800 Å the Lyman bands ($B\ 2p\sigma\,^1\Sigma_u^+ \text{---} X\ 1s\sigma\,^1\Sigma_g^+$) appeared and had a fair intensity as can be seen in figure 16. In this spectral region the Lyman alpha line was dominant.

The (0,0), (0,1), (0,2), (1,3) bands at 3914 Å, 4278 Å, 4709 Å, 4652 Å, respectively, of the N_2^+ First Negative system were selected for cross section measurements. The emission due to the (1,0) band could not be measured for hydrogen atom impact because of the nearness

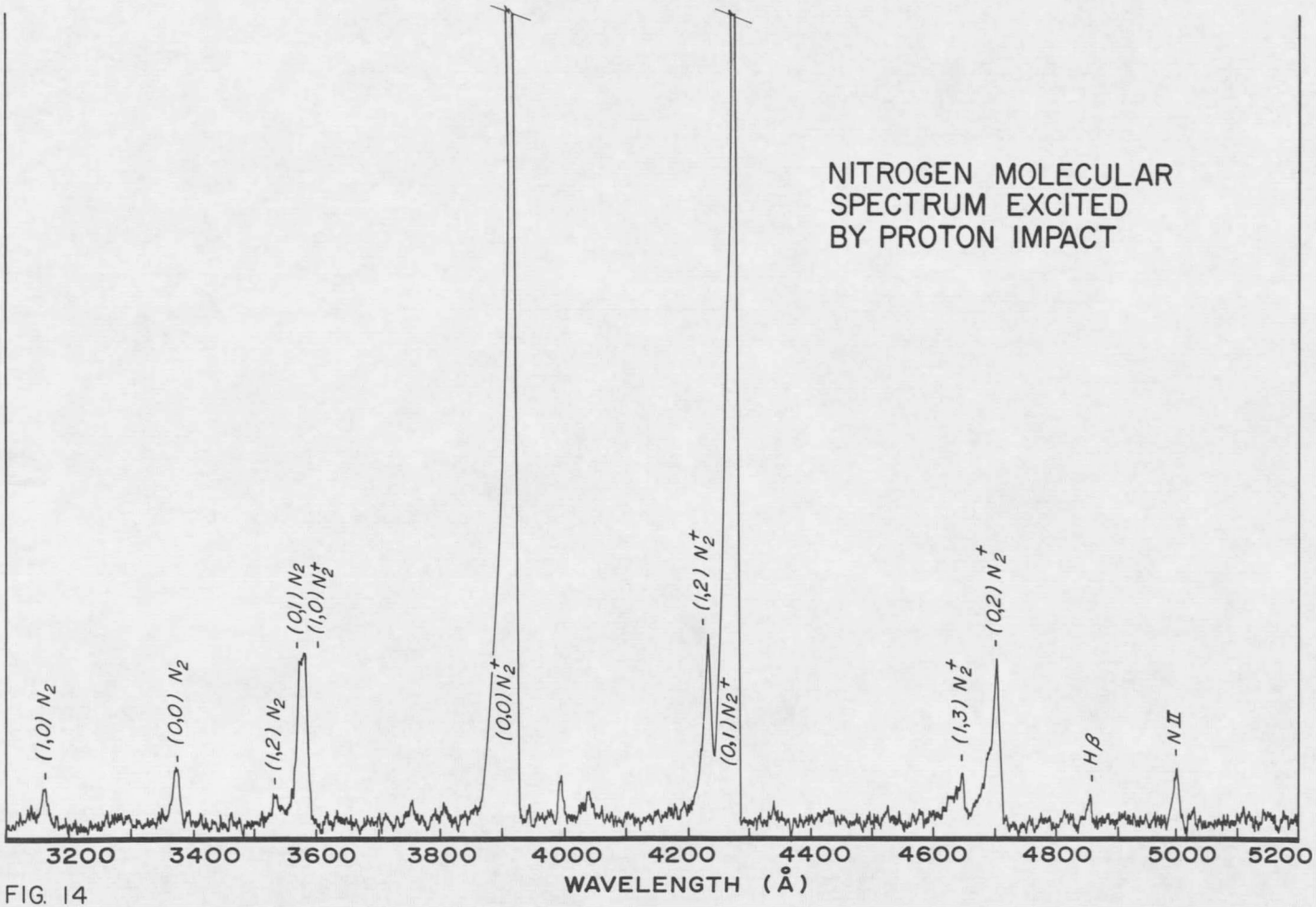
NITROGEN MOLECULAR
SPECTRUM EXCITED
BY PROTON IMPACT
- (1,0) N_2
- (0,0) N_2
- (1,2) N_2
- (0,1) N_2
- (1,0) N_2^+
(0,0) N_2^+
- (1,2) N_2^+
(0,1) N_2^+
- (1,3) N_2^+
- (0,2) N_2^+
- Hβ
- N II
3200
3400
3600
3800
4000
4200
4400
4600
4800
5000
5200
WAVELENGTH (Å)

FIG. 14

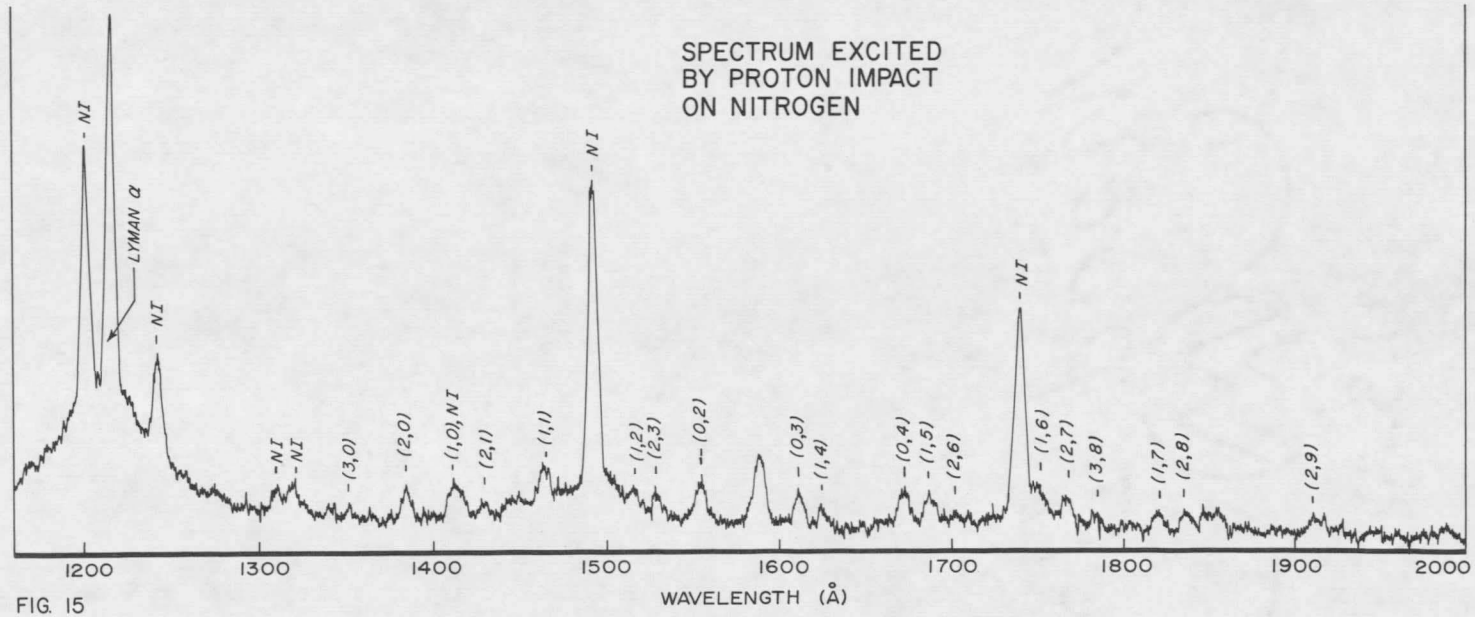
SPECTRUM EXCITED
BY PROTON IMPACT
ON NITROGEN
- NI
LYMAN α
- NI
- NI
- NI
- (3,0)
- (2,0)
- (1,0), NI
- (2,1)
- (1,1)
- NI
- (1,2)
- (2,3)
- (0,2)
- (0,3)
- (1,4)
- (0,4)
- (1,5)
- (2,6)
- NI
- (1,6)
- (2,7)
- (3,8)
- (1,7)
- (2,8)
- (2,9)
1200
1300
1400
1500
1600
1700
1800
1900
2000
WAVELENGTH (Å)

FIG. 15

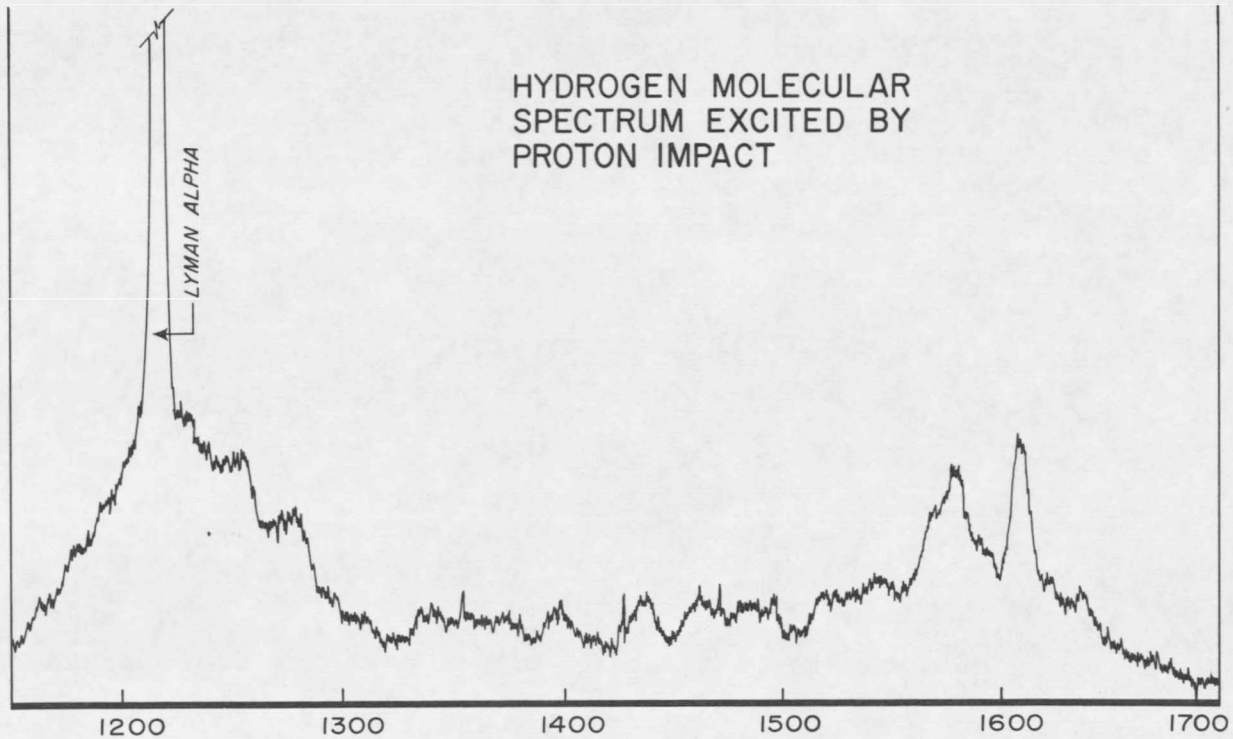
HYDROGEN MOLECULAR
SPECTRUM EXCITED BY
PROTON IMPACT
LYMAN ALPHA
1200
1300
1400
1500
1600
1700
WAVELENGTH (Å)

FIG. 16

of the (0,1) band of the Second Positive system. The (0,0) band at 3371 $\mathring{A}$ appeared to be the only one feasible of measurement in the Second Positive system. In atomic nitrogen the $3s\,^4P---2p\,^4S^o$, $3s\,^2P---2p\,^2P^o$, and $3s\,^2P---2p\,^2D^o$ transitions at 1200 $\mathring{A}$, 1743 $\mathring{A}$, and 1493 $\mathring{A}$, respectively, had sufficient intensities for cross section measurements. The $3d\,^3F^o---3p\,^3D$ transition of the nitrogen ion at 5005 $\mathring{A}$ was also selected.

In hydrogen the Lyman bands, centered at 1606 $\mathring{A}$, were chosen for further investigation.

For both hydrogen and nitrogen target gases the Lyman alpha line at 1216 $\mathring{A}$ had sufficient intensity to permit cross section measurements.

EMISSION CROSS SECTIONS

The data will be classified according to the target gas and the band system or atomic lines which were observed.

Nitrogen Target

N_2^+ First Negative System: Relative emission cross sections as a function of the incident particle energy from 10 kev to 130 kev were measured for the four bands previously mentioned. These measurements were made for both proton and hydrogen atom impact.

After all corrections were made, the (0,0) emission cross sections due to proton impact were normalized to the absolute measurements of Philpot and Hughes [5]. Since the relative measurements of this work had the same energy dependence over the energy interval of 40 to 70 kev as Philpot and Hughes' measurements, the normalization was made in this energy region. The hydrogen atom data was then normalized to the proton

work of this paper. Emission cross sections for the other bands were also normalized to the (0,0) proton impact cross sections. Corrections were made only for the variation in the spectral response of the monochromator. The final results are presented in figures 17-20.

From these curves of cross section as a function of energy, it is observed that the curves for transitions originating from the v'=0 level have the same shape. This characteristic holds for both the proton impact data and the hydrogen atom impact data. Since these transitions all originate from the same upper state and the transition probabilities are independent of the means of exciting the particular level, the shapes are in fact expected to be the same.

The (1,3) band is the only one which originates from a level different from the v'=0 for which emission cross sections by hydrogen atom impact could be measured. These data reveal that the ratio of Q_o/Q_+ appears to be somewhat greater for exciting the v'=1 level than for exciting the v'=0 level, where Q_o and Q_+ are, respectively, the emission cross sections for hydrogen impact and for proton impact.

The effectiveness of the hydrogen atom in exciting transitions in the First Negative system reveals little energy dependence over the energy region of these measurements. It does reveal, however, that the hydrogen atom excitation of the v'=0 level is a significant fraction of the proton excitation, especially at the higher energies. The ratio Q_o/Q_+ is one-half at 40 kev and 2/3 at 90 kev.

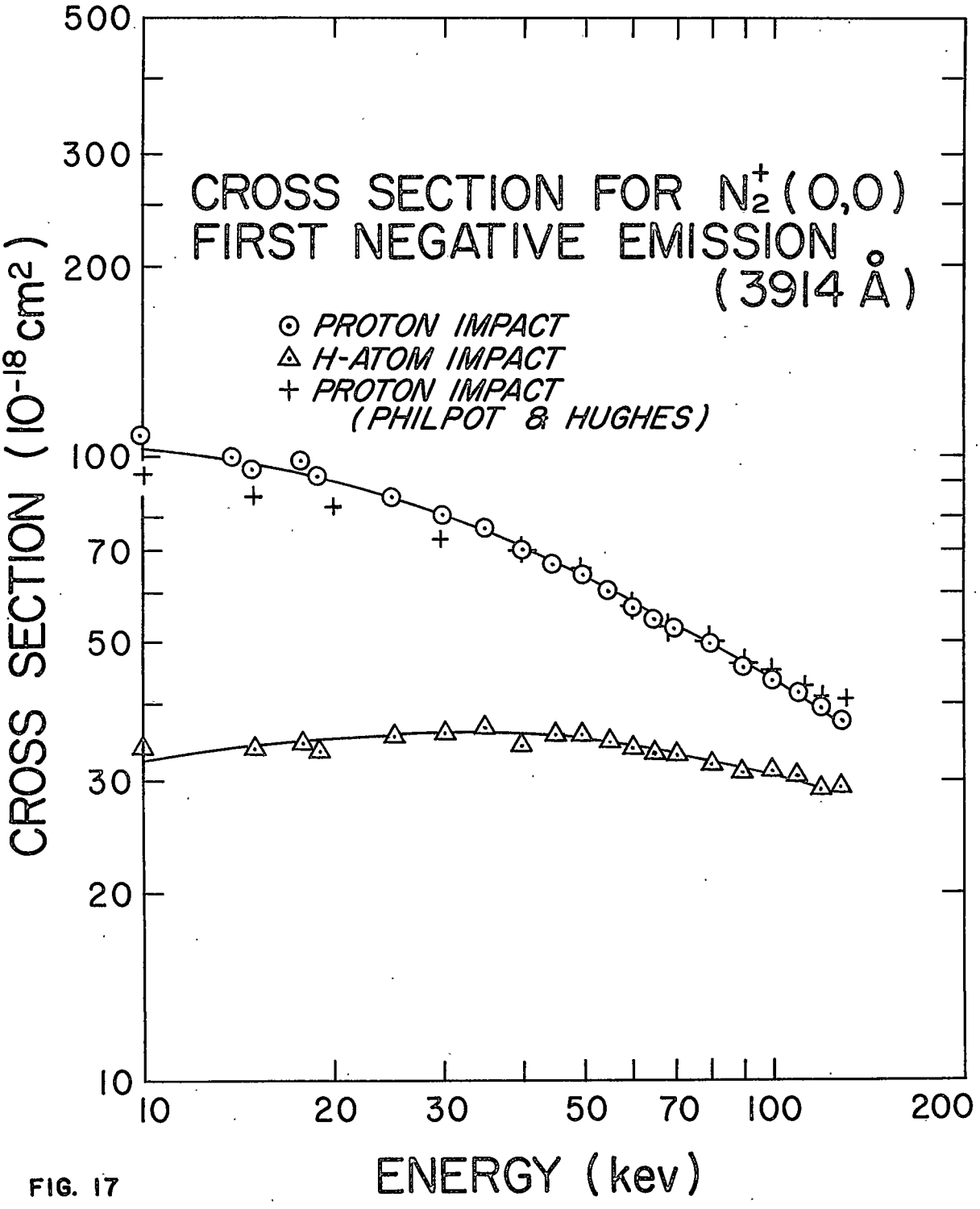
CROSS SECTION FOR N_2^+ (0,0)
FIRST NEGATIVE EMISSION
(3914 Å)
⊙ PROTON IMPACT
△ H-ATOM IMPACT
+ PROTON IMPACT
(PHILPOT & HUGHES)
CROSS SECTION (10^{-18} cm^2)
ENERGY (kev)
500
300
200
100
70
50
30
20
10
10
20
30
50
70
100
200

FIG. 17

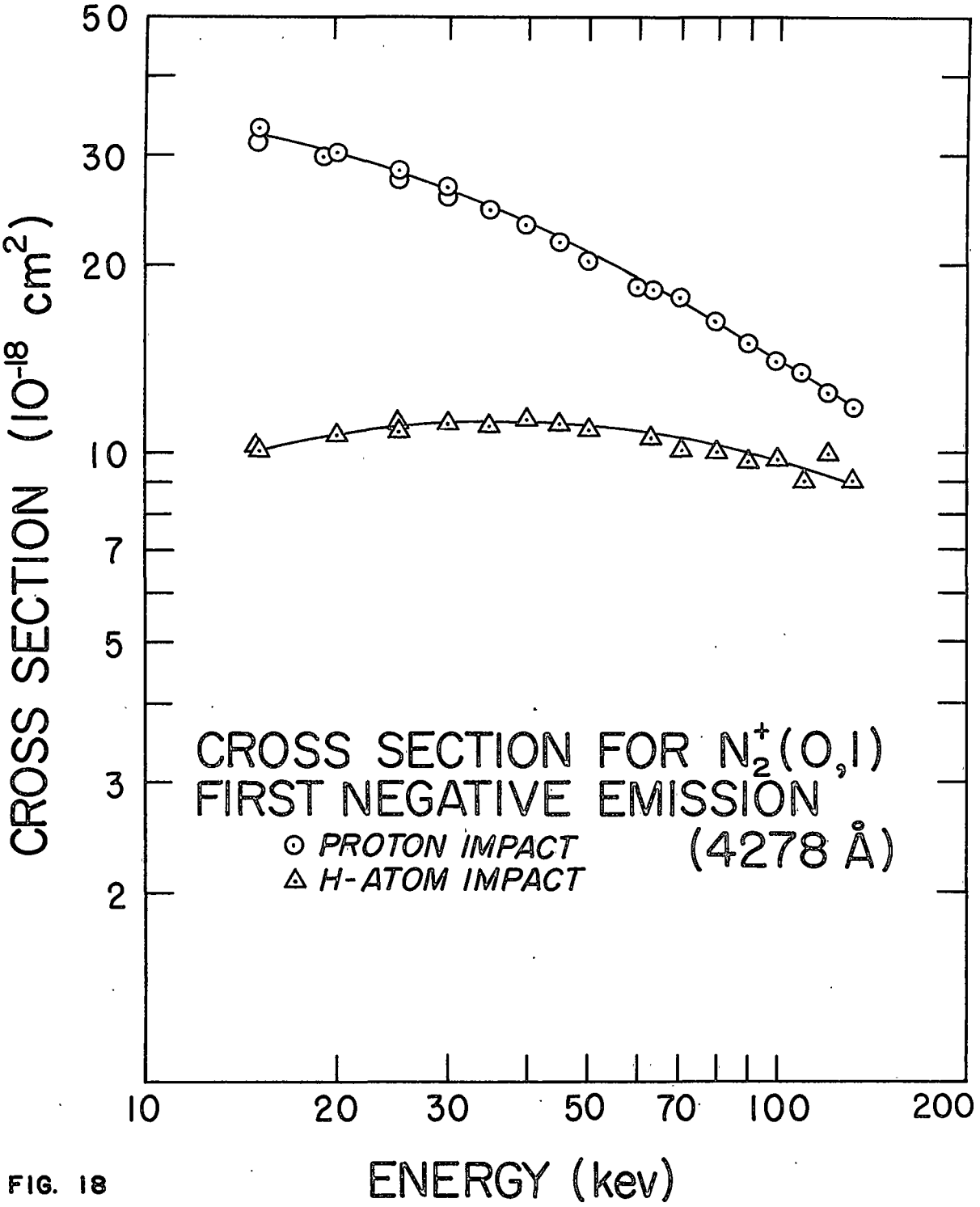
50
30
20
10
7
5
3
2
CROSS SECTION (10^{-18} cm^2)
CROSS SECTION FOR $N_2^+(0,1)$
FIRST NEGATIVE EMISSION
(4278 Å)
⊙ PROTON IMPACT
△ H-ATOM IMPACT
10
20
30
50
70
100
200
ENERGY (kev)

FIG. 18

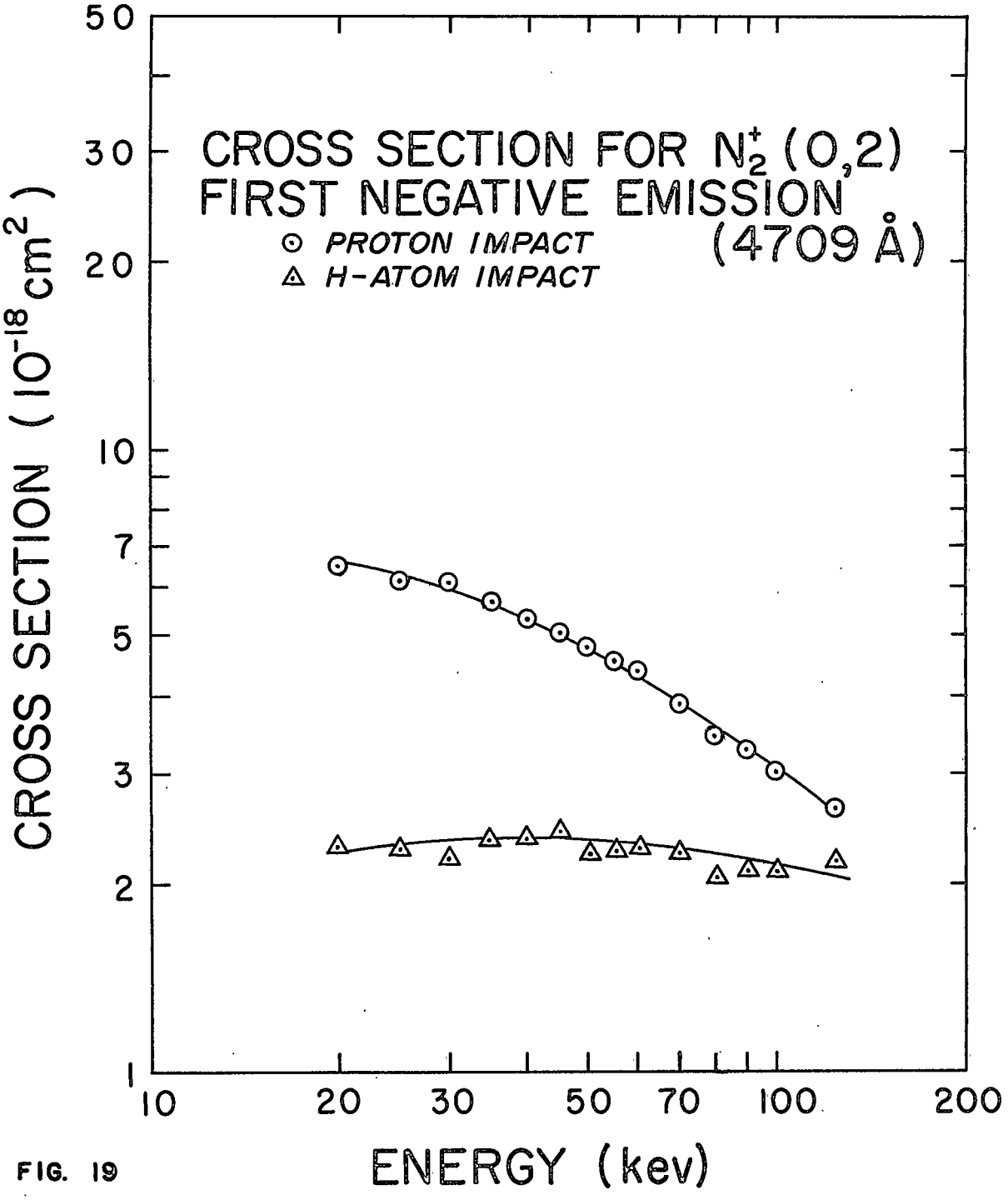
CROSS SECTION FOR N_2^+ (0,2)
FIRST NEGATIVE EMISSION (4709 Å)
⊙ PROTON IMPACT
△ H-ATOM IMPACT
CROSS SECTION (10^{-18} cm^2)
50
30
20
10
7
5
3
2
1
10
20
30
50
70
100
200
ENERGY (kev)

FIG. 19

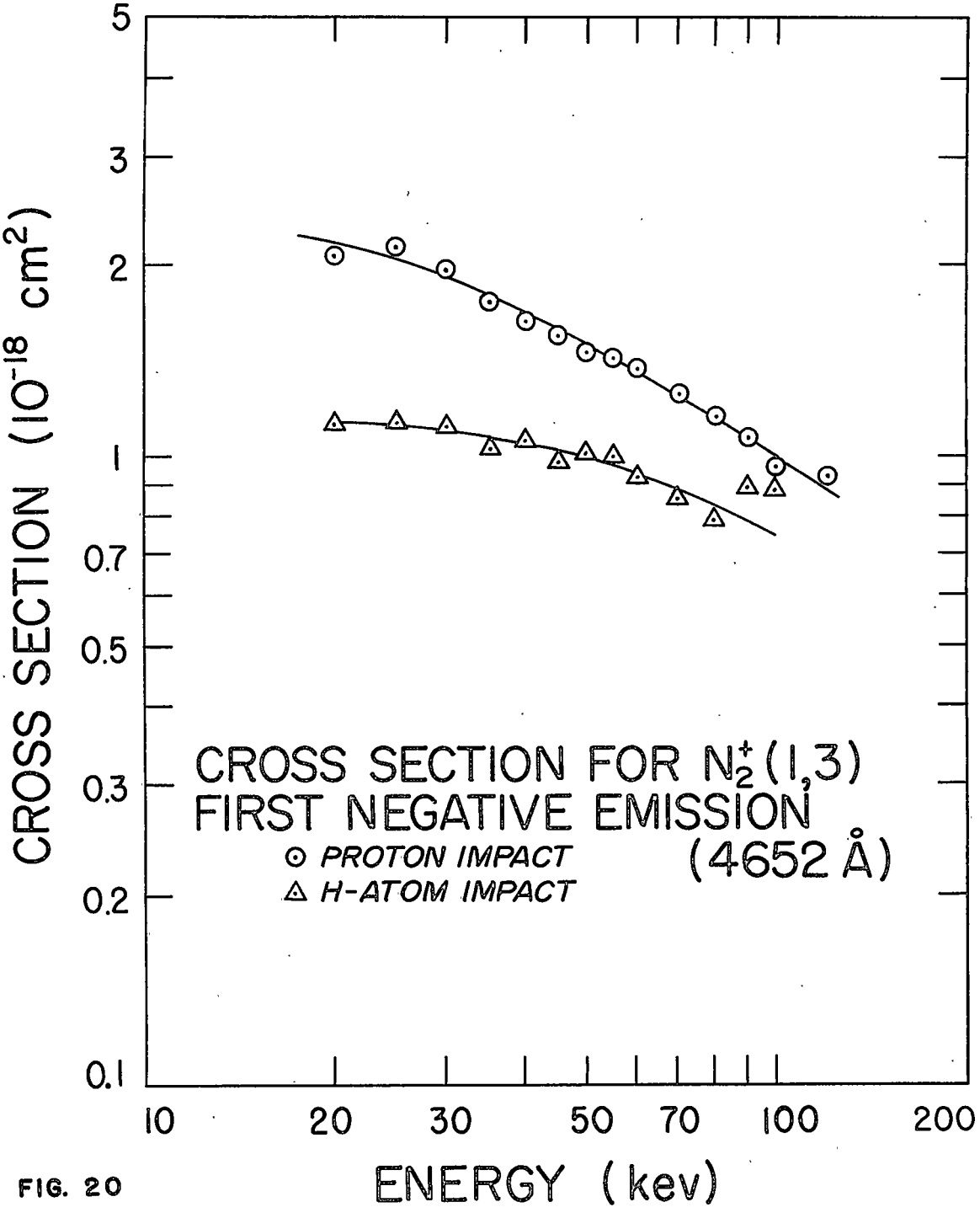
CROSS SECTION (10^{-18} cm^2)
5
3
2
1
0.7
0.5
0.3
0.2
0.1
CROSS SECTION FOR N_2^+(1,3)
FIRST NEGATIVE EMISSION
(4652 Å)
⊙ PROTON IMPACT
△ H-ATOM IMPACT
10
20
30
50
70
100
200
ENERGY (kev)

FIG. 20

The relationship of emission to excitation for the First Negative system is easily obtained since the upper state is populated only by direct excitation and not by cascading. The $C\,^2\Sigma_u^+$ state which lies above the $B\,^2\Sigma_u^+$ state of N_2^+ would not be expected to populate the B state for two reasons. First, the transition between the two states is forbidden. Second, the Franck-Condon principle predicts that the levels of the C state that are most likely to be excited, predissociate[36]. A brief discussion of predissociation is presented in the appendix C. From Chapter I, therefore, $Q_{v'=0} = \sum_{v''} Q_{ov''}$. The cross sections for the excitation of the $v' = 0$ level can then be obtained by measuring the emission cross sections for each of the bands originating from the $v' = 0$ level and summing the results.

The processes and the energy defects are presented in Table I as a guide for determining the possible excitation mechanisms.

Since the excitation produced in conjunction with the charge exchange process requires less energy than the other processes, the author expects process 2 to contribute significantly to the excitation. If the energy dependence of process 2 is the same as the energy dependence of process 1, process 2 cannot explain the observed energy dependence of the First Negative system. As is shown in figure 21, the charge exchange cross section decreases much more rapidly than the emission measurements of this work. Since process 3 has a high cross section, figure 21, the fourth process listed could also contribute to the emission cross section. If one then adds the ionization cross section to the charge exchange cross section, the result is a curve which has

about the same shape as the cross section curve for the excitation of the v' = 0 level of the $B\,^2\Sigma_u^+$ state. This comparison is also shown in figure 21. Now if the energy dependence of the sum of processes 1 and 3 have the same energy dependence as the sum of the processes 2 and 4, there is justification for believing that both processes 2 and 4 contribute to the observed emission.

TABLE I

Some of the Processes Resulting From Collisions of Protons and Hydrogen Atoms with Nitrogen Molecules.

Number	Process	Energy Defect
1	$H^+ + N_2 \text{---} H^o + N_2^+$	1.9 ev
2	$\text{---} H^o + N_2^{+*}$	4.9
3	$\text{---} H^+ + N_2^+ + e$	15.5
4	$\text{---} H^+ + N_2^{+*} + e$	18.5
5	$H^o + N_2 \text{---} H^o + N_2^+ + e$	15.5
6	$\text{---} H^o + N_2^{+*} + e$	18.5
7	$\text{---} H^+ + N_2^+ + 2e$	29.1
8	$\text{---} H^+ + N_2^{+*} + 2e$	32.1
9	$\text{---} H^- + N_2^{+*}$	17.7
10	$H^+ + N_2 \text{---} H^+ + N_2^*$	11.
11	$H^o + N_2 \text{---} H^o + N_2^*$	11.
12	$H^o + N_2 \text{---} H^+ + N_2^* + e$	24.6
13	$H^o + N_2 \text{---} H^{o*} + N_2$	10.2
14	$H^o + N_2 \text{---} H^{o*} + N_2^+ + e$	25.7
15	$H^+ + N_2 \text{---} H^{o*} + N_2^+$	12.1

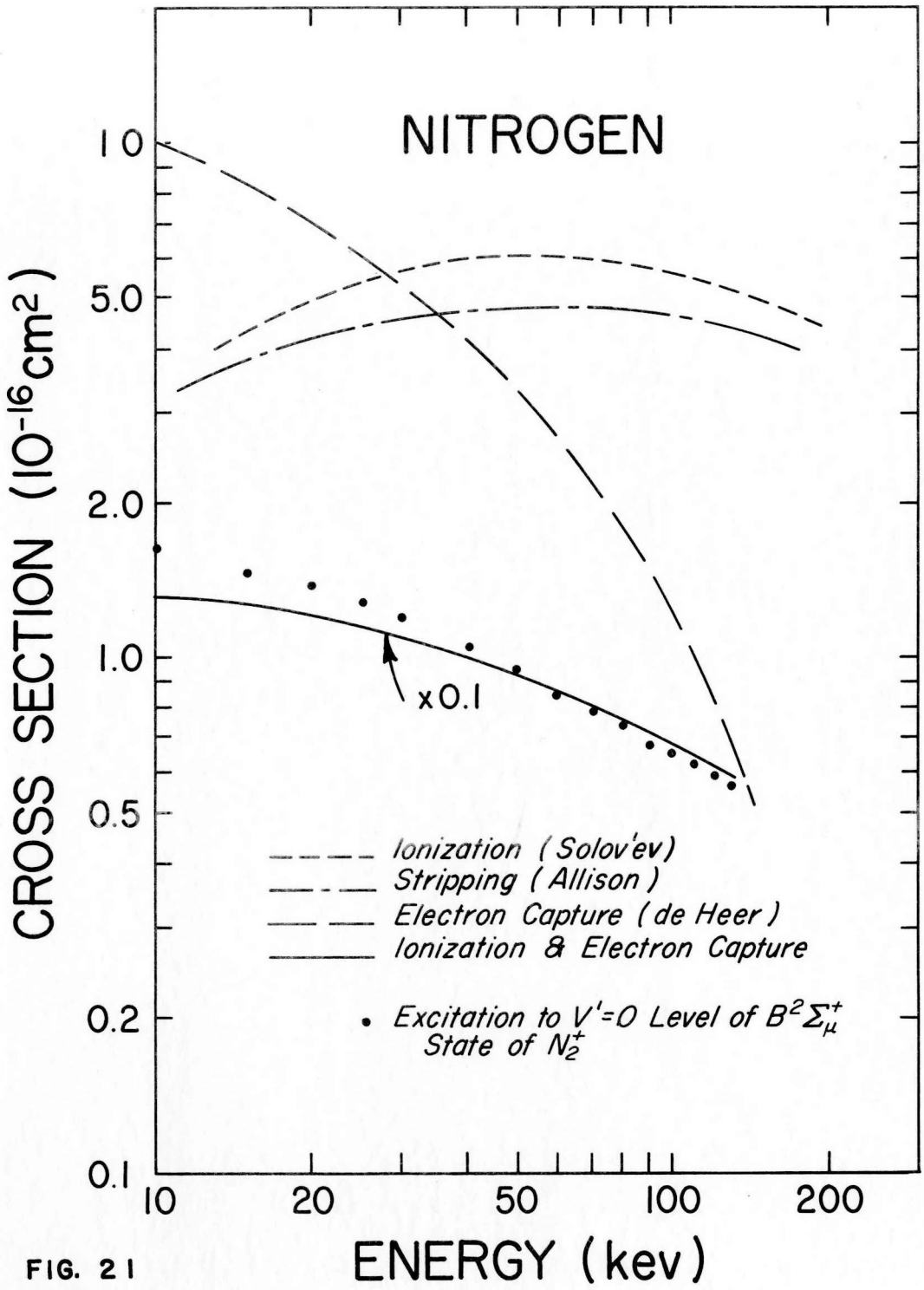
NITROGEN
CROSS SECTION (10-16cm2)
10
5.0
2.0
1.0
0.5
0.2
0.1
x0.1
Ionization (Solov'ev)
Stripping (Allison)
Electron Capture (de Heer)
Ionization & Electron Capture
Excitation to V'=0 Level of B2Σμ+ State of N2+
10
20
50
100
200
ENERGY (kev)

FIG. 21

The curve of the sum of processes 1 and 3 is a measure of the total cross section for the production of N_2^+. The experimental curve is a measure of the cross section for the excitation of the v'= 0 level of the B state of N_2^+. The ratio of these curves would, therefore, approximately represent the fraction of the molecular ions excited to the v'= 0 level to the total number of molecular ions formed. This fraction is on the order of 0.1. Since approximately 80% of the light emitted in transitions from the B state is from the v'= 0 level, the fraction of the molecular ions excited to the B state to the total number of molecular ions formed is still on the order of 0.1.

Excitation cross section calculations for proton impact on nitrogen molecules have not been worked out using either the Born approximation or the distortion approximation. As discussed in Chapter I, however, the energy dependence of the cross section can be predicted by the Born approximation for some processes. The cross section is expected to have an (1/E) ln E dependence for electric dipole transitions and an 1/E dependence for an electric quadrupole transition, where E is the incident particle energy. By plotting Q E as a function of ln E, the functional form of the energy dependence can most easily be exhibited. The graph of Q E as a function of ln E for proton impact, figure 22, indicates an apparent (1/E) ln E dependence of Q at the higher energies. A linear dependence at the higher energies would support the supposition that process 4 becomes important at the higher energies. Process 4 is an ionization plus excitation process which is predicted by the Born approximation to have the (1/E) ln E dependence.

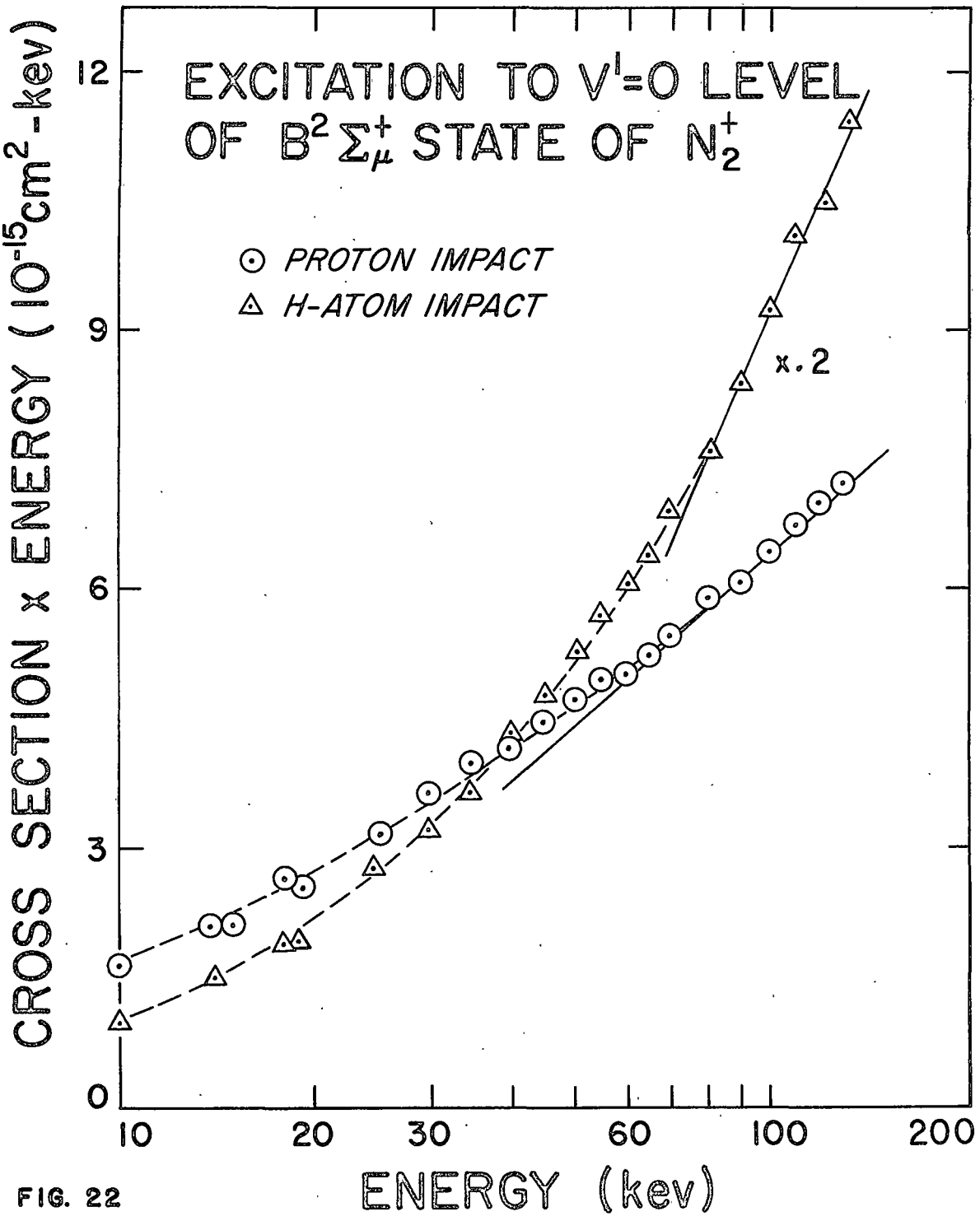
EXCITATION TO V'=0 LEVEL
OF $B^2\Sigma_\mu^+$ STATE OF N_2^+
⊙ PROTON IMPACT
△ H-ATOM IMPACT
x.2
CROSS SECTION x ENERGY (10^{-15}cm^2-kev)
0
3
6
9
12
10
20
30
60
100
200
ENERGY (kev)

FIG. 22

In order to propose a mechanism responsible for the excitation of the B state of N_2^+ by hydrogen atom impact, a few observations will be made.

If one calculates the interaction distance "a" according to the Massey criterion, one obtains a value of 12 Å for proton impact and 6 Å for hydrogen atom impact. These values imply that in the hydrogen atom collisions the systems approach each other more closely than in the proton collisions before interacting.

The curve of Q E as a function of ln E in figure 22 indicates the appearance of a linear region at the higher energies. Such a linear region at the higher energies means an (1/E) ln E dependence of Q which is predicted in proton impact for ionization and excitation processes.

With reference to the processes previously listed, the simple ionization and excitation of N_2 requires the least amount of energy for exciting the B state in hydrogen atom impact. If the collision were more violent, the hydrogen atom could also be excited or ionized leading to process 8. This process, however, requires approximately twice the energy of process 6. Since the cross section for electron capture by the hydrogen atom is small, process 9 is not expected to contribute significantly at these energies.

From these observations the author suggest process 6 as the basic mechanism for the excitation of the B state by hydrogen atom impact. Process 8, however, cannot be ignored as a possible mechanism.

The ratio of oscillator strengths of the transitions from $v' = 0$ level of the B state to the $v'' = 0$ and $v'' = 1$ levels of the X state have been measured and calculated by many researchers. As discussed previously, the data of this paper indicates that the cross section curves for the (0,0) and (0,1) band emissions have the same shape. From these curves, therefore, the ratio $Q_{(0,1)}/Q_{(0,0)}$ can be calculated. The calculated number was 0.33 ± 0.03 which is in agreement with what others have obtained [37-39,5].

N_2 Second Positive System: Emission cross sections were measured for the (0,0) transition of the Second Positive system. These curves are displayed in figure 23. The low light intensities and the stringent pressure requirements prevented measurements of other bands in this system.

As in the case of the First Negative system these data were normalized to the (0,0) band of the First Negative system correcting only for the change in spectral efficiency of the monochromator.

The data reveals an emission cross section due to hydrogen atom impact that decreases rapidly with increasing energy showing no sign of a peak even for the lowest energy at which measurements were made. The emission cross section for proton impact reveals a very small probability of excitation of the upper state of this system. The statistics were quite poor at low energies which left considerable uncertainty in the shape of the cross section curve for proton impact at these energies. There does, however, appear to be a maximum in the curve at about 35 kev.

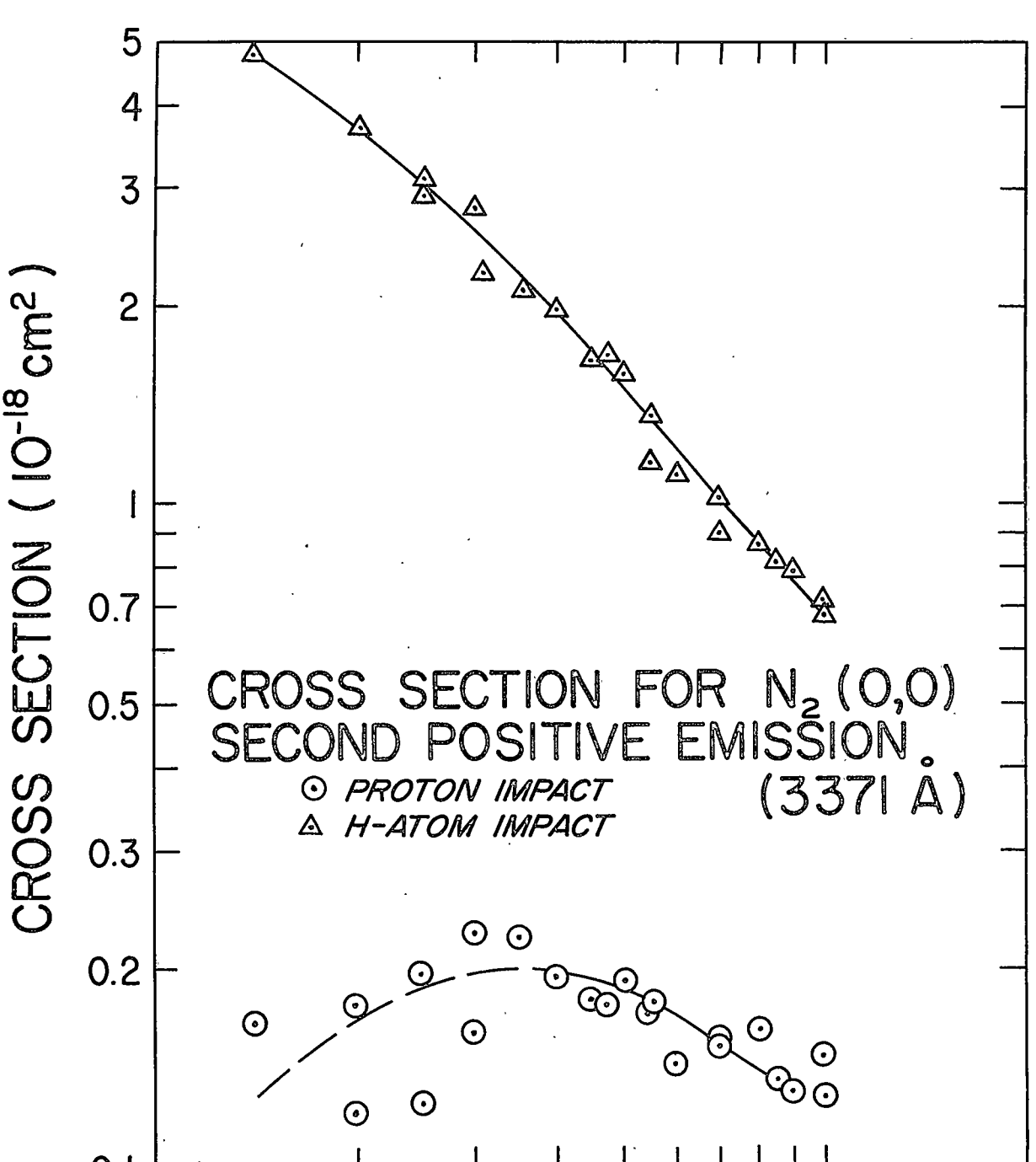
CROSS SECTION (10^{-18} cm^2)
5
4
3
2
1
0.7
0.5
0.3
0.2
0.1
CROSS SECTION FOR N_2 (0,0)
SECOND POSITIVE EMISSION.
PROTON IMPACT
H-ATOM IMPACT
(3371 Å)
10
20
30
50
70
100
200
ENERGY (kev)

FIG. 23

No known states exist above the $C^3\Pi_u$ state which could populate this state by cascading. The emission resulting from the C state, is expected, therefore, to be entirely due to the direct excitation of this state. Likewise, the emission from the (0,0) band is directly proportional to the probability of excitation of the v'= 0 level of the C state.

Due to the predissociation of the C state above the v'= 4 level there are no observed bands that originate from levels higher than v'= 4 [40]. The transitions cut off abruptly above this level indicating that the dissociation is due to the crossing of two bound states as is discussed in appendix C.

The possible processes for the excitation of the C state are presented in Table I.

For hydrogen atom impact process 11 would appear the more likely because of the smaller amount of energy required. This direct excitation process, however, would not be expected to excite a triplet state from a singlet ground state unless electron or spin exchange were involved. For the excitation of the C state, therefore, process 11 cannot be a simple excitation but involves electron or spin exchange mechanisms.

If the hydrogen atom is stripped of its electron in the interaction, process 12 would result. Even though this process requires an additional energy of 13.6 ev, it represents a possible mechanism.

In figure 24 the curve of QE plotted as a function of E does not show the linear behavior at the higher energies which is indicative of

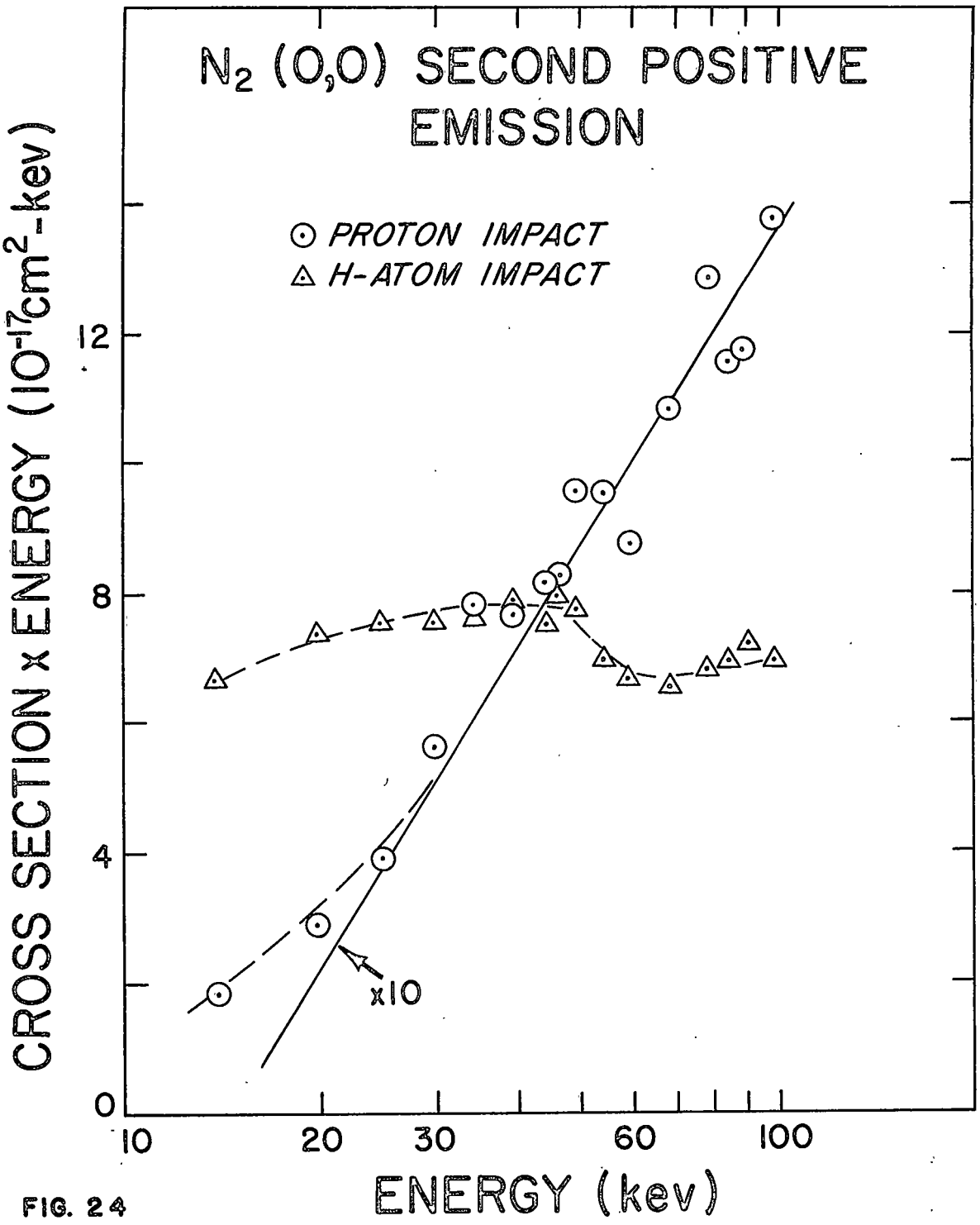
N_2 (0,0) SECOND POSITIVE EMISSION
⊙ PROTON IMPACT
△ H-ATOM IMPACT
CROSS SECTION x ENERGY ($10^{-17}cm^2$-kev)
0
4
8
12
x10
10
20
30
60
100
ENERGY (kev)

FIG. 24

a simple dipole transition. The excitation mechanism, therefore, is more complex, and the structure in the curve complicates the situation even more. Referring to figure 23 the rapid decrease of cross section with energy would predict an exchange mechanism [13].

From these observations the author concluded that both processes 11 and 12 are possible contributors to the excitation of the C state, and that electron exchange is probably the basic mechanism for exciting this triplet state. Hydrogen atom excitation has not been studied by many people, but in the work of Van Eck, et. al. [20] their conclusion is that electron exchange accounts for the excitation of the triplet states of helium.

In the case of proton impact, spin conservation rules do not allow excitation of a pure triplet state [41]. Since excitation of the C state is observed for proton impact, there must be some mechanism permitting the excitation. The curve of QE as a function of ln E, figure 24, indicates that, in spite of the rather poor statistics, there is a definite (1/E) ln E dependence predicted for a simple dipole excitation. If spin-orbit coupling were sufficiently strong, the C state could be a mixture of both singlet and triplet terms. This mixing would then allow for some excitation of the C state by proton impact.

In their studies of electron impact on nitrogen, Lassettre, et. al. [42] claim that the C state is a linear combination of singlet and triplet terms. The singlet element is considered to be small but present.

Lyman Alpha Line: When the proton collides with an atom or molecule it can capture an electron from the target system by the charge exchange process. In the impact the resulting hydrogen atom can also be left in the excited state. If the hydrogen atom is left in the 2p state, the transition producing Lyman alpha radiation will occur. When the hydrogen atom collides with an atom or molecule there is also a finite probability of the excitation of the 2p state.

There are problems associated with measuring the excitation of the fast particle which are not encountered in the target system. These problems result because of the motion of the particle. As discussed in Chaper I, the cross section for exciting the 2p state of hydrogen is obtained by measuring the emission from transitions which populate the 2p state by cascading and by measuring the Lyman alpha emission. Cascading as well as direct excitation would, therefore, contribute to the observed Lyman alpha emission. A further difficulty is encountered because of the finite lifetimes of the states. The incident beam must travel in the target gas a sufficiently long time to establish an equilibrium between excitation and emission. This condition is actually reached only at distances on the order of meters because of the long lifetimes[43] of the higher states which populate the 2p state by cascading. If the beam traveled distances of meters in the target gas, the composition of the beam would no longer be known unless very low pressures were used. The light intensities at such pressures would be too weak for measurements by the techniques used for this work. An important factor in the Lyman alpha measurements

is the presence of atomic nitrogen lines nearby. Since there is a strong NI line at 1200 Å and a weaker line at 1243 Å, monochromator slits equivalent to 8 Å were necessary for the Lyman alpha measurements.

For these reasons some sort of a compromise was required. The experimental conditions of this work provided what appeared to be the best compromise. The technique was to observe the optical emission very soon after the beam entered the excitation chamber. If the lifetimes of the states capable of populating the 2p state by cascading were sufficiently long, the hydrogen atoms in these states would have passed the region of observation before emitting their radiation. If the lifetime of the 2p state were sufficiently short, an equilibrium between the direct excitation to and the emission from the 2p state could then be established. Since a range of particle velocities was used in this work, the optimum condition was not possible for the entire energy range. The contribution to Lyman alpha emission due to cascading from higher levels was calculated to be on the order of 10% at 20 kev and negligible at the higher energies. At the highest energies the observed emission was lower than the equilibrium emission by approximately 10%. The total error in the relative cross section from the lowest to the highest energy was, therefore, on the order of 20%.

The relative cross sections for the production of Lyman alpha as a function of incident particle energy were measured in the energy range from 20 to 130 kev. These results, which were normalized to the

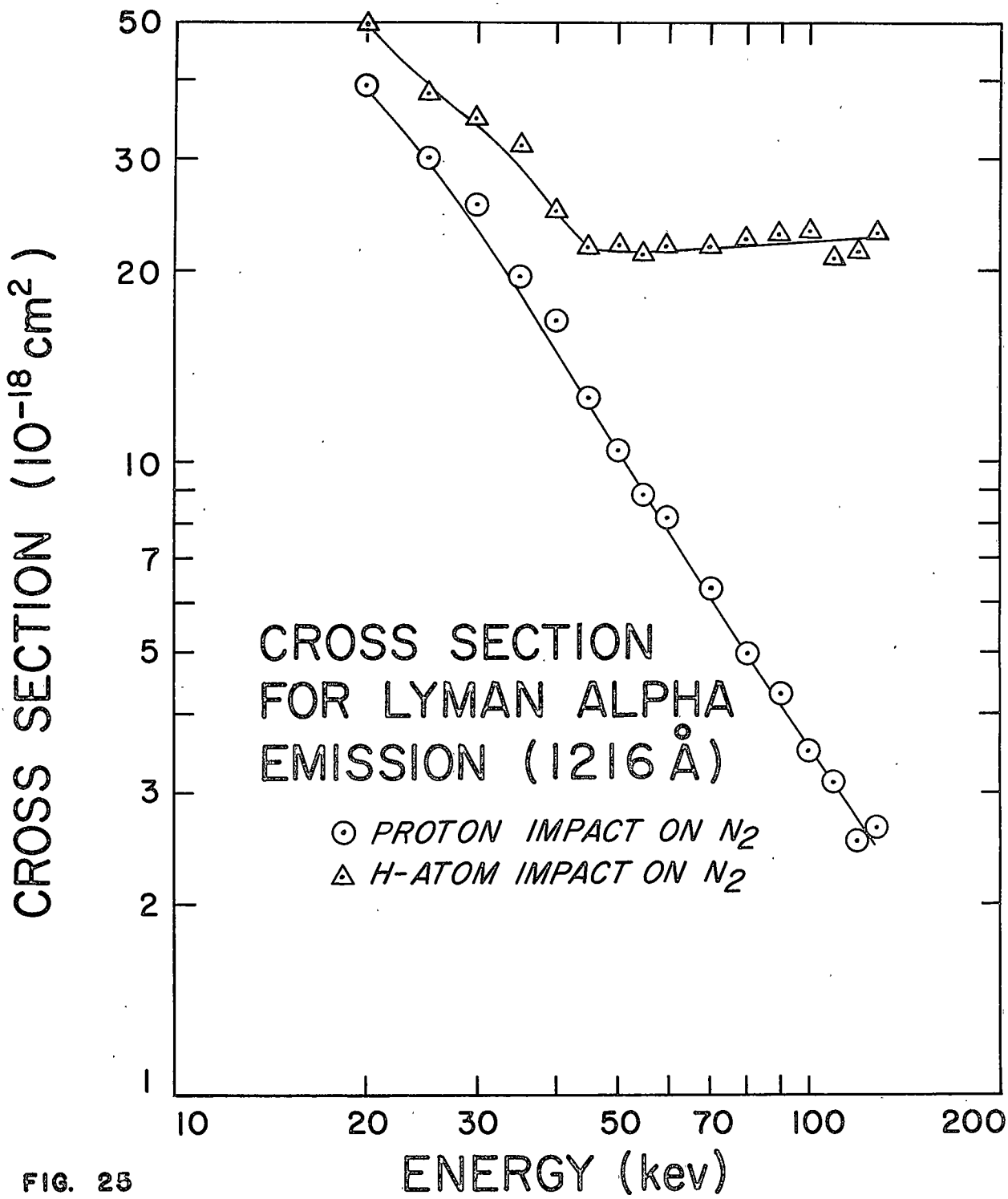
CROSS SECTION (10⁻¹⁸ cm²)
50
30
20
10
7
5
3
2
1
CROSS SECTION
FOR LYMAN ALPHA
EMISSION (1216 Å)
⊙ PROTON IMPACT ON N2
△ H-ATOM IMPACT ON N2
10
20
30
50
70
100
200
ENERGY (kev)

FIG. 25

proton impact data of Van Zyl[8] at 20 kev, are shown in figure 25. No correction was made for the possible systematic errors which were discussed previously.

The proton impact curves show a very rapid decrease in the production of Lyman alpha as the energy of the proton is increased. The production of Lyman alpha by hydrogen atom impact has a higher cross section over the entire energy range than the cross section for proton impact. One different feature in the hydrogen atom cross section curve as compared with the proton cross section curve is the apparent abrupt change in the slope occuring at about 45 kev.

The cross section curve for Lyman alpha emission by proton impact has the same general shape as that of the charge exchange cross section curve reproduced for reference in figure 21. If the errors discussed previously were taken into consideration, the two curves would more nearly have the same shapes. This general relationship between the shapes of the emission curve and the charge exchange curve is expected since the existence of a hydrogen atom in the beam depends upon the charge exchange process. These measurements indicate that about 3% of the hydrogen atoms formed in the beam are excited to the 2p state.

The curve of QE as a function of ln E, figure 26, is not really applicable to this process since the Born approximation predicts an E^{-6} dependence of cross section for charge exchange. The curve does, however, show that the energy decreases less rapidly than the prediction of the Born approximation. The energy dependence of the cross

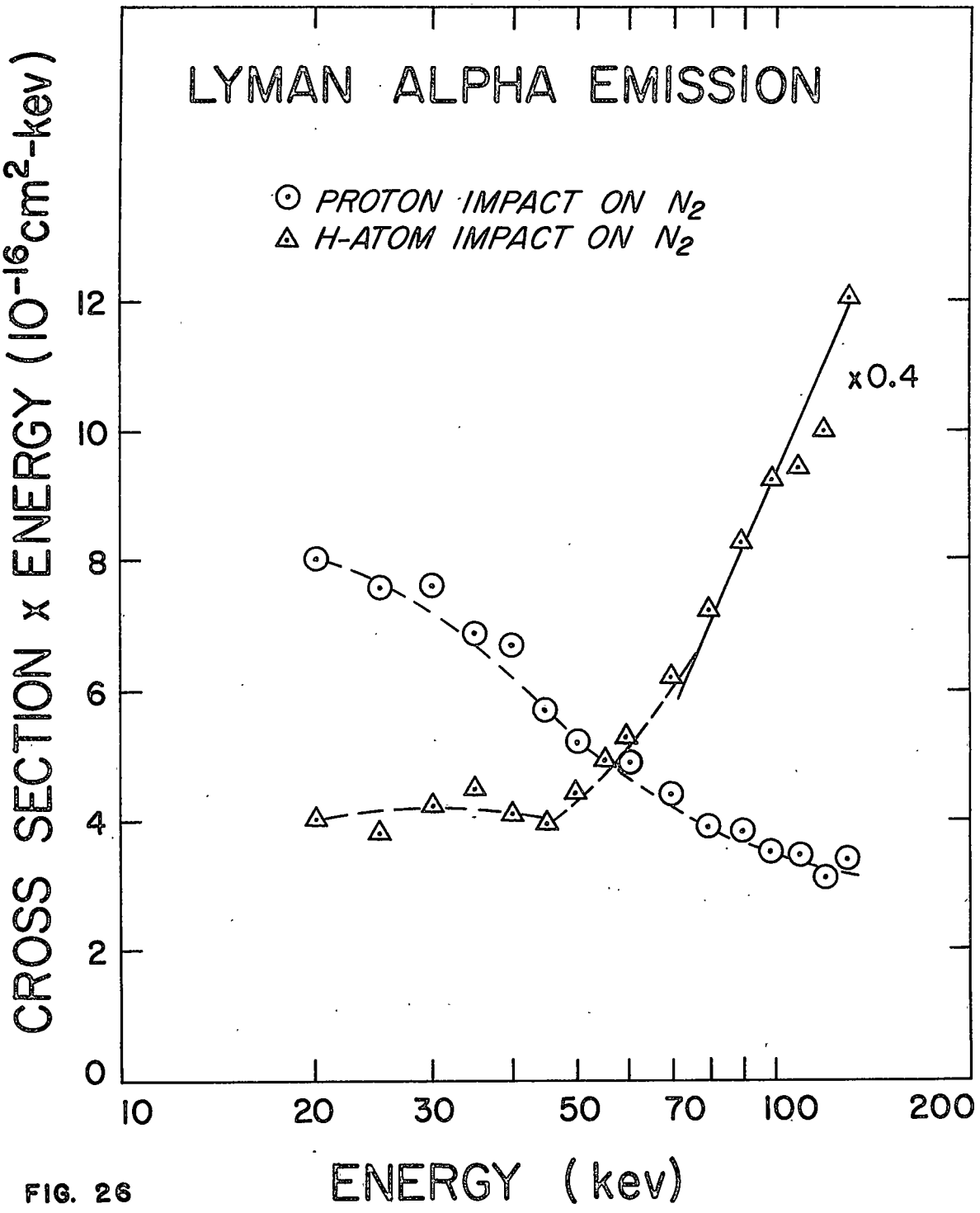
LYMAN ALPHA EMISSION
⊙ PROTON IMPACT ON N_2
△ H-ATOM IMPACT ON N_2
x0.4
CROSS SECTION x ENERGY (10^{-16}cm^2-kev)
0
2
4
6
8
10
12
10
20
30
50
70
100
200
ENERGY (kev)

FIG. 26

section is approximately $E^{-1.6}$.

The processes which are expected to contribute to these emissions are the final three processes listed in Table I.

The change in the slope of the curve of cross section as a function of energy, figure 25, implies that more than one process contributes to the excitation of the 2p state. One possibility is, first, a process for which the cross section decreases very rapidly with energy dominating at the low energies and, second, a process for which the cross section is nearly independent of energy dominating at the high energies.

Experimental data for basic atom-molecule inelastic cross sections is not adequate for making a meaningful analysis of the processes involved in producing Lyman alpha emission. On the basis of this work some observations can be made, however.

If process 3 and process 5 were similar, one would expect the cross sections for process 14 to be nearly constant with energy in the energy region considered in this work. If, further, the cross sections for processes 5 and 6 have the same energy dependence, it is possible that the cross section for process 14 would have the same energy dependence as the cross sections for processes 5 and 6. The only difference between process 6 and 14 is that in 6, N_2^+ is excited and in 14, H^o is excited. These observations and speculations could explain the energy dependence above 45 kev. Even though the energy dependence of curve of QE as a function of ln E in figure 26 is not exactly linear, the higher energy section does seem to show signs of linearity.

If hydrogen atom impact is not significantly different from proton impact in the Born approximation, the linearity of the curve would, again, point to an ionization process, an excitation process or both.

In order to arrive at some understanding of the cross section at lower energies some further observations will be made. Comparing the Lyman alpha results with the emission cross section for the Second Positive system of N_2 due to hydrogen atom impact, one notes shapes that are similar. From figures 24 and 26 it is noted that the breaks in the two hydrogen atom curves occur at about the same energy and that in the low energy region the curves have about the same shape. No definite conclusion can be drawn from these observations except that there appears to be some connection between process 11 and 13. Since process 13 requires an energy of only 10.2 ev, there is no apparent reason for this process not contributing significantly to the excitation of the hydrogen atom.

Atomic and Ionic Nitrogen Lines: Proton and hydrogen atom impact data for the NI lines produced by the $3s\,^2P---2p\,^2P^o$ and the $3s\,^2P---2p\,^2D^o$ transitions and the NII line produced by the $3d\,^3F^o---3p\,^3D$ transition are shown in figures 27-29. The cross section data for the $3s\,^4P---2p\,^4S^o$ transition are shown in figure 30. The emission by proton impact from the NII transition has been measured previously and reported [5,6].

An absolute determination of the emission cross section for the NII line was accomplished by normalizing these data to the proton cross section data for the N_2^+ (0,0) First Negative emission correcting only

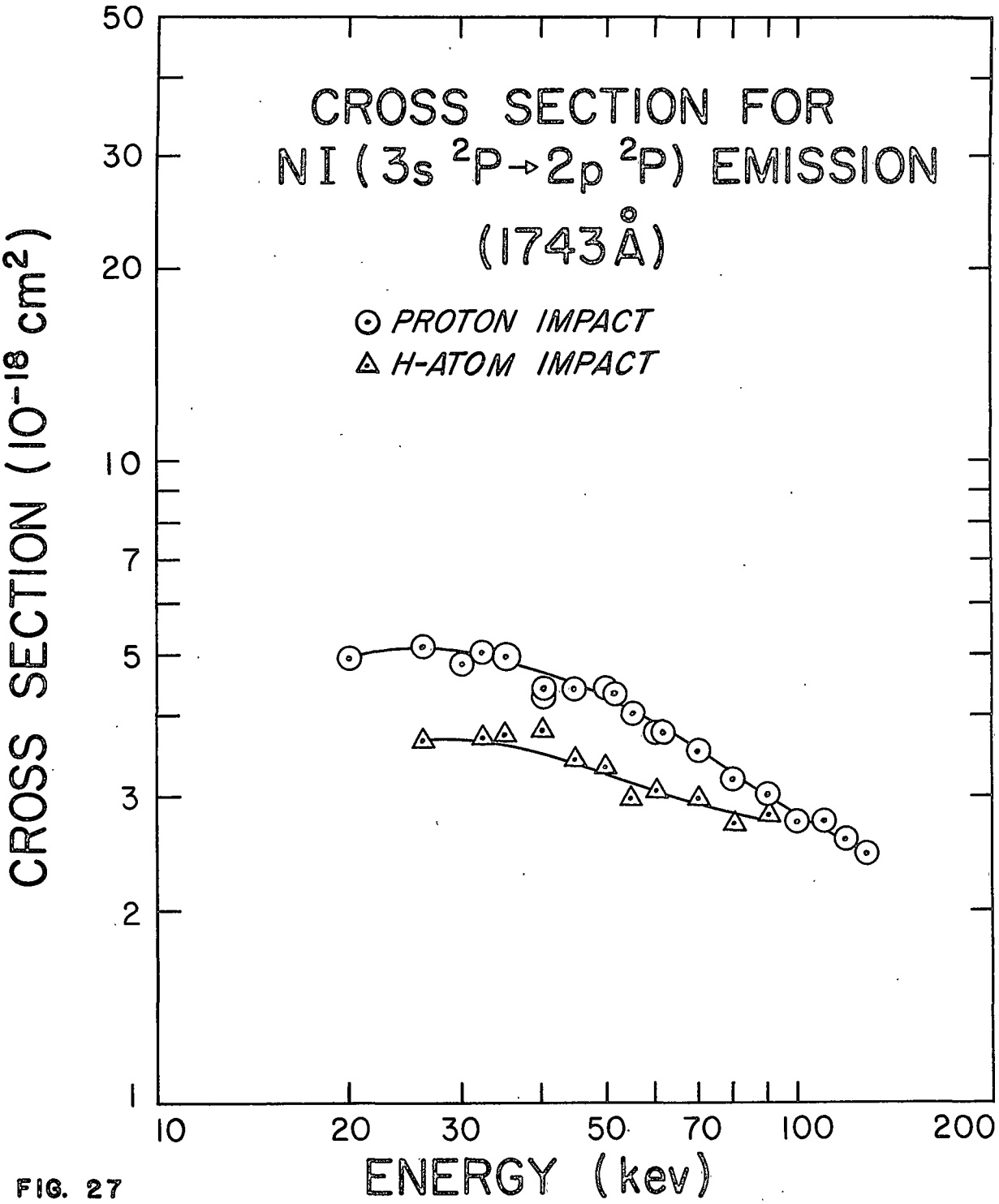
CROSS SECTION FOR
NI (3s ²P→2p ²P) EMISSION
(1743 Å)
⊙ PROTON IMPACT
△ H-ATOM IMPACT
CROSS SECTION (10⁻¹⁸ cm²)
50
30
20
10
7
5
3
2
1
10
20
30
50
70
100
200
ENERGY (kev)

FIG. 27

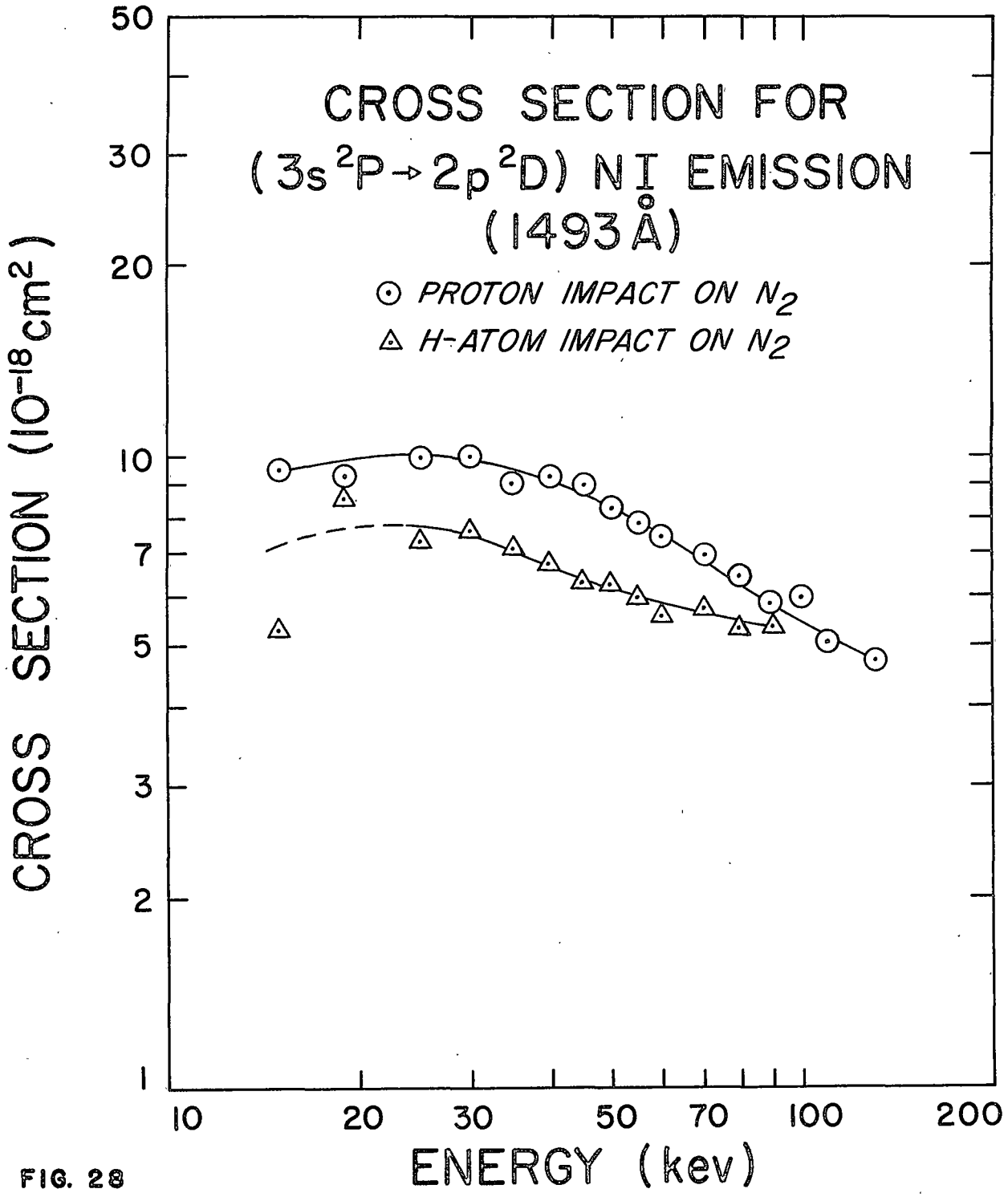
CROSS SECTION FOR
(3s ²P → 2p ²D) NI EMISSION
(1493 Å)
⊙ PROTON IMPACT ON N2
△ H-ATOM IMPACT ON N2
CROSS SECTION (10⁻¹⁸cm²)
50
30
20
10
7
5
3
2
1
10
20
30
50
70
100
200
ENERGY (kev)

FIG. 28

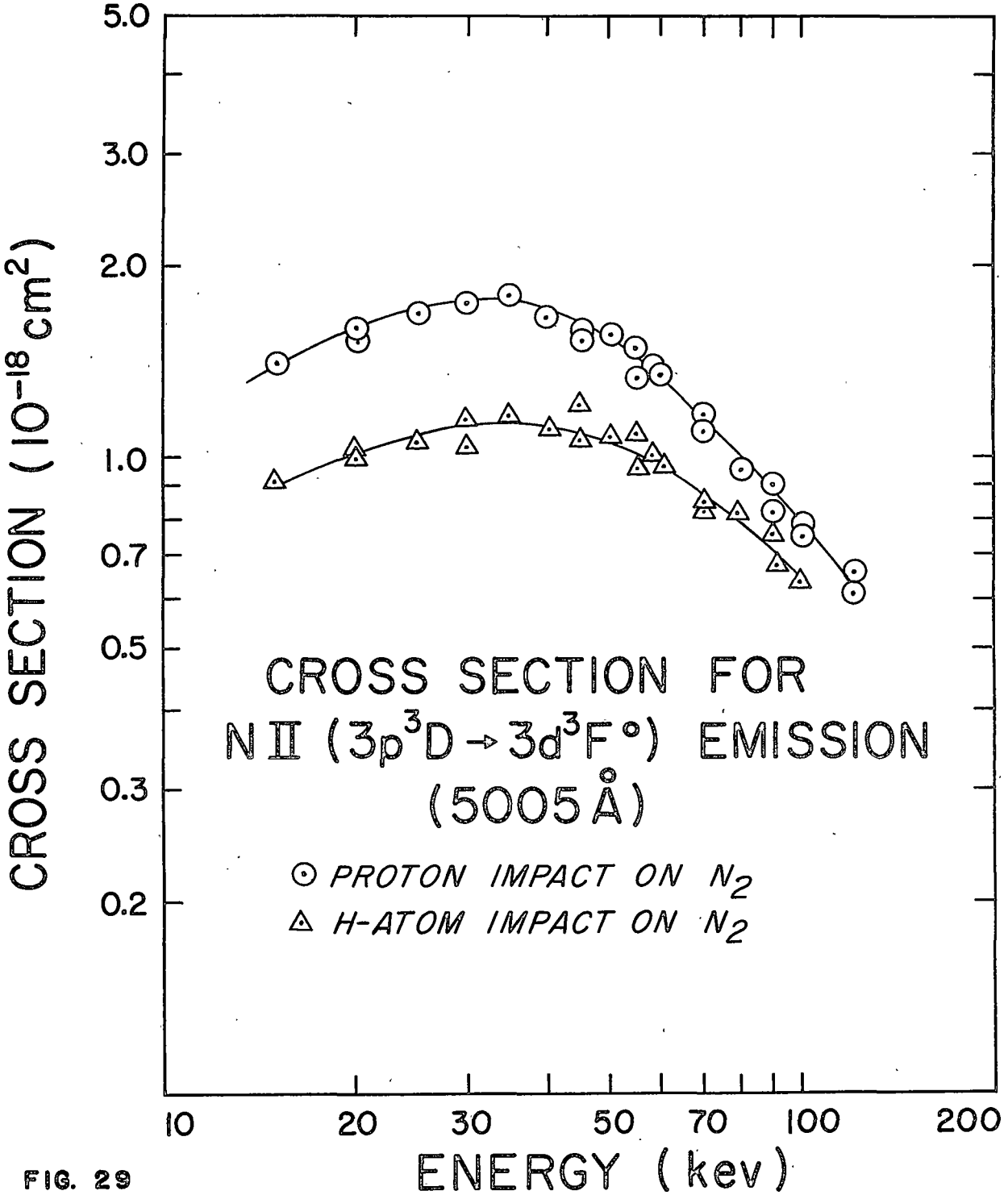
5.0
3.0
2.0
1.0
0.7
0.5
0.3
0.2
CROSS SECTION (10^{-18} cm^2)
CROSS SECTION FOR
N II ($3p^3D \rightarrow 3d^3F^\circ$) EMISSION
(5005 Å)
⊙ PROTON IMPACT ON N_2
△ H-ATOM IMPACT ON N_2
10
20
30
50
70
100
200
ENERGY (kev)

FIG. 29

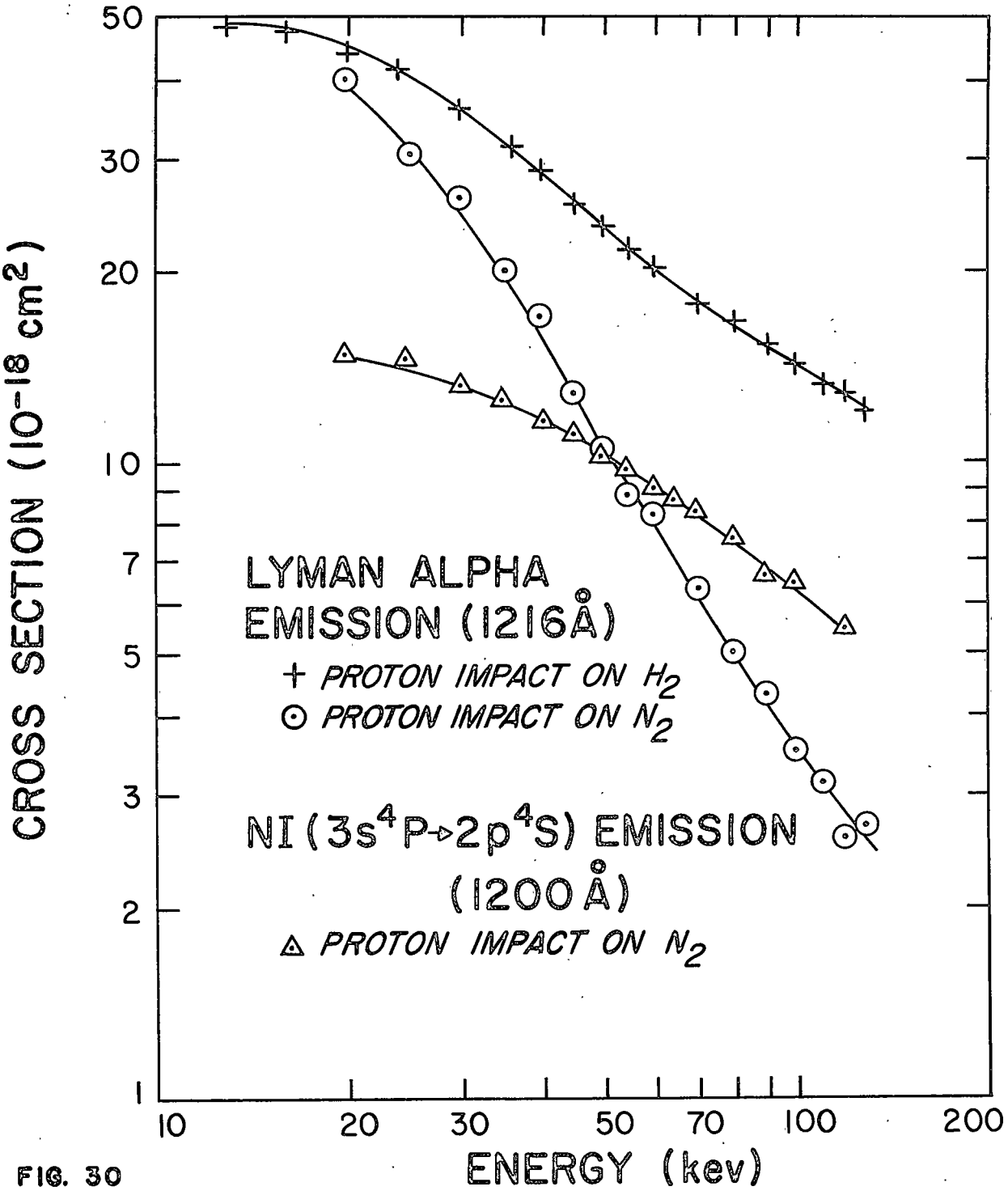
CROSS SECTION (10-18 cm2)
50
30
20
10
7
5
3
2
1
10
20
30
50
70
100
200
ENERGY (kev)
LYMAN ALPHA
EMISSION (1216Å)
+ PROTON IMPACT ON H2
⊙ PROTON IMPACT ON N2
NI (3s4P→2p4S) EMISSION
(1200 Å)
△ PROTON IMPACT ON N2

FIG. 30

for the spectral response of the monochromator.

Absolute values for emission cross sections of the atomic lines were more difficult to obtain because of the wavelength region in which these lines are located. Since the Lyman alpha data were normalized to the measurements of Van Zyl, the cross section measurements for the NI line could, therefore, be normalized to the Lyman alpha data. An absolute determination of the $^4P \text{---} ^4S^o$ emission at 1200 Å was obtained directly since the line lies so near to Lyman alpha. Because of the nearness of the Lyman alpha line, however, there could be an error in the measurements on this line. To obtain absolute values for the other two lines, the assumption was made that the efficiency of the monochromator was essentially the same for Lyman alpha at 1216 Å as for the $^2P \text{---} ^2P^o$ transition at 1743 Å. This assumption seemed reasonable since the grating was blazed for 1500 Å. Then the absolute determination for the $^2P \text{---} ^2D^o$ line was accomplished from the knowledge of the transition probabilities for the $^2P \text{---} ^2P^o$ and $^2P \text{---} ^2D^o$ transitions [44]. It is assumed that the transition probabilities for transitions from the same upper state are independent of the method of excitation.

These data reveal that the atomic nitrogen emissions produced by proton impact have maxima somewhere around 25 kev. For hydrogen atom impact the peaks are not clearly defined because of the statistics. There is, however, very little difference in the magnitudes of excitation by proton impact and hydrogen atom impact. At the lower energies Q_o/Q_+ is about 3/4 and increases with increasing energy.

In the case of the ionic nitrogen line the hydrogen atom cross section is an appreciable fraction of the proton cross section and the emission has a maximum in the area of 40 kev. As is noted the shapes of the curves due to proton impact and due to hydrogen atom impact are about the same.

The results for the ^4P---$^4S^o$ transition are in question both with respect to the relative as well as the absolute values of emission cross section. Because of the closeness to the Lyman alpha line and the Doppler broadening of the Lyman alpha line, the measured emission cross sections for the nitrogen line were probably larger than their actual values. For this reason the emission cross sections due to hydrogen atom impact were not attempted.

No corrections were made for populating the upper states by cascading from higher levels in any of the cross section measurements for the atomic and ionic emissions. Without cross section measurements for lines in the longer wavelength spectral region, it is impossible to accurately account for the cascading effect.

In collisions there are a number of mechanisms for producing as final products either an excited nitrogen ion or an excited nitrogen atom. Two means of dissociating and exciting the atom to the 3s state or the ion to the 3p state will be mentioned. One is to ionize a $\sigma_g 2s$ electron leaving the molecule with about 40 ev of energy[45]. The molecule could find itself in a dissociative state such that either one or both of the end products was left in highly excited states. The other possibility that will be mentioned involves the interaction of

the projectile with more than one electron of the target system. If, for example, two electrons were raised to higher orbitals, and one is ionized by the Auger process, the molecular ion could again be left in a dissociative state capable of producing highly excited products.

The nitrogen molecule has the following configuration:

$KK\ (\sigma_g 2s)^2 (\sigma_u 2s)^2 (\pi_u 2p)^4 (\sigma_g 2p)^2$ [46].

Since both atomic and ionic nitrogen lines were present in the collision processes which were studied, ionization was involved. Consideration will, therefore, be given to the ionization of the various orbital electrons.

If a $\sigma_g 2p$ electron were ionized, the result is the ground state of the molecular ion, $X\ ^2\Sigma_g^+$. If a $\pi_u 2p$ electron is ionized, the $A^2\Pi_u$ state results. If a $\sigma_u 2s$ electron is ionized there results the $B\ ^2\Sigma_u^+$ excited state of N_2^+ from which the First Negative system originates. From the measurements of the excitation of this state, the probability of the $\sigma_u 2s$ electron being ionized is reasonably large. The next orbital from which an electron can be removed is the $\sigma_g 2s$. An electron in this orbital is more tightly bound than the electrons from the orbitals previously mentioned and would require more energy for ionization. If a $\sigma_g 2s$ electron were ionized, one could imagine the molecular ion in an unbound state such as would leave the atom, ion, or possibly both in excited states capable of producing the observed emissions.

Further information is possible from the identification of the particular atomic and ionic lines which were present in the spectral scans. Such an identification would indicate the probable states of the dissociation products which produce the observed atomic and ionic emissions. A study of the spectral scans revealed the following transitions:

$3s\,^4P \text{---} 2p\,^4S^o$	1200 Å	NI
$3s\,^2P \text{---} 2p\,^2P^o$	1743	
$3s\,^2P \text{---} 2p\,^2D^o$	1493	
$3s'\,^2D \text{---} 2p\,^2D^o$	1243	
$3s'\,^2D \text{---} 2p\,^2P^o$	1411	
$3d\,^2P \text{---} 2p\,^2P^o$	1319	
$3d\,^2D \text{---} 2p\,^2P^o$	1311	
$3d\,^3F^o \text{---} 3p\,^3D$	5005	NII
$3p\,^3D \text{---} 3s\,^3P^o$	5680	

The NII line at 5680 Å could not be observed in figure 14 but was observed by the author in other spectral scans. This line has also been reported by other authors[5,6].

It is interesting that the transitions originating from the 3s and 3d levels of atomic nitrogen are strong, but the transitions originating from the 3p and 4p levels are not present at all. Three transitions originating from p levels which should appear are:

$3p\,^2D^o \text{---} 3s\,^2P$	4109 Å	NI
$3p\,^2P^o \text{---} 3s\,^2P$	3830	
$4p\,^2S^o \text{---} 3s\,^2P$	4935	

From these observations it is believed that the dissociation limits of the repulsive states producing the observed emissions are some combinations of $N^+(3d)$, $N^+(3p)$, N(3s), and N(3d).

It is also interesting that emissions from both the $2s^2 2p^2 (^3P)$ nl and the $2s^2 2p^2 (^1D)$ nl families are present in the spectral scans. The ground state of atomic nitrogen is the $^4S^o$ indicating that in the lowest energy state the spins of all the 2p electrons are parallel. The fact that the two families of excited states are present means that the two 2p electrons in the excited atom which results from the dissociation can have their spins either parallel or anti-parallel.

In addition to the transitions recorded above, a line has been observed by Dufay, et. al.[6] at 6482 $\mathring{A}$ for which cross sections were measured. This line was attributed to atomic nitrogen. There are, however, transitions in both atomic and ionic nitrogen at 6482 $\mathring{A}$. In atomic nitrogen the transition is the $4d\,^4F$---$3p\,^4D^o$ and in the ion it is the $3p\,^1P$---$3p\,^1P^o$. From the relative intensities of lines that have been observed and from the differences in the energy dependencies of the cross sections for atomic and ionic emissions, there is no definite evidence for the choice of the atomic transition over the ionic transition.

As shown in figure 31, the graphs of QE as a function of ln E for the NII emission reveal a rather strange behavior. There appears initially an (1/E) ln E dependence of the cross section which changes at higher energies to approximately an 1/E dependence. Figure 32 displays for both proton and hydrogen atom impact approximately an (1/E) ln E

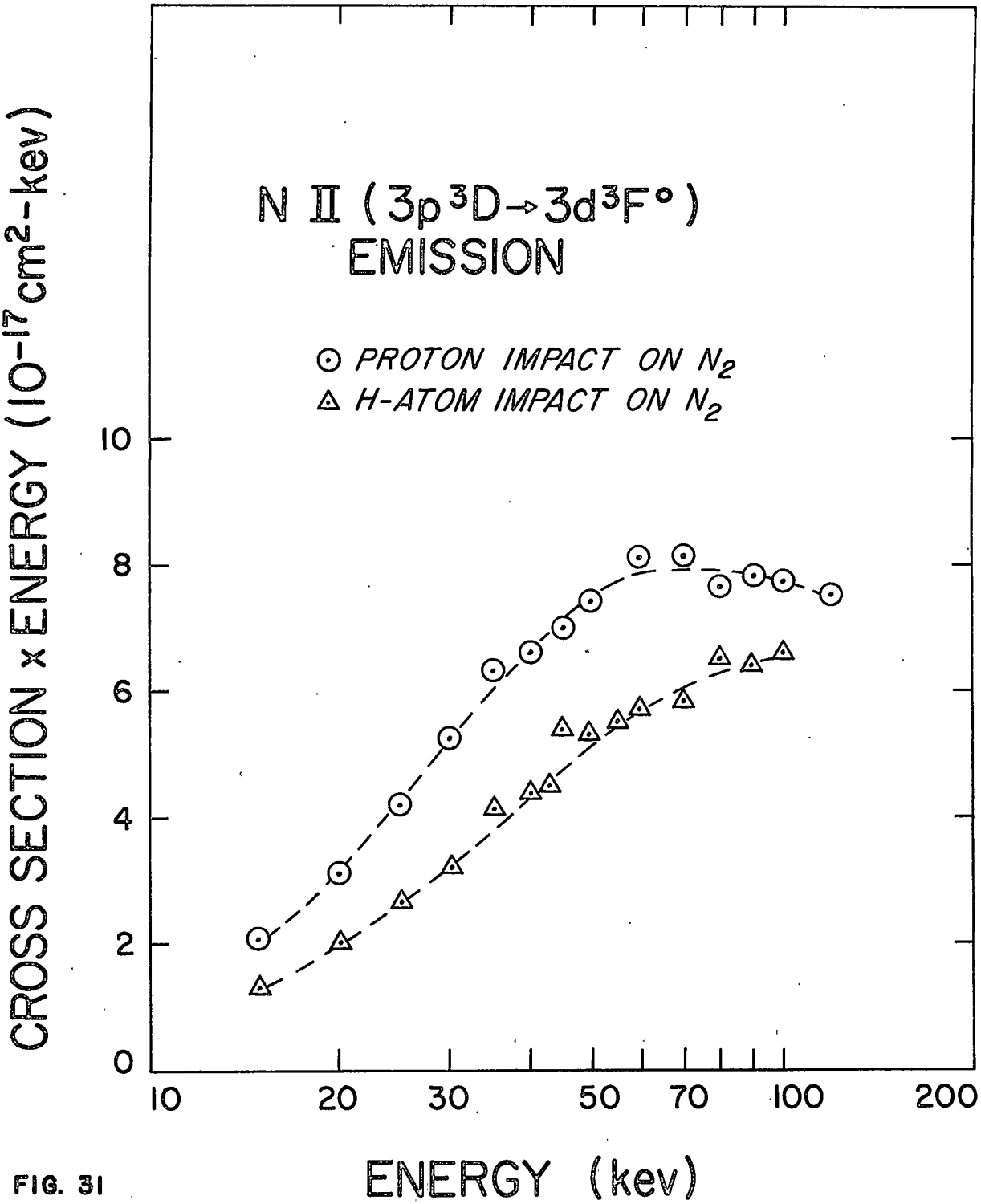
N II (3p ³D → 3d ³F°)
EMISSION
⊙ PROTON IMPACT ON N₂
△ H-ATOM IMPACT ON N₂
CROSS SECTION x ENERGY (10⁻¹⁷ cm²-kev)
0
2
4
6
8
10
10
20
30
50
70
100
200
ENERGY (kev)

FIG. 31

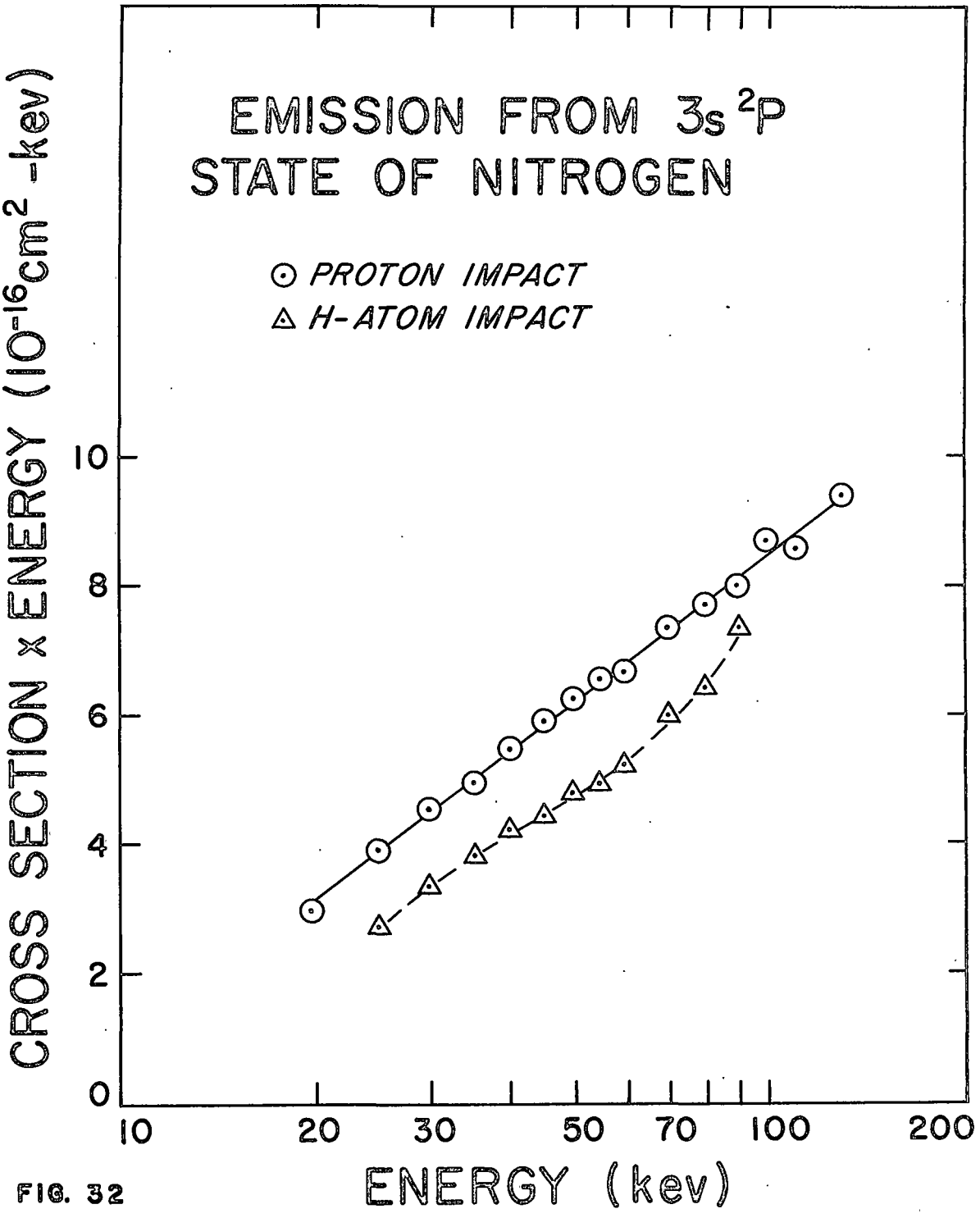
EMISSION FROM 3s ²P
STATE OF NITROGEN
⊙ PROTON IMPACT
△ H-ATOM IMPACT
CROSS SECTION x ENERGY (10⁻¹⁶cm²-kev)
0
2
4
6
8
10
10
20
30
50
70
100
200
ENERGY (kev)

FIG. 32

dependence for the atomic nitrogen emission over the entire energy range.

The (1/E) ln E dependence shown for these lines is not understood. Naively, an (1/E) ln E behavior is expected for a simple process whereas the processes necessary to produce these emissions appear to be complex processes. A dissociation must occur which will leave the atom, ion, or both in excited states. From the differences in the energy dependences of the NII and the NI emissions, it appears that at high energies the mechanism producing the NII emission must be different from the mechanism producing the NI emission.

Hydrogen Target

Lyman Band System: Emission cross section curves for the Lyman bands are shown in figure 33. The emission cross section for hydrogen atom impact was not measured, except for one energy, because of the ineffectiveness of hydrogen atoms in producing excitation and the consequent lower light level.

To obtain these data the monochromator with a slit width equivalent to 16 $\mathring{A}$ was set to include a group of lines centered at 1606 $\mathring{A}$. The group of lines constituted mainly the (4,11), (5,12), and (6,13) vibration bands[47], Geiger[34] has shown, in his electron impact studies, that the v'= 6 level of the B state had a greater probability of being excited than the v'= 4 and the v'= 5 levels. If proton impact were similar, contributions would be expected from all three bands with the greatest from the (6,13) band.

An absolute cross section is not especially meaningful when encompassing a number of bands as is done here. A value was obtained, however,

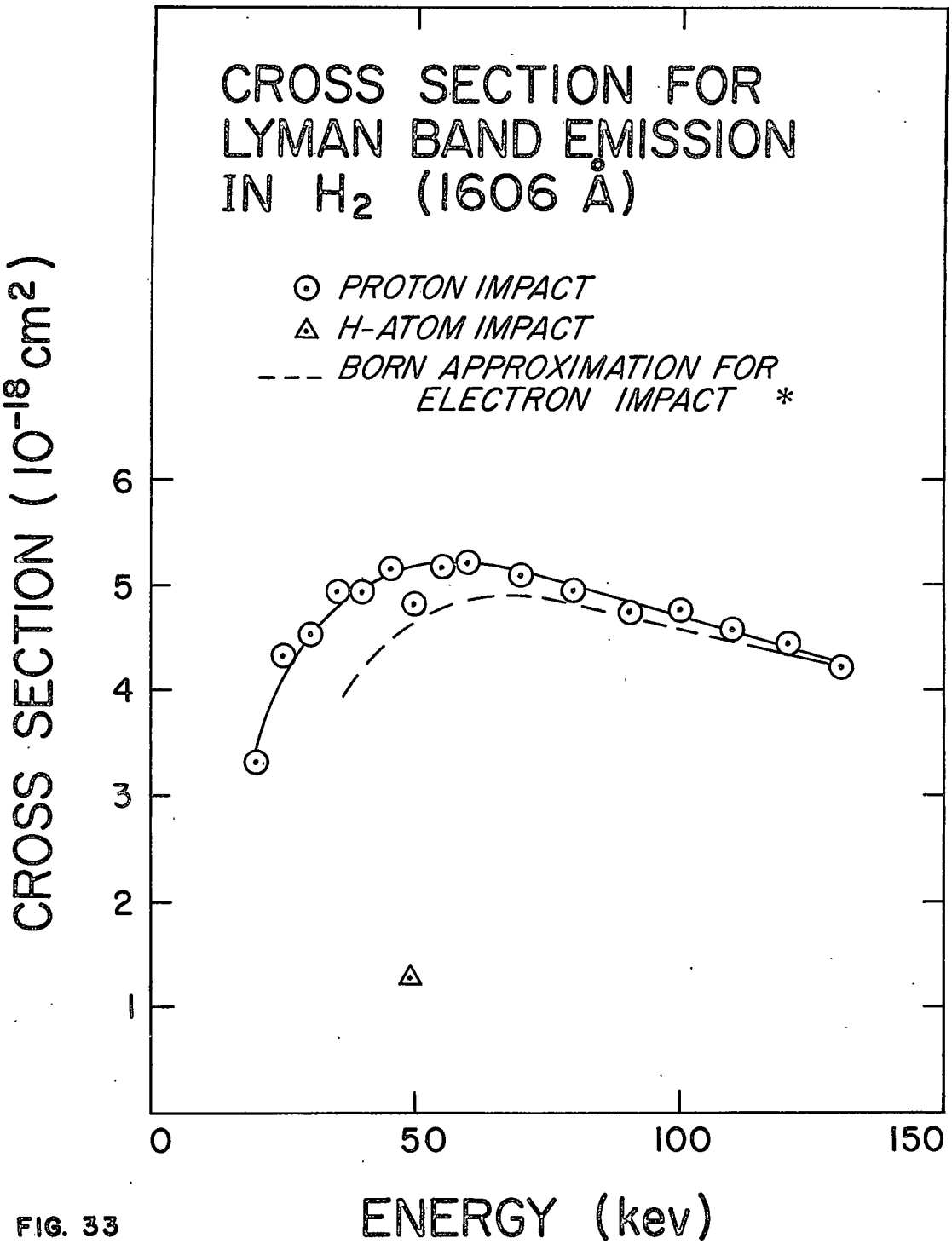
CROSS SECTION FOR
LYMAN BAND EMISSION
IN H_2 (1606 Å)
PROTON IMPACT
H-ATOM IMPACT
BORN APPROXIMATION FOR
ELECTRON IMPACT *
CROSS SECTION (10^{-18} cm^2)
6
5
4
3
2
1
0
50
100
150
ENERGY (kev)

FIG. 33

by normalizing to the Lyman alpha emission and assuming the spectral efficiency of the monochromator to be the same for Lyman alpha at 1216 Å as at 1606 Å. Even though this assumption could cause some error, these absolute values for the cross sections give some indication of the intensity of the group of bands.

Since there are a number of electronic states above the B state, cascading effects must be considered. A study of the known band systems of the hydrogen molecule[46] revealed that the transitions populating the B state by cascading are in the wavelength region from 4000 Å to 6000 Å. When scanning this spectral region, the hydrogen molecular emissions between 4000 Å and 6000 Å were found to be considerably smaller than the Lyman band emissions. From this information it was concluded that cascading was not a large contributor to the populating of the B state.

The emission cross sections were also measured as a function of proton energy for the bands in the spectral region around 1575 Å. The probable bands contributing to this emission were the (5,11), (6,12), (7,13), and (8,14). These measurements showed the same energy dependence as did the bands around 1606 Å.

The author concluded, therefore, that the energy dependence of the emission cross section curve would not differ significantly from the energy dependence of cross section curve for the excitation of the v'= 6 level.

The only process which would be expected to contribute to the excitation of the B state is a simple direct excitation.

$$H^{+} + H_2 \text{ --- } H^{+} + H_2^{*}$$

Of all the data discussed in this paper these represent the clearest example of a simple direct excitation without any complicating process. The emission cross section, therefore, was plotted linearly as a function of energy to depict the characteristic shape expected from theory.

Khare[48] recently calculated the cross section for excitation of the B state by electron impact using the Born approximation. The results of these calculations are compared with the measurements which were made in connection with this paper. The calculations, using the Born approximation for electron impact, can be used for proton impact simply by scaling the relative velocity[14]. Since this calculation involved the excitation of the entire B state and only a fraction of the emission was measured, the data and calculations had to be normalized to each other. The normalization was made at 130 kev. The comparison is shown in figure 33. From the curve of QE as a function of ln E, figure 34, the linear relationship at the higher energies agrees, also, with predictions of the Born approximation.

Lyman Alpha Line: The emission cross section measurements for the Lyman alpha transition due to both proton and hydrogen atom impact are shown in figure 35. These data were normalized to the emission of Lyman alpha produced in the impact of protons on nitrogen.

In this emission data there were contributions both from the charge exchange and excitation of the fast particle and from the dissociation of the hydrogen molecule. When comparing these curves with those for Lyman alpha produced in the collisions with nitrogen, the influence of both the fast beam and the target gas are evident.

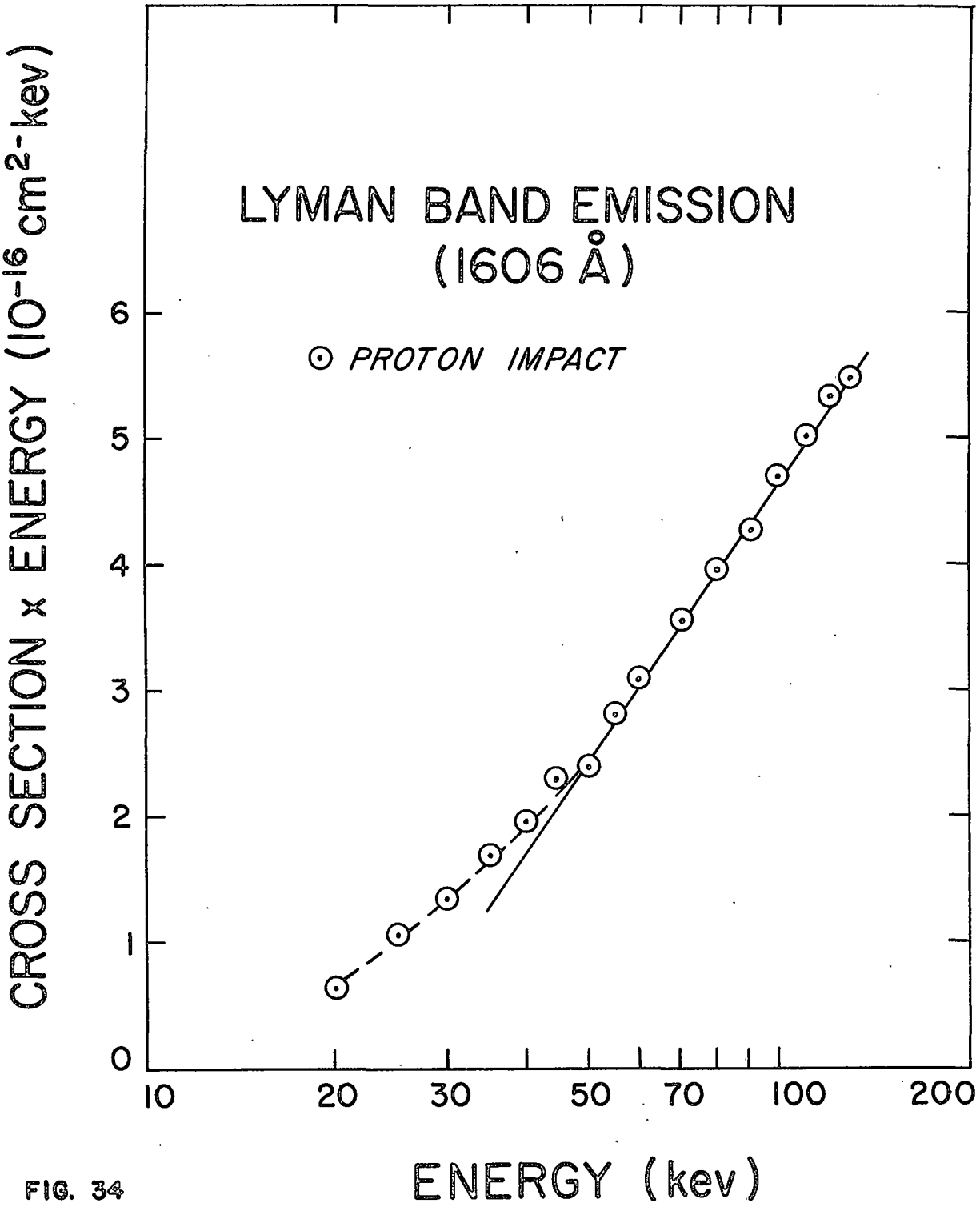
LYMAN BAND EMISSION
(1606 Å)
⊙ PROTON IMPACT
CROSS SECTION x ENERGY (10⁻¹⁶ cm²-kev)
0
1
2
3
4
5
6
10
20
30
50
70
100
200
ENERGY (kev)

FIG. 34

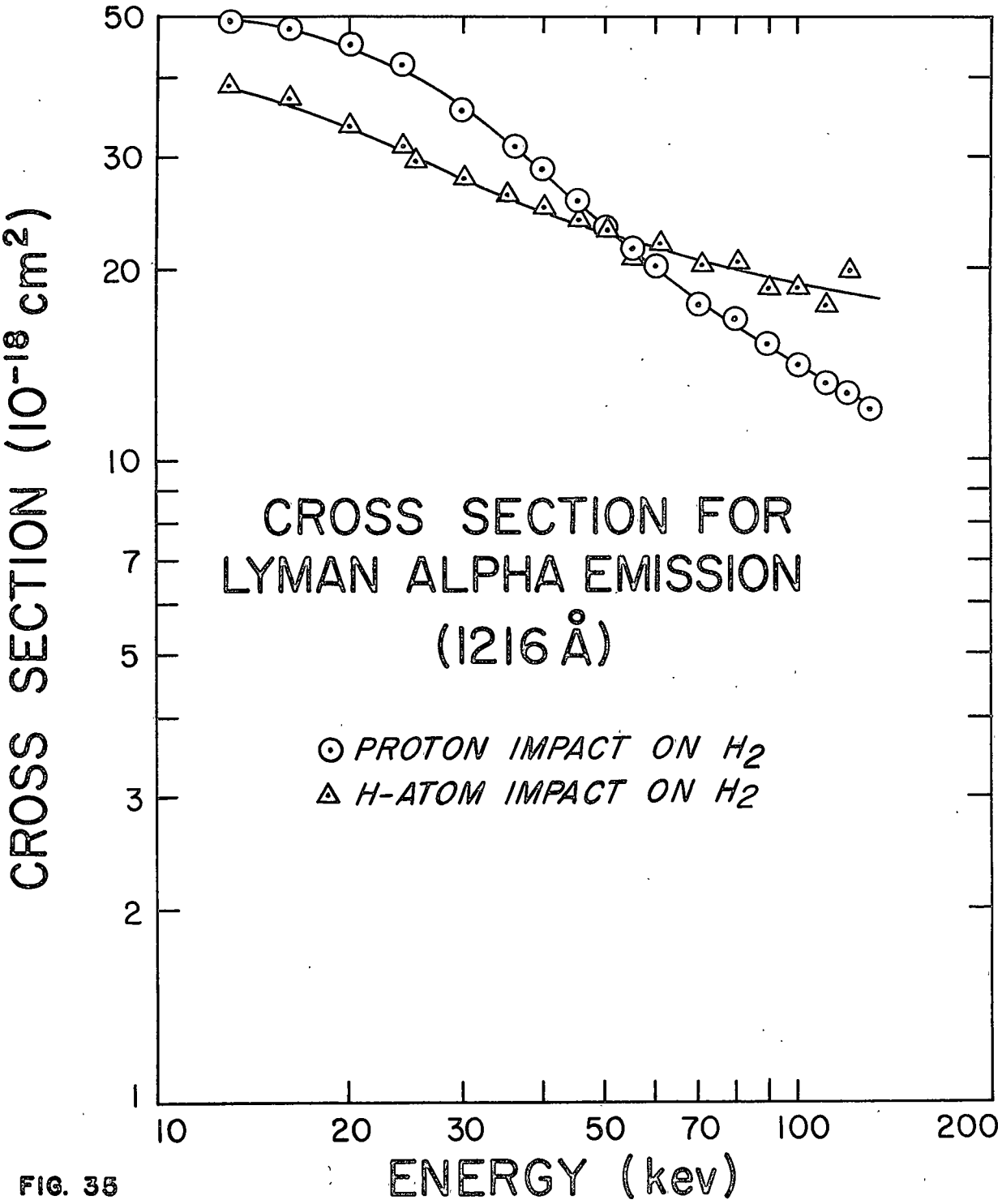
CROSS SECTION FOR
LYMAN ALPHA EMISSION
(1216 Å)
⊙ PROTON IMPACT ON H_2
△ H-ATOM IMPACT ON H_2
CROSS SECTION (10^{-18} cm^2)
ENERGY (kev)
50
30
20
10
7
5
3
2
1
10
20
30
50
70
100
200

FIG. 35

Since the two contributions to the emission are present, only qualitative information is obtainable.

In proton impact the main contribution to the Lyman alpha emission at the higher energies is expected to have been from the dissociation of the hydrogen molecule. This expectation is based upon the fact that the charge exchange cross sections decrease rapidly with energy and the production of Lyman alpha from the fast proton is dependent upon the charge exchange process.

From the results of the Lyman alpha emission produced in the collision of hydrogen atoms with nitrogen and from the energy dependence of the cross section for Lyman alpha produced in the collision of hydrogen atoms with hydrogen molecules, it would appear that the major contribution at the higher energies was from the excitation of the incident hydrogen atom. The curves of QE as a function of ln E, figure 36, also reveal the complexity of the data.

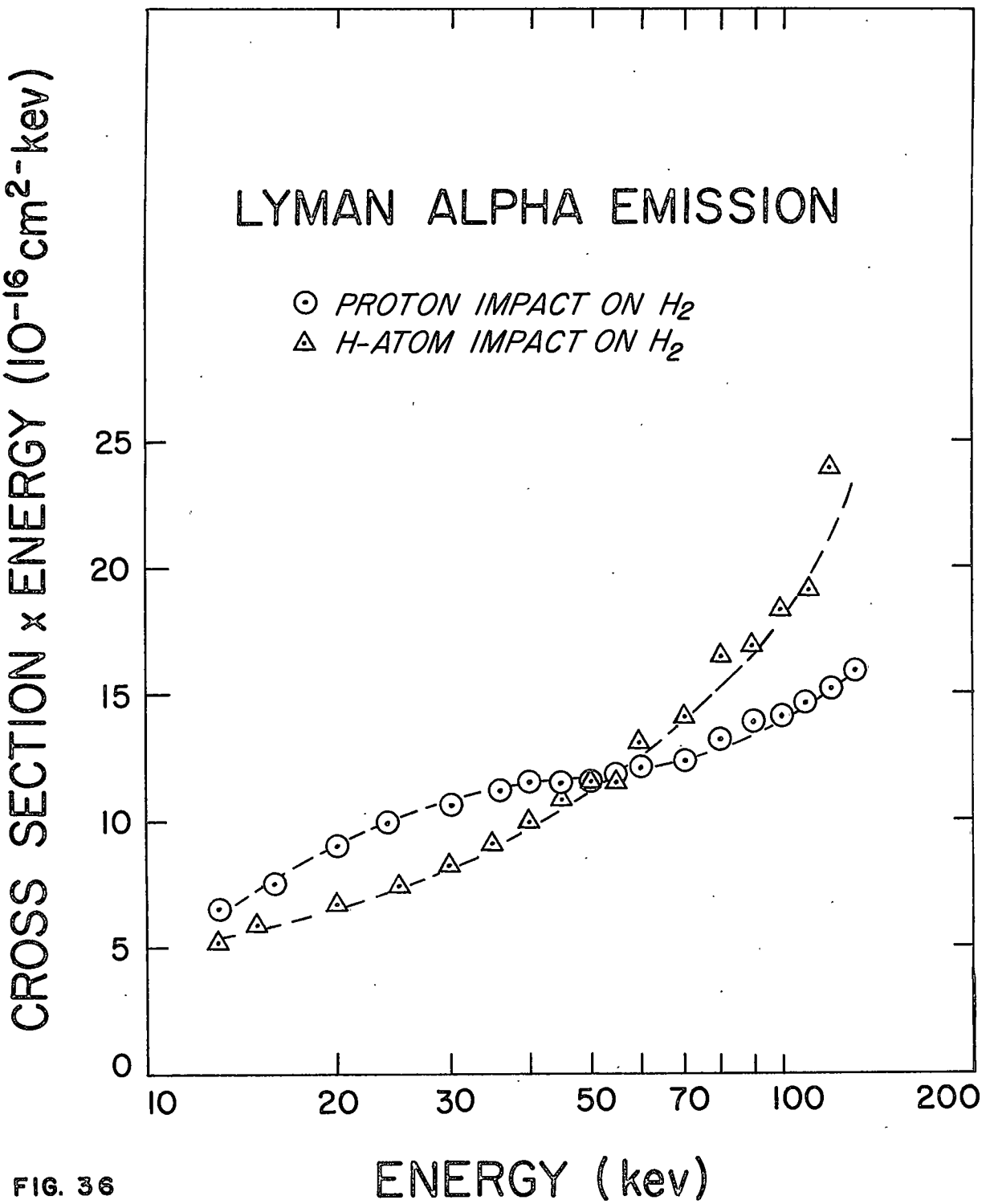
LYMAN ALPHA EMISSION
⊙ PROTON IMPACT ON H_2
△ H-ATOM IMPACT ON H_2
CROSS SECTION x ENERGY (10^{-16} cm^2-kev)
0
5
10
15
20
25
10
20
30
50
70
100
200
ENERGY (kev)

FIG. 36

APPENDIX

A. SLIT WIDTHS

If the entrance slit of the monochromator has the same opening as the exit slit, the theoretical energy distribution at the exit slit has a triangular shape, figure 37. The width of this intensity distribution at one-half the maximum intensity is sometimes called the half intensity band width and can be expressed in angstroms. If the dispersion of the monochromator is given, the half intensity band width is obtained from the product of the slit width and the dispersion. For example, the slit width of one mm was often used in measurements with the Bausch and Lomb monochromator. The half intensity band width would, therefore, be 33 Å since the dispersion of the monochromator was 33 Å/mm.

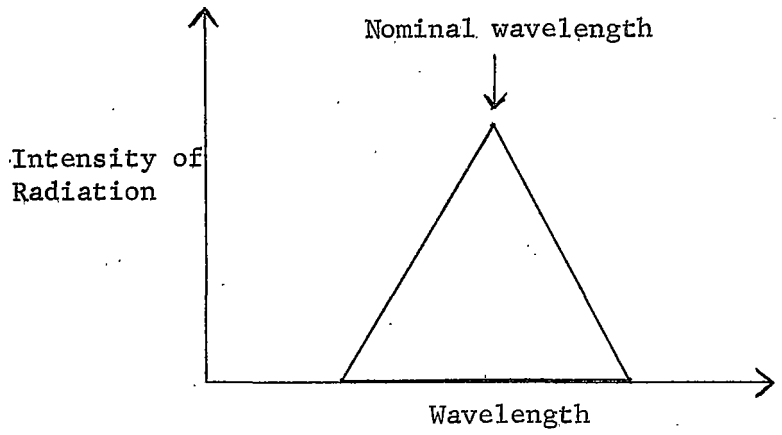

Figure 37. Theoretical Energy Distribution

B. BEAM COMPOSITION CORRECTIONS

If a particle has two primary charged states, the composition of a beam of such particles while passing through a gas can be calculated.

Following the work of Allison[2] two equations are required if all of the particles in the beam are initially in only one of the charge states.

For the case of the proton the two primary charge states are 0 and 1 which correspond, respectively, to the hydrogen atom and the proton. One other charge state exists, -1, which corresponds to the negative ion of hydrogen. The cross section for the production of the -1 charge state is small at low energies and insignificant at the higher energies when compared with the cross section for the production of the other two charge states.

The two equations which are required are:

$$F_0 = F_{0\,\infty}\ (1 - e^{-zpd})$$

and

$$F_1 = F_{1\,\infty}\ (1 - e^{-zpd})$$

F_0 and F_1 are, respectively, the fraction of hydrogen atoms produced in an initially pure proton beam and the fraction of protons produced in an initially pure hydrogen atom beam. $F_{0\,\infty}$ and $F_{1\,\infty}$ are, respectively, the equilibrium fractions of hydrogen atoms and protons in the beam. The pressure of the gas through which the beam traveled is p, in microns and the distance the particles had traveled in the gas is d, in cm. $z = 6.6 \times 10^{13}\ (Q_{01} + Q_{10})$ for diatomic molecules, where Q_{01} is the stripping cross section for hydrogen atoms incident on the target molecules and Q_{10} is the electron capture cross section for protons incident of the target molecules.

$F_{0\,\infty}$, $F_{1\,\infty}$, Q_{10}, and Q_{01} have been measured for the collisions considered in this work[2]. If the pressure in the excitation chamber and the distance that the particles traveled in the gas to the point of observation of the optical emission were measured, the charge state composition of the beam at that point could be calculated.

Calculations were made as a function of energy for each of the experimental conditions. If the correction for the change in the composition of the beam were significant compared with the experimental errors, the measured emission cross sections were corrected for the change in beam composition. The correction was always small except for the correction of the proton emissions from the $N_2(0,0)$ Second Positive band.

The correction always required the knowledge of the emission cross sections for both proton and hydrogen atom impact. An exact correction, therefore, required an iterative process. In this work, however, the author found that for all the emission cross section measurements essentially no correcting was required for the emission measurements due to one or the other of the incident particles. The iterative process was generally limited, therefore, to a single step.

C. PREDISSOCIATION[49]

Predissociation can be described in the following manner. If the potential energy curves of two states with the proper symmetry cross there will be a mixing of the two wave functions of the two electronic states. As a result radiationless transitions may occur between the two states. If one of the states is repulsive, dissociation will begin to

occur when the molecule, in its bound state, is above the dissociation limit of the repulsive state. There will be complete dissociation above the crossing point of the two curves. If both potential energy curves are stable, dissociation will occur from the state with the lower dissociation limit. There will be a radiationless transition to this state which will then dissociate. In this case dissociation begins very sharply at the lower dissociation limit.

LITERATURE CITED

1. A. B. Meinel, Astrophys. J. 113, 50 (1951)

2. S. K. Allison, Revs. Mod. Phys. 30, 1137, (1958)

3. N. P. Carleton and T. R. Lawrence, Phys. Rev. 109, 1159 (1958)

4. W. F. Sheridan, O. Oldenberg, and N. P. Carleton, Second International Conference on the Physics of Electronic and Atomic Collisions, University of Colorado, 1961 (W. A. Benjamin, Inc., New York, 1961), p. 159

5. J. L. Philpot and R. H. Hughes, Phys. Rev. 133, A107 (1964)

6. M. Dufay, et. al. Comptes Rendus 261, 1935 (1965)

7. G. H. Dunn, R. Geballe, and D. Pretzer, Phys. Rev. 128, 2200 (1962)

8. J. S. Murray, S. J. Young, and J. R. Sheridan, Phys. Rev. Letters 16, 440 (1966)

9. J. B. Hasted, Physics of Atomic Collisions (Butterworths, London, 1964) chapters 1, 11, and 12

10. M. Gryzinski, Phys. Rev. 138, A305 (1965)

11. M. Gryzinski, Phys. Rev. 138, A322 (1965)

12. M. Gryzinski, Phys. Rev. 138, A336 (1965)

13. D. R. Bates, Editor, Atomic and Molecular Processes, (Academic Press, London, 1962) Chapter 14

14. A. M. Arthurs, Proc. Cambridge Phil. Soc. 57, 904 (1961)

15. N. F. Mott and H. S. W. Massey, The Theory of Atomic Collisions, Third Edition (Oxford University Press, Oxford, 1965) Chapters XII and XIII

16. F. J. DeHeer, J. Schutten, and H. Moustafa, Physica 32, 1766 (1966)

17. D. R. Bates, H. S. W. Massey, and A. L. Stewart, Proc. Roy. Soc. A216, 437 (1953)

18. D. R. Bates, Proc. Phys. Soc. 73, 227 (1959)

19. R. J. Bell, Proc. Phys. Soc. A78, 903 (1961)

20. J. van Eck, F. J. DeHeer, and J. Kistemaker, Physica 30, 1171 (1964)

21. E. W. Thomas, G. D. Bent, and J. L. Edwards, Report No. ORO-2591-23, U.S. AEC, Oak Ridge, Tennessee (1966) p. 37

22. D. R. Bates and D. S. F. Crothers, Proc. Phys. Soc. 90, 73 (1967)

23. H. S. W. Massey, Rep. Prog. Phys. 12, 248 (1949)

24. J. B. Hasted, Advances in Electronics and Electronic Physics, Volume XIII (Academic Press, New York, 1960)

25. E. S. Solov'ev, R. N. Il'in, V. A Oparin, and N. V. Fedorenko, Soviet Phys. JETP 15, 459 (1962)

26. C. D Moak, H. Reese, Jr., and W. M. Good, Nucleonics 9, 18 (1951)

27. J H. Montague, Phys. Rev. 96, 973 (1955)

28. P. M. Stier, C. F. Barnett, and G. E. Evans, Phys. Rev. 96, 973 (1954)

29. H. Ishii and K. Nakayama, Proc of 8th Vacuum Symposium and 2nd Int. Congress (1961) p. 519

30. N. G. Utterback and T. Griffith, Jr., Rev. Sci. Instr. 37, 866 (1966)

31. N. P. Carleton, Phys. Rev. 107, 110 (1957)

32. F. R. Gilmore, The Rand Corporation Memorandum RM-4034-1-PR (1966)

33. G. H. Dieke and J. J. Hopfield, Phys. Rev. 30, 413 (1927)

34. J. Geiger, Z. Physik 181, 413 (1964)

35. P. K. Carroll, Can. J. Phys. 36, 1585 (1958)

36. P. K. Carroll, Can. J. Phys. 37, 880 (1959)

37. D. T. Stewart, Proc. Phys. Soc. A69, 437 (1956)

38. D. R. Bates, Mon. Nat. R. Astr. Soc. 112, 614 (1952)

39. G. Herzberg, Ann. Phys. Lpz. 86, 191 (1928)

40. G. Buttenbender and G. Herzberg, Ann. Physik (5)21, 577 (1934)

41. E. Wigner, Nach. Gess. Wiss., Gottingen (1927) page 375

42. E. N. Lassettre, A. Skerbele, and V. D. Meyer, J. Chem. Phys. 45, 3214 (1966)

43. E. U. Condon and G. H. Shortley, The Theory of Atomic Spectra Cambridge University Press, London, 1935), p. 136

44. P. S. Kelly, Astrophys. J. 140, 1247 (1964)

45. B. J. Ransil, Revs. Mod. Phys. 32, 239 (1960)

46. G. Herzberg, Spectra of Diatomic Molecules (D. Van Nostrand, Princeton, New Jersey, 1950), p. 345

47. G. Herzberg and L. L. Howe, Can. J. Phys. 37, 636 (1959)

48. S. P. Khare, Phys. Rev. 149 33 (1966)

49. Alf Lofthus, The Molecular Spectrum of Nitrogen (Spectroscopic Report No. 2, University of Oslo, 1960)

FIGURE CAPTIONS

Fig. 1 A view of the section of the apparatus which has direct significance to the experiment.

Fig. 2 A schematic of the excitation chamber used in the vacuum ultraviolet spectral work.

Fig. 3 The control system for the power to the diffusion pump.

Fig. 4 The fine current control for the analyzing magnet.

Fig. 5 The Magnetic field of the analyzing magnet as a function of current.

Fig. 6 The beam collector which served as the Faraday cage and the secondary emission detector.

Fig. 7 A partial energy level diagram of N_2 and N_2^+ taken from the work of Gilmore[32].

Fig. 8 Curves of potential energy as a function of internuclear distance for some of the electronic states of H_2[33].

Fig. 9 A partial energy level diagram of H_2 showing the X, B, and C states with some of the vibrational levels[34].

Fig. 10 Light intensity/incident proton as a function of pressure for the production of the (0,0) band of the N_2^+ First Negative system.

Fig. 11 Light intensity/incident hydrogen atom as a function of pressure for the production of the (0,0) band of the N_2^+ First Negative System.

Fig. 12 Light intensity/incident proton and relative cross section as a function of pressure for the production of the (0,0) band of the N_2 Second Positive system.

Fig. 13 Light intensity/incident proton as a function of energy for the production of the Lyman bands of H_2.

Fig. 14 Spectrum produced by a 7 microamp beam of 55 kev protons incident upon nitrogen gas at a pressure of 5.7 microns. Monochromator slits equivalent to 7 Å.

Fig. 15 Spectrum produced by a 10 microamp beam of 55 kev protons incident on nitrogen gas at a pressure of 25 microns. Monochromator slits equivalent to 4 Å.

Fig. 16 Spectrum produced by a 10 microamp beam of 55 kev protons incident on hydrogen gas at a pressure of 27 microns. Monochromator slits equivalent to 5.5 Å.

Fig. 17 Cross section for the production of the (0,0) band of the N_2^+ First Negative system by proton and hydrogen atom impact. Normalization was made to the absolute cross sections for proton impact measured by Philpot and Hughes[5].

Fig. 18 Cross section for the production of the (0,1) band of the N_2^+ First Negative system by proton and hydrogen atom impact.

Fig. 19 Cross section for the production of the (0,2) band of the N_2^+ First Negative system by proton and hydrogen atom impact.

Fig. 20 Cross section for the production of the (1,3) band of the N_2^+ First Negative system by proton and hydrogen atom impact.

Fig. 21 Cross sections for the ionization of N_2 in proton impact[25], for electron capture of protons incident on N_2 [16], and for the stripping of hydrogen atoms incident in N_2 [2]. Cross sections

also for the sum of the ionization and electron capture compared with the excitation of the $v' = 0$ level of the $B\ ^2\Sigma_g^+$ state of N_2^+ produced by protons incident on N_2.

Fig 22 Cross section for the excitation of the $v' = 0$ level of the N_2^+ First Negative system by proton and hydrogen atom impact plotted in terms of QE as a function of ln E.

Fig. 23 Cross section for the production of the (0,0) band of the N_2 Second Positive system by proton and hydrogen atom impact.

Fig. 24 Cross section for the production of the (0,0) band of the N_2 Second Positive system by proton and hydrogen atom impact plotted in terms of QE as a function of ln E.

Fig. 25 Cross section for the production of the Lyman alpha line by protons and hydrogen atoms incident on nitrogen.

Fig. 26 Cross section for the production of Lyman alpha line by proton and hydrogen atom impact on nitrogen plotted in terms of QE as a function of ln E.

Fig. 27 Cross section for the production of the $3s\ ^2P---2p\ \ ^2P^o$ NI line by proton and hydrogen atom impact.

Fig. 28 Cross section for the production of the $3s\ ^2P---2p\ ^2D^o$NI line by proton and hydrogen atom impact.

Fig. 29 Cross section for the production of the $3d\ ^3F^o---3p\ ^3D$ NII line by proton and hydrogen atom impact. The order of the states is reversed in the figure.

Fig. 30 Comparisons of the cross sections for the production of the

Lyman alpha line by protons incident on N_2 and H_2 and the 3s ^4P---2p $^4S^o$ NI line by proton impact.

Fig. 31 Cross section for the production of the 3d $^3F^o$---3p ^3D NII line by proton and hydrogen atom impact plotted in terms of QE as a function of ln E. The order of the states is reversed in the figure.

Fig. 32 Total cross sections for emissions from the 3s ^2P state of nitrogen due to proton and hydrogen atom impact plotted in terms of QE as a function of E.

Fig. 33 Cross sections for the emission of the Lyman bands centered at 1606 Å produced by proton and hydrogen atom impact. *Comparison is made with the Born approximation calculations of Khare[49]. Normalization is at 130 kev.

Fig. 34 Cross sections for the emission of the Lyman bands centered at 1606 Å produced by proton impact, plotted in terms of QE as a function of ln E.

Fig. 35 Cross sections for the production of the Lyman alpha line by protons and hydrogen atoms incident on H_2.

Fig. 36 Cross sections for the production of the Lyman alpha line by proton and hydrogen atom impact plotted in terms of QE as a function of ln E.